Construction and evaluation of a temperature dependent laminar burning velocity model for inerted hydrogen, methane and carbon monoxide mixtures

Jon Tolaas
University of Bergen, Department of Physics and Technology
Bergen, Norway

A thesis in partial fulfillment of the requirements for the degree of
Master of Science in the subject of Physics; Process Safety Technology

Abstract

The laminar burning velocity is an important mixture property providing information about different gas mixtures' reactivity. It is extensively used in the computational fluid dynamics (CFD) program FLACS to calculate explosion parameters such as explosion pressures, for risk management. Inaccuracy in FLACS' laminar burning velocity model sometimes causes it to misrepresent explosion pressure trends. This model is curve fitted towards experimental results and is not calculated as a function of physical models, such as thermal diffusivity and reaction rate. The aim of this study is to construct and evaluate a product temperature dependent laminar burning velocity model with a greater physical basis. The research was confined to four different fuel − air gas mixtures, including 67 distinct mixtures, and the laminar burning velocity (S_L) model was calibrated towards a range of experimental data sets.

Neither FLACS nor the S_L model are adequately precise in the current works' domain. The S_L model shows better agreement with experiments than FLACS for the $CO - air$, $CH_4 - air$ and $CH_4 - O_2 - CO_2$ mixtures, and a slightly better agreement for the $H_2 - O_2 - CO_2$ mixtures, while FLACS shows a slightly better agreement for the $C_3H_8 - air$ mixtures. It is hard to ascertain whether FLACS or the S_L model show better agreement with experiments for the $H_2 - air$ and $H_2 - air - steam$ mixtures. The S_L model shows good prospect, and it is conceivable that with further enhancement it may be capable of replacing the model currently implemented in FLACS. In order to determine this, the S_L model needs to be recalibrated towards the less fitted mixtures in the current work, and be calibrated and validated towards other gas mixtures at various conditions.

Acknowledgements

First and foremost, I would like to thank my supervisor Bjørn J. Arntzen (UoB) for providing me with an exciting topic for my thesis. His helpful feedback, explanations and motivational talks throughout this process have been much appreciated.

I would also like to thank Pawel J. Kosinski for taking the time to help me find valuable literature, and Kjetil Heitmann for helping me with computer related issues.

Next, I would like to thank the University of Bergen for providing a great learning environment. To all the amazing people I share office with; thank you for enjoyable lunch breaks, encouraging words and great cooperation. You have made the period as a master student a memorable time. A special thanks to Tone and Wulme for offering feedback, as well as Erlend for proofreading.

Finally, I wish to express my deepest gratitude to my parents who are always supportive.

Bergen, June 2017
Jon Tolaas

Contents

Nomenclature

Abbreviations

CFD	Computational fluid dynamics
FLACS	Flame Acceleration Simulator
LFL	Lower flammability limit
UFL	Upper flammability limit

Greek letters

α	Thermal diffusivity	$[m^2/s]$
δ	Flame thickness	$[m]$
ω	Mole based reaction rate	$[mol/m^3 \cdot s]$
ω	Reaction rate	$[s^{-1}]$
ρ	Density	$[kg/m^3]$

Latin letters

$[A], [B], [C]$	Concentration of species A,B,C	$[mol/m^3]$
$\dot{m}''$	Mass flux of reactants	$[kg/m^2 \cdot s]$
$\frac{\dot{Q}}{V}$	Volumetric heat transfer rate	$[j/m^3 \cdot s]$
$\overline{\dot{m}'''_F}$	Average mass production of fuel	$[kg/m^3 \cdot s]$
a	Geometry and mixture dependent constant	$[m^{-1}]$
A_{prex}	Pre-exponential factor	$[s^{-1}]$
C_p	Heat capacity at constant pressure	$[j/K]$
C_{ps}	Specific heat capacity at constant pressure	$[j/kg \cdot K]$
D	Mass diffusivity	$[m^2/s]$
E	Expansion factor	$-$
E_a	Activation energy	$[j/mol]$
H	Enthalpy	$[j]$

H_s	Specific enthalpy	[j/kg]
K	Rate coefficient	[s^{-1}]
k	Thermal conductivity	[$j/m \cdot K \cdot s$]
Le	Dimensionless Lewis number	–
M	Molecular weight	[g/mol]
n	Mole	[mol]
P	Pressure	[Pa]
Q	Heat	[j]
R	Radius from ignition point	[m]
R	Universal gas constant	[$j/K \cdot mol$]
RSS	Residual sum of squares of laminar burning velocity	[m^2/s^2]
S	Burning velocity	[m/s]
S_L	Laminar burning velocity	[m/s]
S_T	Turbulent burning velocity	[m/s]
S_{QL}	Quasi laminar burning velocity	[m/s]
T	Temperature	[K]
T_M	Mean temperature for the diffusion zone	[K]
U_R	Reactant flow	[m/s]
V	Volume	[m^3]
v	Dimensionless oxidizer to fuel mass ratio	–
W	Species mass fraction term	–
X	Air composition input parameter	–
x	Mole fraction	–
x	Moles of species	[mol]
Y	Mass fraction	–
y	Moles of species	[mol]

Subscripts and superscripts

0	Initial quantity
a, b, c, z	Reaction orders
F	Fuel
i, j, m	Species indices
i, n	Numeric indices
mix	Mixture
O	Oxidizer
o	Standard reference state
P	Product
R	Reactant
$stoich$	Stoichiometric
Z	Final species included in rate law

List of Figures

List of Tables

1. Introduction and motivation

Today, there is an increased focus on environmental protection, and thus clean fuels like syngas are attracting more interest. Simultaneously, the ever growing energy demand increases the commitment to other energy sources like nuclear energy, where hydrogen gas explosions can cause severe damage like it did in Fukushima in 2011. The energy demand also drives the Norwegian petroleum industries into more desolate, vulnerable locations like the Bering sea, where gas explosions can have disastrous consequences, and must be prevented.

Gas explosions occur when a flammable gas mixes with air and is ignited. Explosion parameters, such as maximum pressure, determine the consequence load of an accident. Information about these parameters may be used to preserve safety standards, e.g by designing more rigid structure layouts. Explosion parameters may be approximated through experiments, numerical studies or a combination of both. The computational fluid mechanics (CFD) program FLACS is used in industry to predict explosion parameters, by simulating explosion scenarios. The laminar burning velocity (S_L) is an important mixture property and is extensively used in FLACS calculations. Therefore, realistic S_L values are important in order to correctly assess potential risks.

Nowadays, detailed kinetic calculation software may be used to model S_L. However, if such S_L models were to be implemented in FLACS, running the program would be too time consuming. In FLACS, S_L values for different explosive mixtures are curve fitted towards experimental values. Inerted mixtures, e.g nitrogen or carbon dioxide diluted mixtures, are sometimes misrepresented by the laminar burning velocity correction models in FLACS. With the aim of improving the S_L values, a simple, more physically based model for S_L will be constructed and evaluated.

2. Background

This chapter presents combustion theory and the CFD program FLACS. Developed at the Christian Michelsen Institute from 1980, FLACS is a CFD tool that specialises in safety applications. Since development started, the code has continually been validated and updated. Today, FLACS's capabilities include the simulation of gas explosions, jet fires, pool fires and blast waves.

2.1 Literature survey

This section presents a literature overview of laminar burning velocity measurements and theories.

2.1.1 Experimental investigations of laminar burning velocity

The laminar burning velocity may be approximated by a combination of, or one of the following measurements [1, 2, 3]:

- The flow velocity of reactants in a steady flame.
- Pressure versus time in an explosion chamber.
- Optical observation of the flame front.

These experimental schemes can employ different flame configurations, including [4, 5]:

- Heat flux method/flat burner:

  A premixed stream of fuel and air flows through a perforated plate where it is stabilized by adjusting the flow rate.

- Spherical flame:

  The spherical flame configuration can be divided into constant pressure or volume setups. In the constant pressure setup, a soap bubble is filled with a premix and ignited in open air. The bubbles radial increase is recorded. In the constant volume setup a bomb is filled with a premix and pressure data is recorded.

Experimental results - now and then

The information in this section is gathered from a journal article by Ranzi et al. [6] unless stated otherwise. The authors of the article have done great work consolidating and investigating an extensive amount of experimental laminar burning velocity data.

A vast number of experiments have been conducted to measure the laminar burning velocity for different fuel mixtures. In the mid-1980s, an approach to eliminate the stretch effects in measurements was proposed by Wu and Law. As a result, the scatter in maximum laminar burning velocity between different experimental measurements was reduced, e.g from ± 25 cm/s to less than ± 2 cm/s for $CH_4 - $ air mixtures at atmospheric pressure, shown in Figure 2.1. Nevertheless, a large scatter in data still exist for other fuels such as hydrogen (approximately 30%), caused by differences in flame configuration and measurement techniques [1].

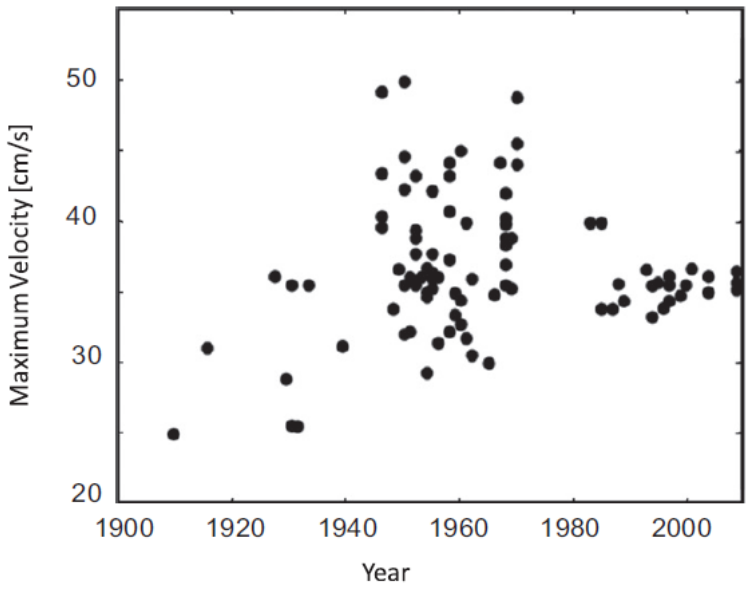

Figure 2.1: Historical measurement of maximum laminar burning velocity for $CH_4 - $ air mixtures at atmospheric pressure and room temperature, taken from Law C.K [7].

2.1.2 Laminar burning velocity theories

The information in this section is collected from Arntzen and Crows PhD theses and the combustion book by Turns [8, 9, 10].

Mallard and Le Châtelier published the thermal flame theory in 1883. Since then there has been proposed a vast amount of laminar burning velocity theories with varying level of detail. Various assumptions and approximations make these theories differ from each other, e.g the number of space coordinates which quantities depend on (dimensionality), the quantities' dependence on time (steady state versus transient state), the number of reactions included in the reaction rate law and the inclusion or neglection of transport phenomena such as thermal diffusion. These laminar burning velocity theories can be classified as diffusion theories, thermal theories and comprehensive theories as described below:

- Diffusion theories:

  The laminar burning velocity is generally accepted to be proportional to the mass transport of atoms and radicals by diffusion, and reaction rate, $S_L^2 \propto -D \cdot \omega$.

- Thermal theories:

  The laminar burning velocity is generally accepted to be proportional to the thermal diffusivity, and reaction rate, $S_L^2 \propto -\alpha \cdot \omega$.

- Comprehensive theories:

  An attempt is made to make a complete description of the laminar flame, including expressions for concentrations and velocities of all the involved chemical species.

In 1959, Spalding developed a simple model for laminar burning velocity prediction, which included only essential physics. It relies on one-dimensional conservation equations applied with simplified experimental transport equations, with chemical kinetics occurring in a one step global reaction. The current work is based upon this model.

In 1986, Kuo concluded that if one approximates the reaction rate with an Arrhenius expression, the burning velocity is essentially determined by the product temperature.

Nowadays the reaction rate may be calculated by detailed kinetic software package models. CHEMKIN is one such software package, which generates reaction pathways and consists of lists of elementary reactions with associated rate coefficient expressions which have been calibrated towards experimental values [11].

2.2 Combustion

Combustion, or burning, is often associated with the appearance of a warm flame and smoke. The four elements necessary for burning to occur are:

- Fuel
- Oxdidizer
- Heat
- Chain reactions

This section introduces some fundamental combustion concepts and definitions, starting with these four elements.

2.2.1 Fuel and oxidizer

Fuel and oxidizer can exist in the gaseous, liquid or solid phase. However, they must be in the gaseous phase for combustion to occur. In combustion, the oxidizer is usually the oxygen in air, while there exists a vast amount of different fuels, e.g hydrogen and methane. Mixtures of fuel and oxidizer are named reactants. Unless stated otherwise, normal air is presumed to contain approximately 21% oxygen and 79% nitrogen in this research. The ratio of nitrogen to oxygen in such air is 3.76. Subscripts $_F$ and $_O$ will denote fuel and oxidizer, respectively.

According to the Merriam-Webster dictionary [12], combustion can be described as a rapid exothermic chemical reaction. When fuel and oxygen species collide, they form heat and product species. The heat originates from the breaking of chemical bonds in fuel and oxidizer. The chemical composition and quantity of product species is determined by the chemical compositions and quantities of reactants. Typical products are often water, carbon dioxide and nitrogen. Equation (2.1) displays the general reaction equation for the complete reaction of a coincidental hydrocarbon in normal air, collected from Turns [9]:

$$\mathrm{C_xH_y} + (\frac{\mathrm{y}}{4} + \mathrm{x}) \cdot (\mathrm{O_2} + 3.76 \cdot \mathrm{N_2}) \longrightarrow \mathrm{x} \cdot \mathrm{CO_2} + (\frac{\mathrm{y}}{2}) \cdot \mathrm{H_2O} + (\frac{\mathrm{y}}{4} + \mathrm{x}) \cdot 3.76 \cdot \mathrm{N_2}\ . \qquad (2.1)$$

Small letters x and y, as well as numbers, denote the moles of the respective species.

Premixed and nonpremixed combustion

A distinction is made between premixed and nonpremixed combustion. In nonpremixed combustion, fuel and oxidizier react and mix together simultaneously, and the combustion is controlled by the transport of fuel and oxidizer to the flame. In premixed combustion, fuel and oxidizer are mixed before they react [13]. From a safety aspect, premixed blends are more of a concern as a much greater amount of fuel and oxidizer are ready to react than in the nonpremixed case. This research handles premixed combustion.

Characterising a complete reaction

A flame is said to be stoichiometric if fuel and oxidizer consume each other completely in the reaction. On the contrary, if the blend consists of excess fuel or oxidizer, it is categorized as fuel rich or lean, respectively. Equation (2.2) represents the combustion of a fuel-lean premix, where excess oxygen is left after the combustion.

$$\mathrm{H_2} + \mathrm{O_2} + 3.761 \cdot \mathrm{N_2} \longrightarrow \mathrm{H_2O} + 0.5 \cdot \mathrm{O_2} + 3.761 \cdot \mathrm{N_2} \ . \tag{2.2}$$

The equivalence ratio (ϕ) is a comparison parameter useful to relate the mixture composition to the stoichiometric, and is defined as [2]:

$$\phi = \frac{(\frac{n_F}{n_O})_{mix}}{(\frac{n_F}{n_O})_{stoich}} = \frac{(\frac{x_F}{x_O})_{mix}}{(\frac{x_F}{x_O})_{stoich}} \ , \tag{2.3}$$

where ϕ is equivalence ratio, n is mole and x is mole fraction. Subscripts mix and $stoich$ denote mixture and stoichiometric, respectively. In the results chapter, mole fraction is used to quantify the amount of fuel. Mole fraction can be calculated from ϕ by:

$$x_{F_{mix}} = \phi \cdot (\frac{x_F}{x_O})_{stoich} \cdot x_{O_{mix}} \ . \tag{2.4}$$

Flammability limits

As the fuel fraction decreases or increases, one of two concentrations is eventually reached where the mixture is no longer able to propagate a flame, called the lower and upper flammability limit (LFL, UFL), respectively.

2.2.2 Heat

The Merriam-Webster dictionary [14] defines heat as "the energy associated with the random motion of molecules". Heat is needed for a combustible mixture to ignite, and for the combustion to become self-sustained, which requires heat to be transferred from products to reactants. The current work includes constant, atmospheric pressure. For constant pressure processes, the first law of thermodynamics states that: $dH = dQ$, where H denotes enthalpy and Q denotes heat. The heat of reaction is calculated by:

$$\Delta H_{reaction} = H_{products} - H_{reactants} \ . \tag{2.5}$$

The heat capacity of a system at constant pressure, $C_p = \frac{dQ}{dT}$, describes the infinitesimal temperature change dT when an infinitesimal amount of heat dQ is added. It is used to calculate temperature elevated enthalpies:

$$H_i = H_i^o + \int_{298\,\mathrm{K}}^{T} C_p dT \ , \tag{2.6}$$

where H_i is the enthalpy of species i at temperature T, H_i^o is the standard enthalpy of formation of species i at standard reference state o (where $T = 298\,\mathrm{K}$) and $\int_{298\,\mathrm{K}}^{T} C_p dT$ is the enthalpy change caused by change in temperature [2].

2.2.3 Chain Reactions

A mixture may ignite upon being exposed to a heat source. However, if the mixture is to burn, it has to undergo radical chain reactions. In a radical chain reaction, very reactive species named radicals are formed from the stable reactants. Radicals expand in "chain branching steps" by forming two additional radicals when reacting with stable species, visualised in Figure 2.2:

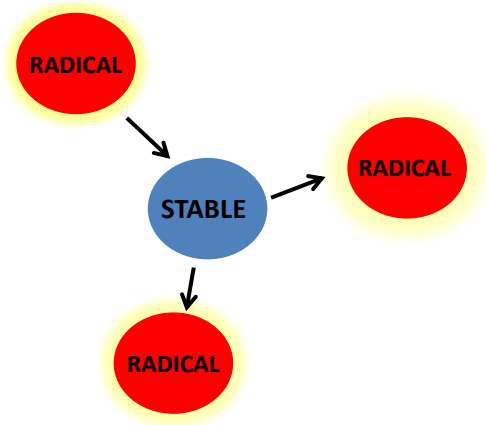

Figure 2.2: Chain branching step

This exponential increase in reactivity ends with the "chain terminating" step where radicals react to stable species, visualised in Figure 2.3:

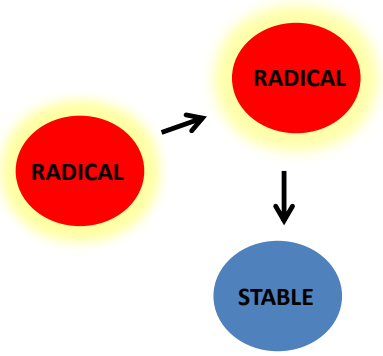

Figure 2.3: Chain terminating step

The heat released in these chain reactions is vital for burning.

2.2.4 Reaction rates and reaction mechanisms

Unless stated otherwise, the equations and information in this section has been taken from Warnatz' combustion book [2].

From a safety aspect, knowledge about the reaction rates of different gas mixtures is crucial. Reaction rates are key in defining hazard inducing parameters such as explosion pressure and amount of smoke. Many gaseous mixtures exhibit the fastest reaction rate at the stoichiometric composition. The reaction rate is controlled by the amount of successful molecular collisions per unit time. Reaction rates can be empirically formulated as so-called rate laws:

$$\omega = -K[A]^a[B]^b[C]^c... \; . \tag{2.7}$$

Equation (2.7) displays the reaction rate, ω, for a mixture of reactant species A, B and C. Exponents a, b and c are reaction orders with respect to these species. $[A]$, $[B]$, $[C]$ denote the concentration of the species. K is called the rate coefficient, which strongly depends in a nonlinear way on temperature, and can be described using Arrhennius law:

$$K = A_{prex}\, e^{(-\frac{E_a}{RT})} \; . \tag{2.8}$$

The activation energy E_a represents an energy barrier to overcome if the reactants are to ignite. T is the reaction temperature and R is the universal gas constant. The term $\frac{E_a}{R}$ is often omitted for T_a, named activation temperature. The pre-exponential factor A_{prex} is sometimes called the frequency factor and is proportional to the number of times molecules collide [15]. If species B and C in Equation (2.7) remain constant over the course of the reaction, the rate law may be simplified by excluding them:

$$\omega = -K[A]^a \; . \tag{2.9}$$

In combination with Equation (2.8),

$$\omega = -A_{prex}\, e^{(-\frac{T_a}{T})}[A]^a \; . \tag{2.10}$$

Combustion is a complex chemical event which consist of a wide range of elementary reactions with different reaction rates. Elementary reactions occur the exact same way on the molecular level as described in the reaction equation. The reaction orders of elementary reactions are always constant and usually consist of integers. This is not the case for net reactions, which only include the initial reactants and end-products. Simplified rate laws can be constructed from them. In a real combustion event, thousands of intermediate elements are formed and undergo reactions. One can gain adequate resolution of these reactions by constructing rate laws for each one, however, this is very time consuming. A detailed net reaction may require very advanced reaction orders, varying with time or other parameters like concentration, temperature etc. The rate laws in this research will be used to express a net reaction.

2.2.5 Laminar burning velocity

The information and equations in this section are gathered from Eckhoff's explosion hazard book [13] and the journal article by Dahoe et al. [1], unless stated otherwise. Subscripts $_R$ and $_P$ will denote reactant and product, respectively.

The burning velocity (S), is the pace at which the flame eats into the unburned reactants. Idealistically, the laminar burning velocity (S_L), is the lowest velocity at which a smooth, adiabatic flame can propagate through a uniform, quiescent gas mixture. Realistically the flame is not adiabatic as it loses heat to the surroundings, and non-uniformities in the flow field induce stretch effects on the flame. This stretching leads to the burning velocity varying at different locations in a cross-section of the flame. The laminar burning velocity for a given mixture is unique. To describe a complex phenomena like combustion, the laminar burning velocity is extremely useful as it contains information about gas mixtures' reactivity [6]. The structure of a premixed laminar flame is visualized in Figure 2.4.

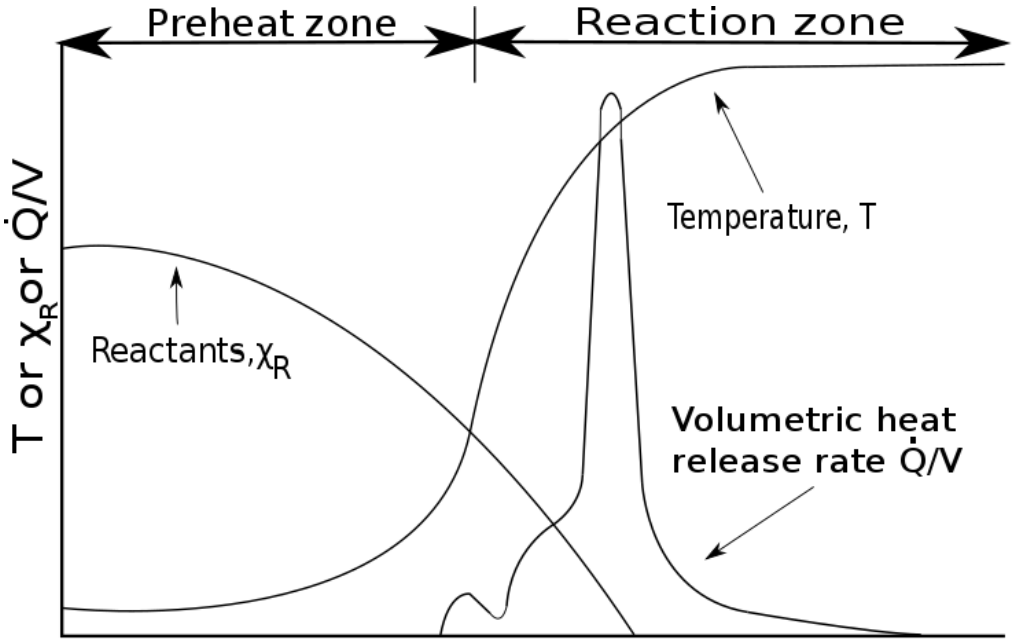

Figure 2.4: Laminar flame structure, where x_R is molefraction of reactants, T is temperature and $\frac{\dot{Q}}{V}$ is the volumetric heat release rate. Based on a figure from Turns [9].

Flame velocity

The flame velocity is influenced by the relative direction and magnitude of the flowing reactants (U_R) to the burning velocity (S). For a 1D pipe system where ignition occurs in the closed end, illustrated in Figure 2.5, the expansion of hot products will push the unburned gas in the same direction as the flame propagates. The flame speed (S_{FL}) is then

the sum of S and U_R.

$$S_{FL} = S + U_R \,, \tag{2.11}$$

which can also be expressed as

$$S_{FL} = S \cdot E \,, \tag{2.12}$$

where E is the expansion factor, caused by the decrease in density of the hot products ($E = \frac{S_{FL}}{S}$).

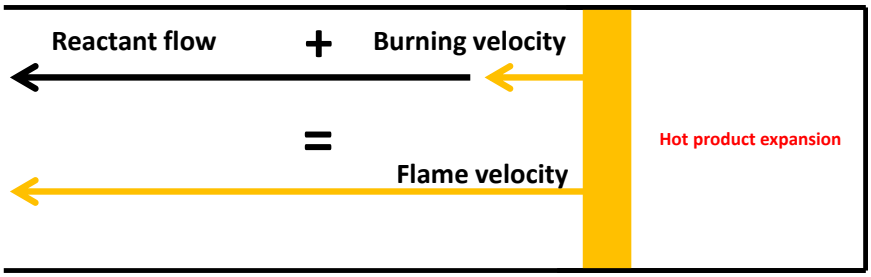

Figure 2.5: Visualisation of the difference between flame velocity and burning velocity. Combustion in an one-way open tube with ignition in the closed end. Based on a figure from Eckhoff [13].

Flame types

The combustible mixtures discussed so far have been assumed to either be quiescent or in steady flow. In steady flow, velocities at different spatial locations in the fluid remain constant over time, and layers of fluid slide on top of each other without vertical mixing. However, most flames are turbulent. Turbulent flow fields are characterized by rapid fluctuations in velocity and vertical mixing between fluid layers in the stream. As the turbulent flow stretches the flame, it increases the area between reactant and flamezone, hence increasing the flame velocity. Different flame types are summarized in Table 2.1:

Table 2.1: Flame types

Fuel/Oxidizer Mixing	Fluid Motion	Examples
Premixed	Turbulent Laminar	Gas explosion Flat flame
Nonpremixed	Turbulent Laminar	Diesel engine Candle fire

2.3 CFD and FLACS

In industry, high quality risk management requires rigid safety standards and barriers in order to minimize potential accident loads and consequences from combustion events [16]. Safety is costly, so there should be some logical reasoning behind such implementations. Some options are:

- Analytic evaluation:

  May give a pointer to the damage load of a potential accident, but lacks the required detail.

- Experimental evaluation:

  Produces valuable explosion parameter data by constructing small scale accident scenarios. However, large scale "realistic" experiments are very expensive.

- CFD simulation:

  Advanced CFD programs have the potential to accurately predict accident data, by simulating accident scenarios and solving for physical parameters in space and time. Results are validated towards experiments. FLACS is one such CFD program, used in industry risk management.

2.3.1 The governing equations of CFD

The governing equations - the continuity, momentum and energy conservation equations are the founding stones on which all CFD programs such as FLACS are based upon. They arise from different physical principles. Information about them can be found in John D. Andersons CFD book [17].

2.3.2 FLACS combustion model

The combustion model in FLACS include conservation equations of [8]:

- Mass (the continuity equation)
- Momentum
- Energy
- Mass fraction of fuel (or products)
- Mixture Fraction
- Turbulent Kinetic Energy
- Dissipation rate of turbulent kinetic energy

These equations are coupled with the ideal equation of state for a gas:

$$PV = nRT \ , \tag{2.13}$$

where P is pressure and V is volume.

The equation set is then discretisized and dedicated suitable boundary conditions in order to solve for physical variables in space and time, on a grid of chosen resolution. Information about these CFD terms can be found in the CFD book by John D. Anderson [17]. Submodels are used to account for details such as flammability limits and the effect of inert gases.

Laminar burning velocity in FLACS

In FLACS, the laminar burning velocity is extensively used as input in submodels and conservation equations to calculate other parameters. This section explains how the laminar burning velocity is modelled and used in FLACS today. The information and equations are taken from Arntzen [8] and Turns [9].

For a specific mixture, the laminar burning velocity model in FLACS extracts curve fitted tabulated S_L values. Next a wide range of submodels may be invoked to correct for factors such as initial pressure and temperature conditions, air composition and the quantity of inert gases [18]. The laminar burning velocities in FLACS are curve fitted towards experiments conducted by Jahn and presented by Lewis and von Elbe [19], which Figure 2.6 shows are in the lower range compared to other measurements presented in the journal article by Dahoe et al. [1].

The laminar burning velocity of a propagating flame increases with the distance from the ignition point, because of flame instabilities. A quasi laminar enhancement factor is used in FLACS to include this effect:

$$S_{QL} = S_L \cdot (1 + a \cdot R)^{\frac{1}{2}} \ , \tag{2.14}$$

where R is the radius from ignition point and a is a parameter dependent on factors related to the gas mixture and geometry in vicinity of the ignition point.

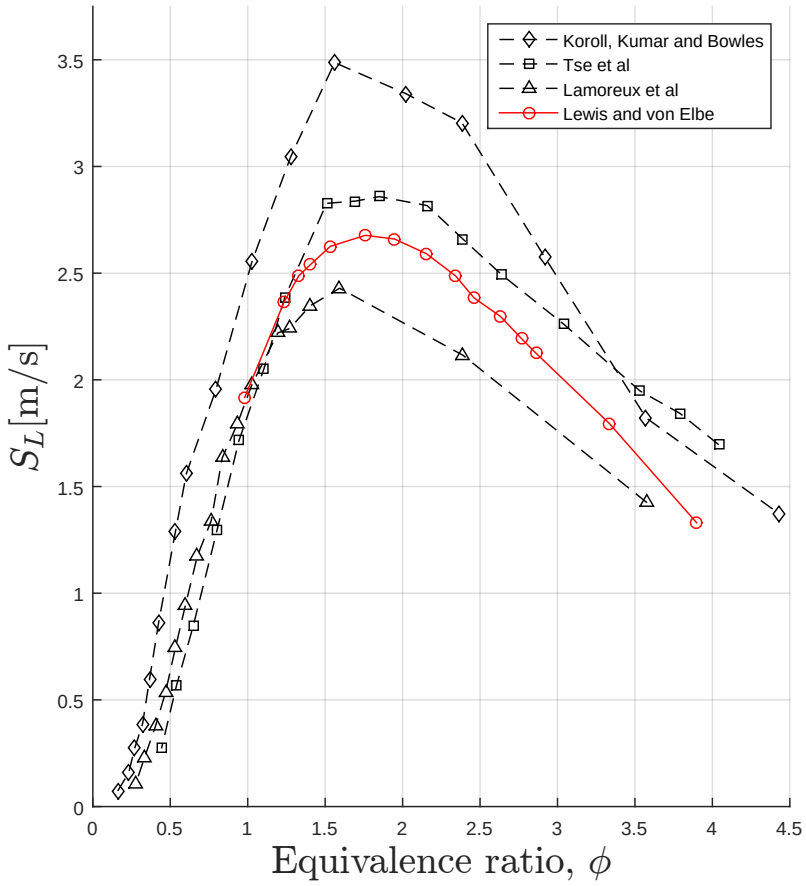

Figure 2.6: Discrepancies in measured $H_2 - air$ mixture laminar burning velocities at atmospheric pressure and room temperature, data collected from Lewis and von Elbe [19] and Dahoe et al. [1].

In FLACS, the turbulent burning velocity (S_T) is modelled as a function of laminar burning velocity. Arntzen [8] suggests that by making S_T a function of ω, turbulent burning velocity values may be improved.

2.4 A product temperature dependent laminar burning velocity model

Turns [9] presents Spaldings simplified laminar burning velocity analysis. All the theory and equations in this chapter have been taken from that analysis unless stated otherwise.

The laminar burning velocity is a function of fuel type, concentration, pressure, temperature etc. By coupling the principles of the previous chapters, the analysis presents the key steps in deducing a framework model for S_L as a function of product temperature, which is a principal parameter affecting burning velocity [8].

Assumptions of Spaldings laminar flame analysis

The following assumptions are applied to the conservation equations:

- Products are formed in a one-step global reaction.
- One dimensional, constant-area and steady flow.
- Kinetic and potential energies, viscous shear work and thermal radiation are neglected.
- Constant pressure.
- Diffusion of mass and heat are governed by the experimental Fick's and Fourier's laws, respectively.
- The Lewis number, $Le = \frac{\alpha}{D}$, which measures the ratio of thermal diffusivity to molecular diffusivity, is unity [20].
- The ideal gas law is considered to be valid.

Spalding also assumed that all species' heat capacities were equal and constant, as well as the oxidizer being present in excess proportions. This was not assumed in the current work.

2.4.1 Spaldings laminar flame analysis

Spaldings laminar flame analysis is presented in the combustion book by Turns [9] on pages 261-269. The conservation equations are adapted to the control volume illustrated in Figure 2.7, which represents a laminar flame.

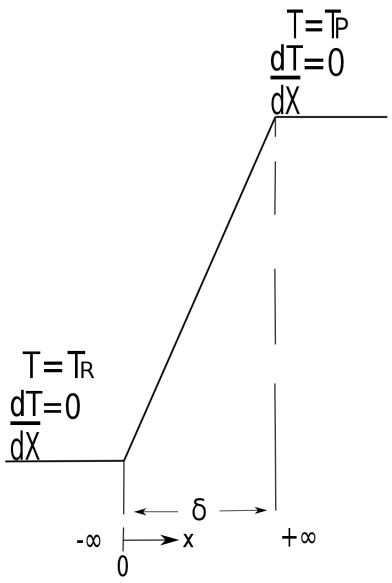

Figure 2.7: Linear laminar flame temperature model. Based on a figure from Turns [9].

As Figure 2.7 visualizes, the boundary conditions upstream of the flame are:

$$T(x \to -\infty) = T_R \ , \tag{2.15}$$

and

$$\frac{\partial T}{\partial x}(x \to -\infty) = 0 \ , \tag{2.16}$$

where T_R is the temperature in reactants. The boundary conditions downstream of the flame are:

$$T(x \to +\infty) = T_P \ , \tag{2.17}$$

and

$$\frac{\partial T}{\partial x}(x \to +\infty) = 0 \ , \tag{2.18}$$

where T_P is the temperature in products. Integrating the energy conservation equation over δ yields the following expression [9]:

$$\dot{m}''(T_P - T_R) = -\frac{\Delta H_{s,reaction}}{C_{ps}} \cdot \delta \cdot \overline{\dot{m}}_F''' \ , \tag{2.19}$$

where $\Delta H_{reaction,s}$ is specific enthalpy, C_{ps} is specific heat capacity at constant pressure, $\dot{m}''$ is the mass flux of reactants and δ is the flame thickness. $\overline{\dot{m}}_F'''$ is the average mass production of fuel, that is mass reaction rate. Because fuel is consumed over the course of the combustion, $\overline{\dot{m}}_F'''$ is negative. There are two unknowns in Equation (2.19), δ and $\dot{m}''$. They are found by integrating the energy equation once more, over the low temperature region of the flame, from $x = -\infty$ to $x = \delta/2$. It is plausible to assume that $\overline{\dot{m}}_F''' \approx 0$ in this

interval and that the majority of reactions occur in the upper half to high temperature region of the flame. The following relation is obtained:

$$\frac{\dot{m}''\delta}{2} - \frac{k}{C_{ps}} = 0 \ , \tag{2.20}$$

where k is thermal conductivity. A simple expression for the laminar burning velocity can then be obtained by solving Equations (2.19) and (2.20) simultaneously:

$$S_L^2 = -2\alpha(v+1)\overline{\dot{m}_F'''} \cdot \frac{1}{\rho_R} \ , \tag{2.21}$$

where v is the mass amount of oxidizer consumed per mass amount of fuel for a stoichiometric mixture, used in Turns [9] to define the species mass conservation equations. ρ_R is the density of the reactants, which is calculated from the densities of species in the mixture:

$$\rho = \sum_i^m \rho_i n_i + \rho_j n_j + ... + \rho_m n_m \ , \tag{2.22}$$

where n represents moles and i, j, m represent species. Species densities are calculated by use of the ideal gas law:

$$PV = nRT \longrightarrow \rho = \frac{PM}{RT} \ , \tag{2.23}$$

where M is molecular weight. In order to express S_L as a function of temperature, the reaction rate is approximated by a transformed Arrhennius equation that is a function of mass fraction:

$$\omega = -A_{prex}\, e^{(-\frac{T_a}{T})} \rho_P^{a+b} \cdot (\frac{Y_F}{M_F})^a \cdot (\frac{Y_O}{M_O})^b \ , \tag{2.24}$$

where ρ_P is the density of the burnt products. More mole density terms such as $(\rho_P \cdot \frac{Y_O}{M_O})^b$ can be included in Equation (2.24), which may increase the accuracy of the approximated reaction rate. Equation (2.24) can be transformed to $\dot{m}_F'''$ by multiplying it by the fuels molecular weight, M_F:

$$\overline{\dot{m}_F'''} = -A_{prex}\, e^{(-\frac{T_a}{T})} \rho_P^{a+b} \cdot (\frac{Y_F}{M_F})^a \cdot (\frac{Y_O}{M_O})^b \cdot M_F \ . \tag{2.25}$$

Inserting this expression for $\dot{m}_F'''$ into Equation (2.21) yields a framework model for S_L, here presented in general form for species F,O to Z:

$$S_L^2 = 2\alpha(v+1)A_{prex}\, e^{(-\frac{T_a}{T})} \frac{\rho_P^{a+b+...+z}}{\rho_R} \cdot (\frac{Y_F}{M_F})^a \cdot (\frac{Y_O}{M_O})^b \cdots (\frac{Y_Z}{M_Z})^z \cdot M_F \ . \tag{2.26}$$

Distinct models for S_L can be constructed from this framework model, determined by differences in modelling of the dependent variables and the amount of mole density terms such as $(\rho_P \cdot \frac{Y_O}{M_O})^b$.

3. Methodology

The methodology of the research can be divided into four parts:

- Development of a laminar burning velocity model, based on Spaldings framework model.
- Gathering of temperature, concentration and burning velocity data by digitalization of experiments, simulation in FLACS and utilization of a chemical calculator.
- Calculation of S_L values in Microsoft Excel, and construction of an algorithm in MATLAB which calculates the unknown parameters that give best fits between experimental data and the S_L model.
- Linearisation of reaction rate parameters to make the S_L model convenient to use.

3.1 Choosing submodels to approximate thermodynamic parameters in the laminar burning velocity model

This section presents how the framework S_L model for laminar burning velocity, Equation (2.26), was transformed by implementation of submodels for the dependent variables. Four different fuel − air gas mixtures, including 67 distinct mixtures were included in the research:

Table 3.1: Gas mixtures in research

Mixture	T [°C]	Special conditions	Number of mixtures
$H_2 - air - steam$	[50 °C, 150 °C, 200 °C]	Steam concentration $[0\% - 12\%]$	14
$H_2 - air$	25 °C	$\frac{O_2}{O_2+N_2}$ in the range $[0.125 - 0.985]$	14
$H_2 - O_2 - CO_2$	25 °C	$\frac{O_2}{O_2+N_2+CO_2}$ in the range $[0.16 - 1], 1.5\%$ N_2 in O_2	12
$CH_4 - air$	25 °C	$\frac{O_2}{O_2+N_2}$ in the range $[0.16 - 0.985]$	7
$CH_4 - O_2 - CO_2$	25 °C	$\frac{O_2}{O_2+N_2+CO_2}$ in the range $[0.3 - 0.985], 1.5\%$ N_2 in O_2	8
$CO - air$	25 °C	$\frac{O_2}{O_2+N_2}$ in the range [0.985-0.13]	8
$C_3H_8 - air$	+25 °C	Varying temperature, $[25, 60, 110, 130]$ °C	4

Choosing appropriate submodels to approximate parameters is very important when building a model. There exist a vast number of submodel options to approximate

parameters in the laminar burning velocity model. They come with varying degree of detail, accuracy and extrapolability. The submodels included in the S_L model were a result of the wish for a convenient model with a greater physical basis than what is already implemented in FLACS. There exist more accurate, advanced models for all the estimated physical parameters. However, a thorough comparison and evaluation of several such models would have been too time consuming for the time frame of the current work.

3.1.1 Reaction temperature and mean temperature for the diffusion zone

- Approximating reaction temperature as product temperature:

  Burning products in the vicinity of the flamezone have a similar temperature magnitude as the reaction temperature. The reaction temperature (T) was approximated by the product temperature (T_P) in this research. This made it possible to use product temperatures calculated by the use of chemical calculator, as explained in Section 3.2.2.

- Mean temperature for the diffusion zone:

  Turns [9] reasoned that because conduction occurs over the entire flame thickness, a mean temperature for the diffusion zone (T_M) should be used to model thermal diffusivity. The same reasoning is used in the S_L model of the current work:

$$T_M = \frac{1}{2}(T_P + T_R) \ , \tag{3.1}$$

3.1.2 Thermal diffusivity

The thermal diffusivity is defined in the CRC Handbook of Chemistry and Physics as [21]:

$$\alpha = \frac{k}{\rho \cdot C_{ps}} \ , \tag{3.2}$$

where k is thermal conductivity.

In this research, α was calculated by estimating k, ρ and C_{ps} as functions of the mean temperature for the diffusion zone and inserting them into Equation 3.2. The following subsections presents how k and C_{ps} were modelled.

Heat Capacity

In FLACS, specific enthalpy of formation data for different species are represented by 2nd degree polynomials. These polynomials were constructed by Arntzen [8] when he curve fitted fifth degree CHEMKIN polynomials:

$$H_{s,i} = aT + bT^2/2 - d \ , \tag{3.3}$$

where coefficients a, b and d are species specific, e.g 13 600, 1.719 and 4.13 for H_2, respectively.

Assuming constant pressure, the first law of thermodynamics states that $dH = dQ = C_p dT$. This implies that derivation of the specific enthalpy of formation polynomial used in FLACS with respect to temperature will yield an approximation of C_{ps}, here evaluated at the mean temperature for the diffusion zone (T_M):

$$C_{ps,i} = \frac{\partial H_{s,i}}{\partial T} = a + bT_M \ . \tag{3.4}$$

A general mass fraction weighting mixing rule was used to calculate mixtures' specific heat capacities:

$$C_{ps,mix} = \sum_i^m Y_i C_{ps,i} + Y_j C_{ps,j} + \cdots + Y_m C_{ps,m} \ , \tag{3.5}$$

where i, j and m denote species in the mixture and Y denotes mass fraction.

Thermal conductivity

Thermal conductivity (k) is proportional to temperature. Experimental thermal conductivity values found in Perry's chemical engineer's handbook [22] and the engineering toolbox [23] may be approximated by:

$$k = k_0 \cdot (\frac{T_M}{T_{M,0}})^{0.83} \ . \tag{3.6}$$

Equation (3.6) was constructed in an explicit way. Subscript 0 denotes the initial value of the respective parameter. Thermal conductivity k is a function of the initial thermal conductivity and mean temperature for the diffusion zone, k_0 and $T_{M,0}$ respectively, as well as the new mean temperature for the diffusion zone, T_M. Information about explicit calculations can be found in Andersons [17] CFD book.

Figure 3.1 shows how the thermal conductivity model, Equation (3.6), compares to experiments for some of the species in the current work. Equation (3.6) was curve fitted towards O_2, N_2 and H_2 thermal conductivities, which it shows fine agreement with. Thermal conductivities for CH_4, CO, C_3H_8 and H_2O are underestimated, but show

agreeing trends. Thermal conductivities for other gases than H_2, N_2 and O_2 may be improved by varying the exponent (0.83 in the current work) in Equation (3.6) with a physical parameter, e.g molecular weight. There exist more accurate and sophisticated models to approximate thermal conductivity. These k models were considered, but deemed too advanced in terms of the extent and time constraint of this research. Some k models are presented at pages 60-70 in Warnatz's combustion book [2].

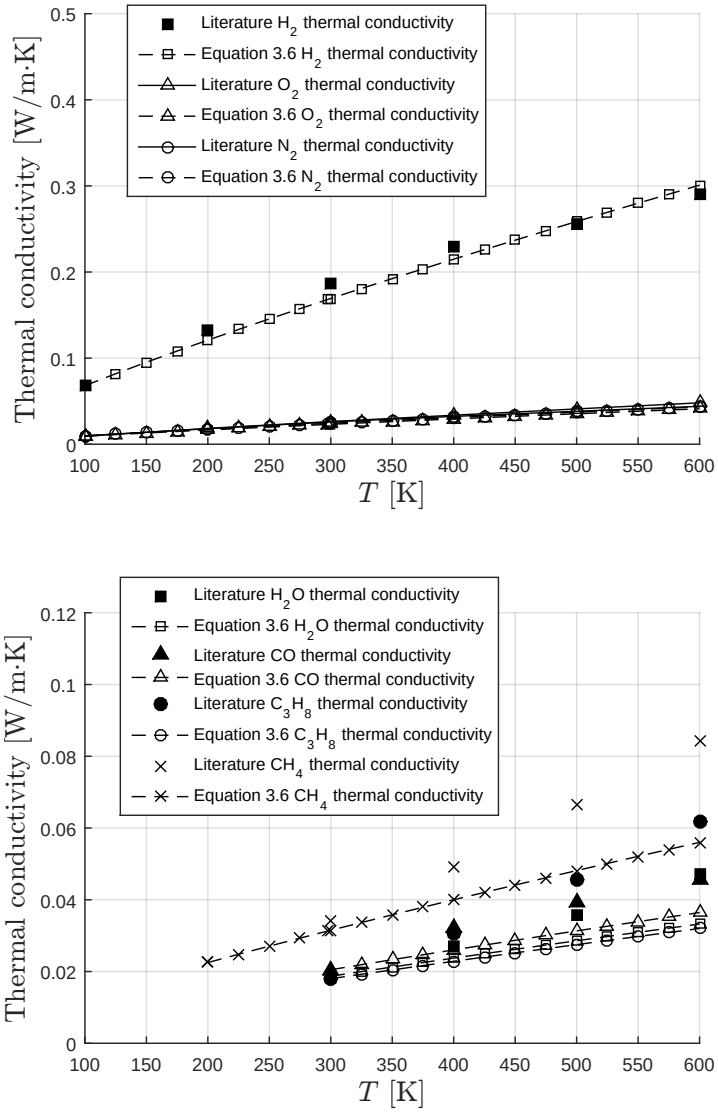

Figure 3.1: Comparison of modelled (Equation (3.2)) thermal conductivities and literature thermal conductivities from tabulated values in Perry's chemical engineering handbook and the engineering toolbox [22, 23].

Thermal conductivity mixing rule

An empirical thermal conductivity mixing rule constructed by Mathur et al. and presented in Warnatz combustion book [2], Equation (3.7), was used to calculate the thermal conductivities of mixtures. It approximates the thermal conductivity of a gas mixture from the thermal conductivities and mole fractions of mixture species, with an accuracy of 10-20 %. Increased accuracy can be achieved by a more sophisticated expression which includes correction factors that depend on viscosities of species in the mixture, found on page 62 in Warnatz's combustion book.

$$k_{mix} = \frac{1}{2} \cdot [\sum_{i}^{m} x_i k_i + (\sum_{i}^{m} \frac{x_i}{k_i})^{-1}] \,, \tag{3.7}$$

where x_i and k_i are the mole fraction and thermal conductivity of species i, respectively.

The choice to vary thermal diffusivity with temperature

In this section, thermal diffusivity differences at various temperatures are presented in order to justify why, in opposition to Spaldings [9] analysis, thermal diffusivity was chosen to vary with temperature even though it makes the S_L model less convenient to use.

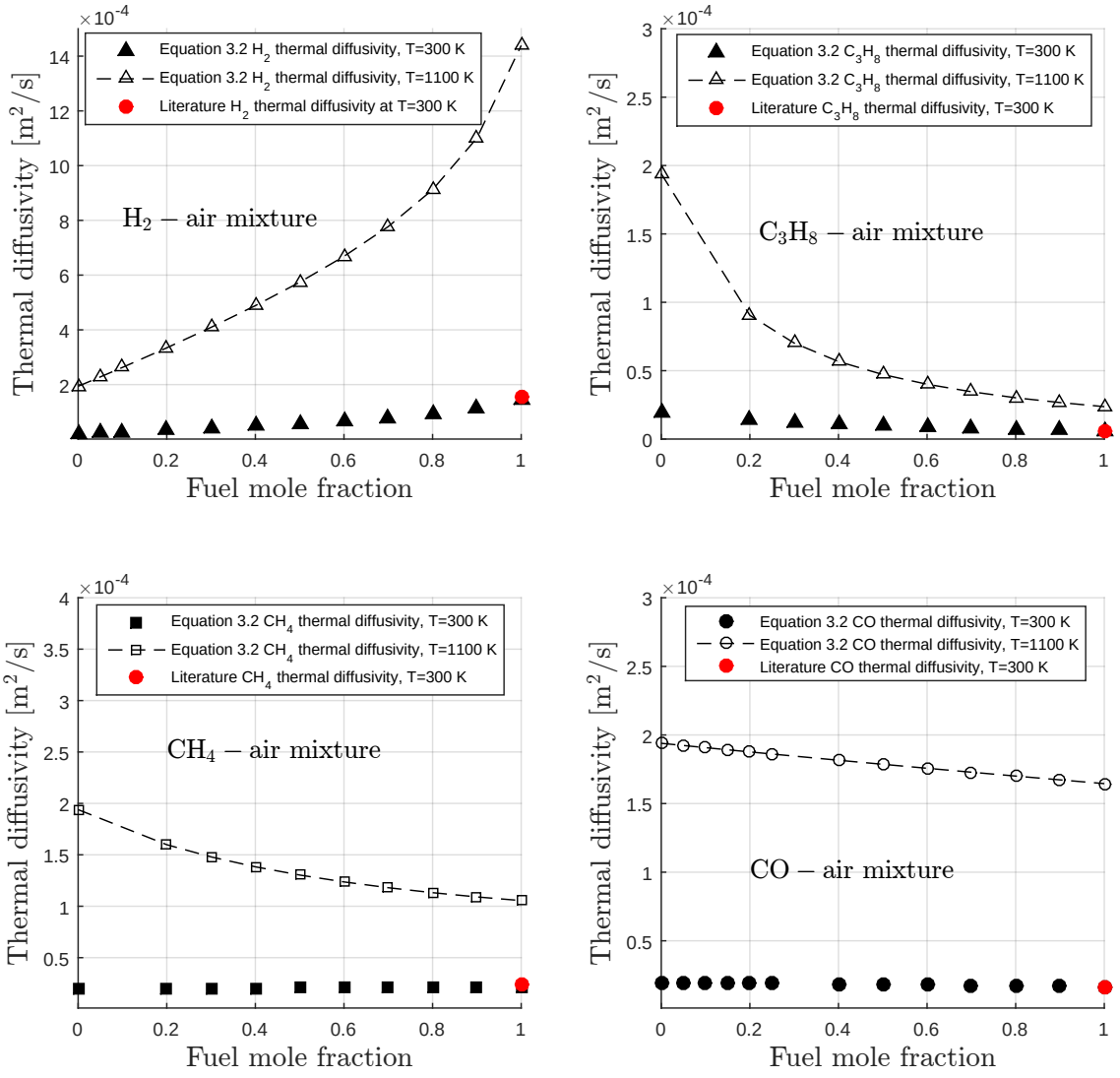

Figure 3.2: Modelled thermal diffusivities using Equation (3.2) at 300 K and 1100 K for $H_2 - air$, $CH_4 - air$, $C_3H_8 - air$ and $CO - air$ mixtures. Literature values at 300 K marked by the red dots have been taken from Perry's chemical engineering handbook and the engineering toolbox [22, 23].

Figure 3.2 visualizes the difference between mixture thermal diffusivities calculated by Equation 3.2 at 300 K or 1100 K. The mean temperature for the diffusion zone can typically be around 1100 K. Literature values at 300 K coincide with α values from

Equation(3.2), marked by the red dots. It is evident from Figure 3.2 that increasing temperature can greatly increase the thermal diffusivity, especially for effective heat conductors like hydrogen. Another literature comparison, visualised in Figure 3.3, was completed for some of the species in the research to investigate if Equation (3.2) produced realistic species thermal diffusivities in the temperature range 100 K to 600 K:

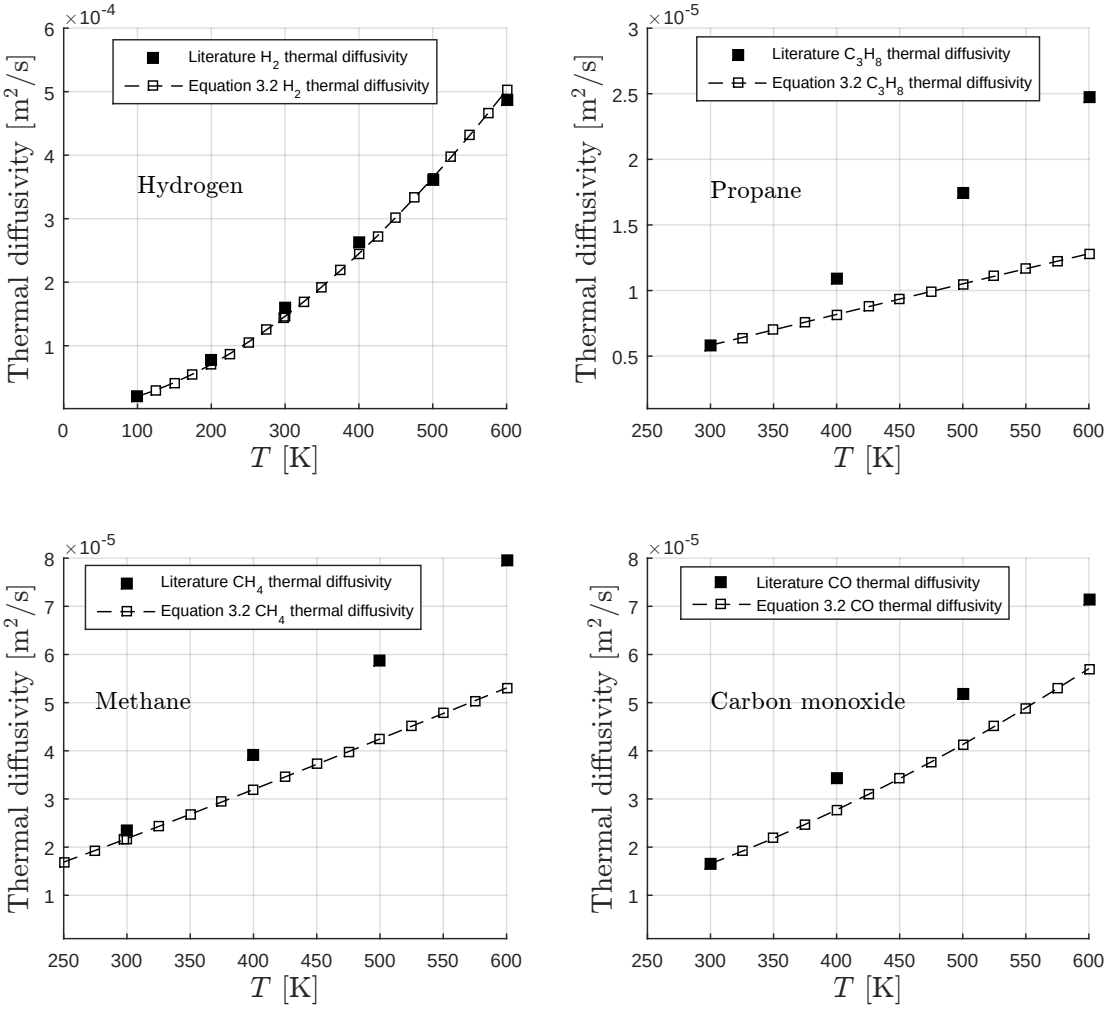

Figure 3.3: Comparison of thermal diffusivities modelled by Equation (3.2) and literature thermal diffusivities at elevated temperatures for H_2, C_3H_8, CH_4 and CO. Literature values have been taken from Perry's chemical engineering handbook and the engineering toolbox [22, 23].

Figure 3.3 shows that H_2 thermal diffusivities calculated by Equation (3.2) agree with literature values. While Equation (3.2) underestimates the thermal diffusivities of the other compared species to various degrees, calculated values show trend similarities with

literature in the temperature range 250 K to 600 K. However, this deviation might increase as the mean temperature for the diffusion zone can typically be around
1100 K. Calculated propane thermal diffusivities deviate the most. Deviations are likely to be caused by underestimation in the thermal conductivity model, which may be improved by calibrating it towards literature values for more species. Nevertheless, all curves show increasing thermal diffusivity with temperature, and while the thermal diffusivity might get underestimated, a temperature-varying thermal diffusivity lies the foundation for a greater physically based S_L model.

Later on in the research, it was found that Welty [24] estimated thermal diffusivity as:

$$\alpha \propto \frac{1}{P^{\frac{5}{4}} \cdot C_{ps}} \cdot (\frac{T}{M})^{7/4} \, . \tag{3.8}$$

A comparison between Equation (3.8) and the chosen thermal diffusivity model, Equation (3.2), was completed. Equation (3.8) was scaled by 647 to produce a literature agreeing H_2 thermal diffusivity at 300 K. This multiplicator was used for all species in the comparison. Some results are presented in Table 3.2. Equation (3.8) is both more accurate than Equation (3.2), and dependent on pressure. Because the current work only includes constant, atmospheric pressure, the pressure dependence of Equation (3.8) was not evaluated. However, replacing the current thermal diffusivity model with Equation (3.8) is suggested as it will both improve the S_L model at atmospheric pressure and has the potential to further improve the S_L model at elevated pressures.

Table 3.2: Thermal diffusivity model comparison

Species, Temperature [K]		$\alpha = \frac{647}{P^{\frac{5}{4}} \cdot C_{ps}} \cdot (\frac{T}{M})^{7/4}$ [m^2/s]	$\alpha = \frac{k}{\rho \cdot C_{ps}}$ [m^2/s]	Literature α [m^2/s]
H_2,	300	$1.60 \cdot 10^{-5}$	$1.46 \cdot 10^{-4}$	$1.60 \cdot 10^{-4}$
H_2,	400	$2.63 \cdot 10^{-4}$	$2.44 \cdot 10^{-4}$	$2.62 \cdot 10^{-4}$
H_2,	500	$3.84 \cdot 10^{-4}$	$3.64 \cdot 10^{-4}$	$3.60 \cdot 10^{-4}$
C_3H_8,	300	$5.83 \cdot 10^{-6}$	$5.82 \cdot 10^{-6}$	$5.82 \cdot 10^{-6}$
C_3H_8,	400	$1.10 \cdot 10^{-5}$	$8.17 \cdot 10^{-6}$	$1.09 \cdot 10^{-5}$
C_3H_8,	500	$1.74 \cdot 10^{-5}$	$1.05 \cdot 10^{-5}$	$1.73 \cdot 10^{-5}$
CH_4,	300	$2.72 \cdot 10^{-5}$	$2.17 \cdot 10^{-5}$	$2.35 \cdot 10^{-5}$
CH_4,	400	$3.89 \cdot 10^{-5}$	$3.19 \cdot 10^{-5}$	$3.92 \cdot 10^{-5}$
CH_4,	500	$5.08 \cdot 10^{-5}$	$4.24 \cdot 10^{-5}$	$5.86 \cdot 10^{-5}$
CO,	300	$3.21 \cdot 10^{-5}$	$1.65 \cdot 10^{-5}$	$2.08 \cdot 10^{-5}$
CO,	400	$3.40 \cdot 10^{-5}$	$2.77 \cdot 10^{-5}$	$3.44 \cdot 10^{-5}$
CO,	500	$5.16 \cdot 10^{-5}$	$4.12 \cdot 10^{-5}$	$5.16 \cdot 10^{-5}$

3.1.3 Stabilizing the reaction rate

Mole densities, such as $(\rho_P \cdot \frac{Y_{O_2}}{M_{O_2}})^b$, which are used by Spalding in his analysis presented by Turns [9], proved to be very sensitive to small changes in concentrations, thereby making it hard to construct linear expressions for species reaction orders, e.g oxygen's reaction order b, by curve calibration later on in the research. To counteract this effect and stabilize the reaction rate, mole densities were replaced by dimensionless "species mass fraction terms" (W). These new terms were normalized by the stoichiometric species mass fractions instead of molecular weight, and were not multiplied by the product density ρ_P, as shown here for an arbitrary fuel: $W_F = (\frac{Y_F}{Y_{F,stoich}})^a$. This simplified scheme was convenient, as FLACS calculates the laminar burning velocity as a function of species mass fractions, and because it made it easy to approximate initial pre-exponential factors (A_{prex}), as explained in Section 3.3.2. From this point onward, species mass fraction terms will be denoted $W_{species}$, e.g $(\frac{Y_{O_2}}{Y_{O_2,\text{stoich}}})^b$ will be denoted "W_{O_2}". In that manner, the density ratio $\frac{\rho_B^{a+b+\ldots+z}}{\rho_R}$, and molecular weight of fuel M_F, were excluded from Spaldings laminar burning velocity model (Equation (2.26)) when constructing the S_L model.

However, this induced a lack in pressure dependence on the S_L model. Another possible scheme is to express mole density as:

$$\frac{\rho_P Y_F}{M_F} = (\frac{Y_F}{Y_{F,stoich}}) \cdot (\frac{Y_{F,stoich}}{M_F}) \cdot \rho_P \ , \tag{3.9}$$

which implemented into Spaldings laminar burning velocity expression, Equation (2.26), leads to:

$$S_L^2 = 2\alpha(v+1)A_{prex}\, e^{-\frac{T_a}{T_P}} \cdot (\frac{Y_F}{Y_{F,stoich}})^a \cdot (\frac{Y_{F,stoich}}{M_F})^a \cdot (\frac{Y_O}{Y_{O,stoich}})^b \cdot (\frac{Y_{O,stoich}}{M_O})^b \cdots \frac{\rho_P^{a+b+\ldots}}{\rho_R} \cdot M_F \ . \tag{3.10}$$

As mentioned, this scheme was not implemented in order to make the S_L model convenient to use, but may be considered an enhancement option in the future.

3.1.4 Overview of the preliminary laminar burning velocity model

Implementation of the chosen models for thermal diffusivity, reaction temperature, mean temperature for the diffusion zone and inclusion of the species mass fraction terms yielded the following model for S_L:

$$S_L^2 = 2\alpha(v+1)A_{prex}\, e^{(-\frac{T_a}{T_P})} \cdot (\frac{Y_F}{Y_{F,stoich}})^a \cdot (\frac{Y_O}{Y_{O,stoich}})^b \cdots (\frac{Y_Z}{Y_{Z,stoich}})^z \ . \tag{3.11}$$

Or alternatively:

$$S_L^2 = 2\alpha(v+1)A_{prex}\, e^{(-\frac{T_a}{T_P})} \cdot W_F \cdot W_O \cdots W_Z \ , \tag{3.12}$$

where:

- $T_M = \frac{1}{2}(T_P + T_R)$
- $\alpha = \frac{k}{\rho \cdot C_{ps}}$
- $k = k(\frac{T_M}{T_{M,0}})^{0.83}$
- $C_{ps,i} = \frac{\partial H_{s,i}}{\partial T_M} = a + bT_M$
- $v = (\frac{Mass_O}{Mass_F})_{stoich}$
- $\rho = \sum_i^m \rho_i n_i + \rho_j n_j + ... + \rho_m n_m$

The following quantities had to be obtained in order to close the S_L model:

- The pre-exponential factor A_{prex}.
- The product temperature T_P, in order to calculate T_M and T_a.
- Concentraton data from experiments, in order to calculate Y_F and $Y_{F,stoich}$, as well as v for the different mixtures.
- Concentration and temperature data in order to calculate ρ, C_p, k and α.
- Laminar burning velocity data from experiments, to calculate fitted reaction orders in included species mass fractions terms, such as "a" in $(\frac{Y_F}{Y_{F,stoich}})^a$.

3.2 Data collection to close the laminar burning velocity model

This chapter describes how thermodynamic data necessary to close Equation (3.11) were gathered.

3.2.1 Concentration and burning velocity digitalization

Data from H_2, CH_4 and CO mixtures with varying air compositions and CO_2 dilutions was digitalized from the results presented by Lewis and von Elbe [19]. Collections of H_2 data from a vast number of experiments were also digitalized from results presented by Dahoe et al. [1]. The data for $H_2 - air - steam$ mixtures was digitalized from the results of Liu and MacFarlane [25]. Data for $C_3H_8 - air$ mixtures was digitalized from the results of Razus et al. [26].

The first digitalization method was to screen-shot pdf files containing curves of the results, and then use the pixel coordinate visualizer in Microsoft Paint to store pixel coordinate data in Microsoft Excel, shown in Figure 3.4:

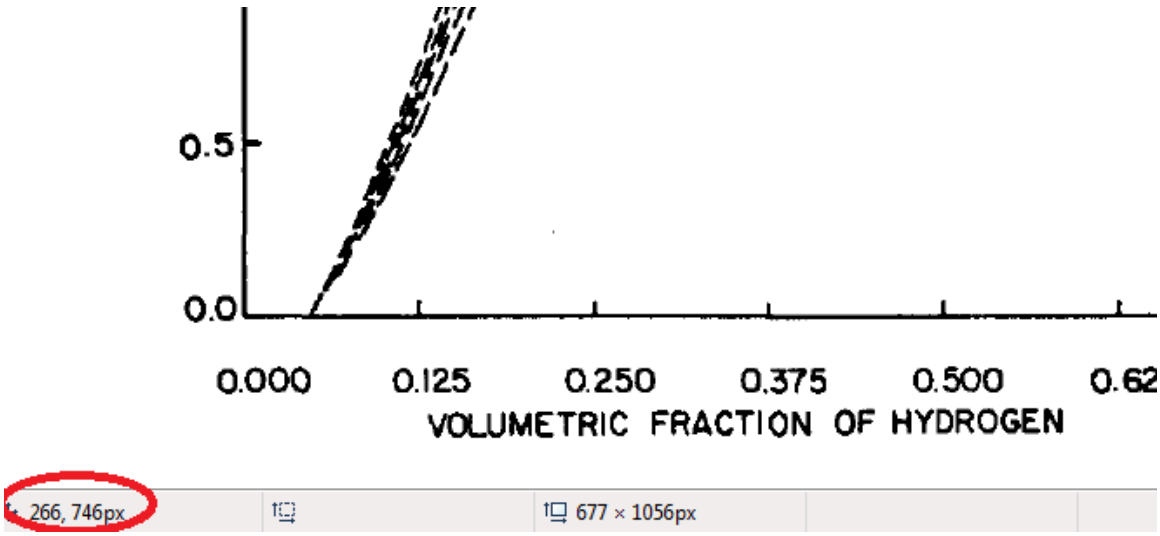

Figure 3.4: Digitalization of laminar burning velocity experiments by storing pixel coordinate data, which is marked by the red ring.

The pixel coordinate data was then transformed to concentration and burning velocity data in Microsoft Excel, shown in Figure 3.5.

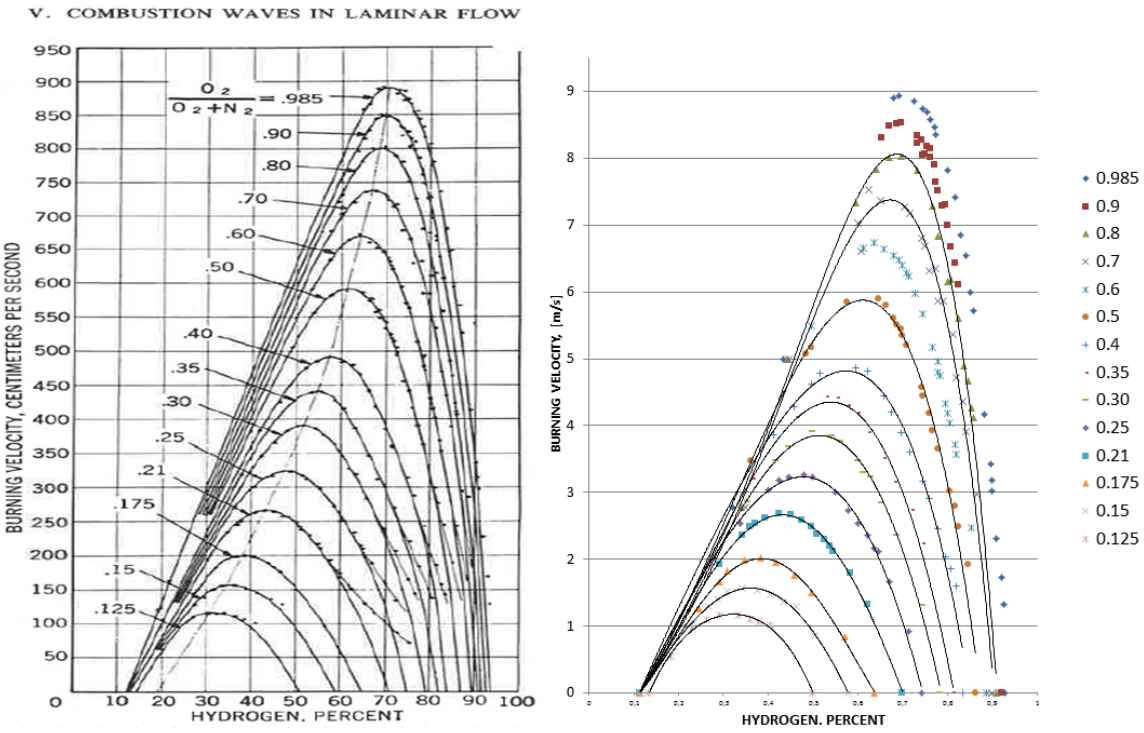

Figure 3.5: Digitalization of laminar burning velocity experiments for $H_2 - \text{air}$ mixtures by Lewis and von Elbe [19]. Experimental results pdf to the left and digitalized datapoints to the right.

This method of digitalization was only utilized for the $H_2 - \text{air}$, $H_2 - \text{air} - \text{steam}$ and $H_2 - O_2 - CO_2$ mixtures as it was found very ineffective. The remaining mixtures were digitalized by using a MATLAB function named GRABIT [27]. This method was much less time consuming as the function made it possible to calibrate axes dimensions of image files and then extract co-ordinates by clicking on them.

3.2.2 Product temperature approximation

The product temperature was approximated by the use of a chemical calculator developed at Colorado State University. It uses data from the CHEMKIN thermodynamic database and implements the STANJAN algorithm developed by Bill Reynolds to calculate various equilibrium properties such as temperature, concentration and pressure [28]. Initial conditions were set equal to that of the experiment in question (for the most part 293.15 K and 101325 Pa). Constant pressure and enthalpy were chosen as calculation constraints. The possible product species (for the hydrocarbon mixtures) were set to H_2O, OH, H_2, H, CO_2, CO, NO and NO_2. The setup is shown in Figure 3.6:

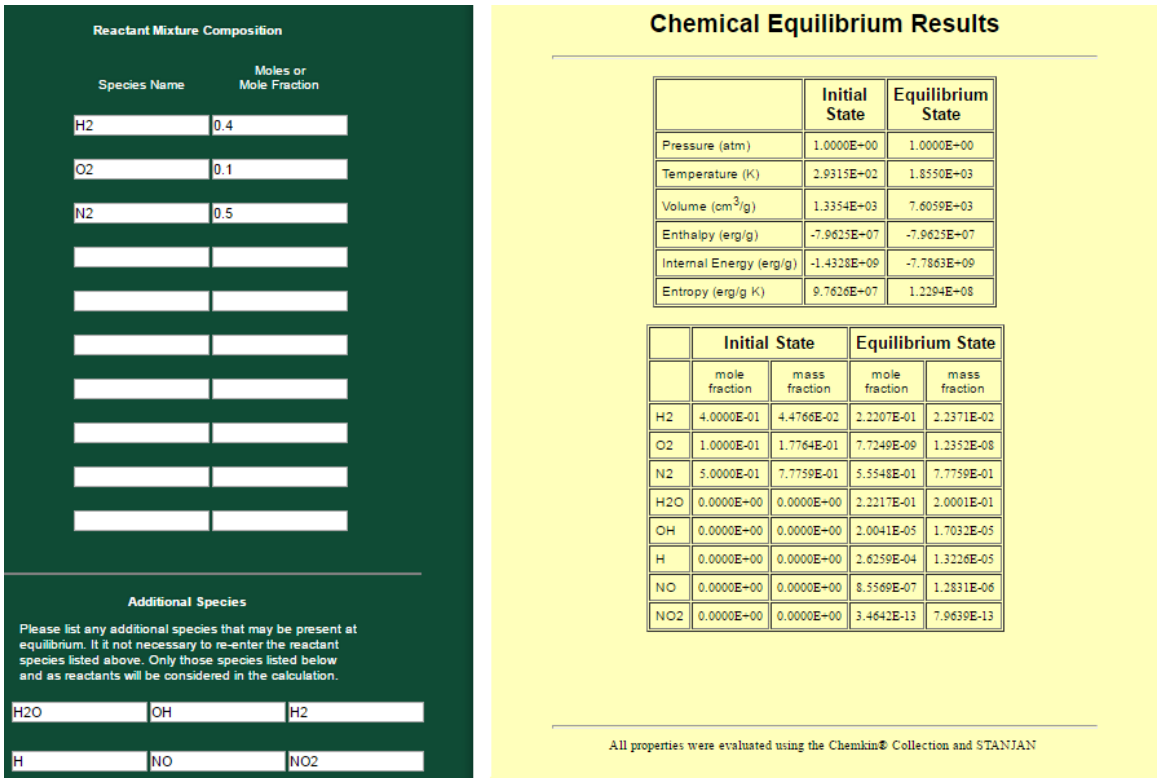

Figure 3.6: Snapshot of the chemical calculator used to calculate the equilibrium temperatures of mixtures in the research. The reactant mixture composition is set in the green window to the left. Equilibrium results are displayed in the yellow window to the right.

3.2.3 FLACS laminar burning velocities

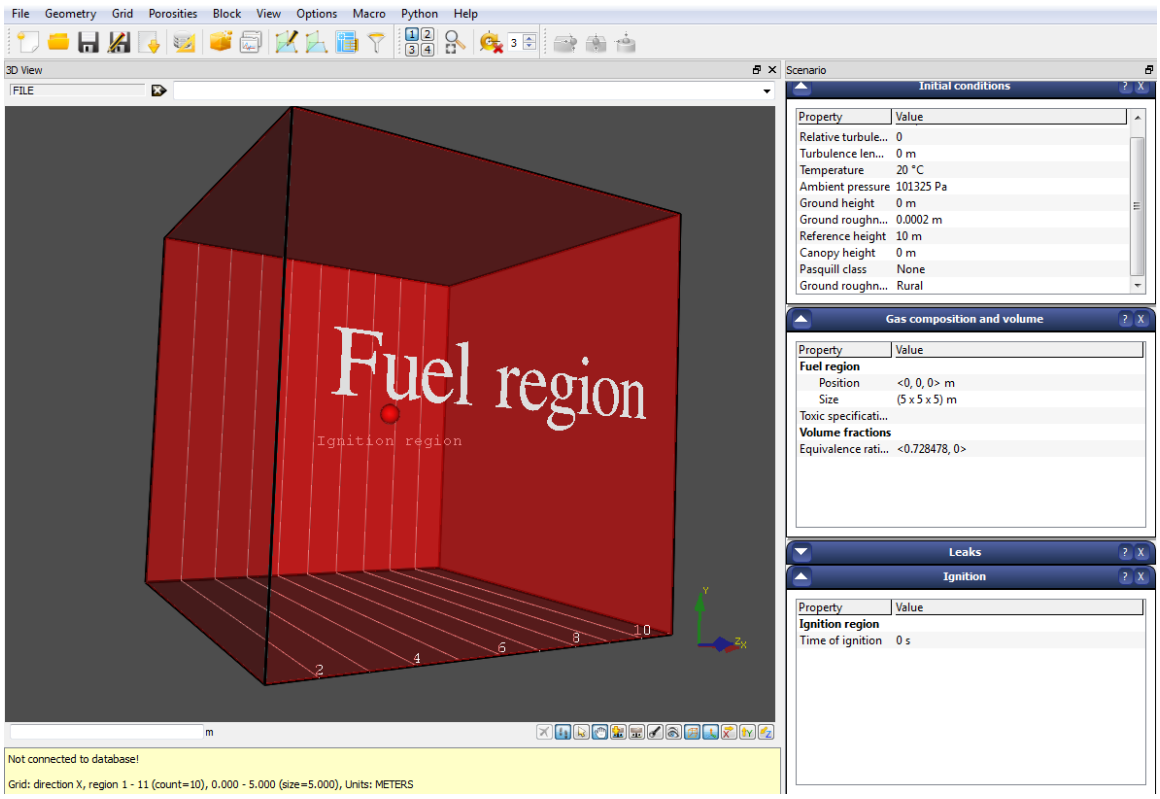

Figure 3.7: Simulation of a nonconfined gas cloud combustion in FLACS in order to obtain laminar burning velocities

Simulations in FLACS always output the laminar burning velocity, which in FLACS "depends on the fuel concentration relative to the concentration of oxygen as well as on the type of fuel" [29]. Because of this, no special care was taken into choosing appropriate CFD parameters like mesh size, initial conditions, boundary conditions etc. A nonconfined gas cloud of $5 \times 5 \times 5$ meters was constructed in FLACS, with ignition point positioned in the middle of the cloud, as shown in Figure 3.7. In hydrogen combustion, FLACS always outputs the laminar burning velocity with and without the *Le* correction factor. Because the outputs without this correction factor fit the shape of experimental curves the best, they were used for comparison later in the research. FLACS calculated laminar burning velocity data was recorded for all mixtures.

3.3 Calculation of laminar burning velocity

With burning velocities and concentrations from experiments and FLACS as well as product temperatures from the chemical calculator gathered, the S_L model was set up for calculation in Microsoft Excel. The mass fractions of species, stoichiometric mass fractions of species, specific heat capacities, thermal conductivities and densities, were calculated as described in Section 3.1.4. The reaction rate parameters A_{prex}, T_a and an adequate amount of species mass fraction terms, e.g W_F, were needed to close the S_L model.

3.3.1 The unknown reaction rate parameters' influence on the laminar burning velocity model

Through trial, the influence of the unknown reaction rate parameters on the S_L model was investigated in Microsoft Excel:

- A_{prex}:

  The pre-exponential factor worked as a multiplier and would only increase the magnitude of the laminar burning velocity curve, illustrated in Figure 3.8:

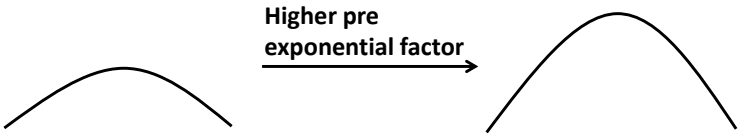

Figure 3.8: The effect of varying A_{prex} on the laminar burning velocity curves.

- T_a:

  Because the activation temperature is in the exponential term, $e^{(-\frac{T_A}{T_P})}$, in Equation (3.11), a high activation temperature would make the burning velocity curve less sensitive to changes in product temperature (T_P) by attaining a flatter shape, illustrated in Figure 3.9:

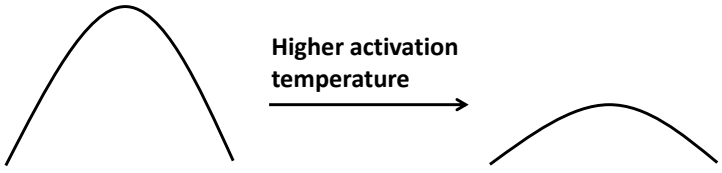

Figure 3.9: The effect of varying T_a on the laminar burning velocity curves.

- Species mass fractions terms:

  Species mass fraction terms, e.g $(\frac{Y_{\mathrm{H_2}}}{Y_{\mathrm{H_{2,stoich}}}})^a$, would change both the magnitude and the shape of the curve. In the reaction order range -3 to 3, including either W_F or W_O shifted the curve to the right or left. A more pronounced change in shape was observed when including at least two species mass fraction terms. Only adding one species mass fraction term was found inadequate with regard to the desired shape. Therefore, atleast W_F and W_O were included in the S_L model for all mixtures. The effect is shown in Figure 3.10:

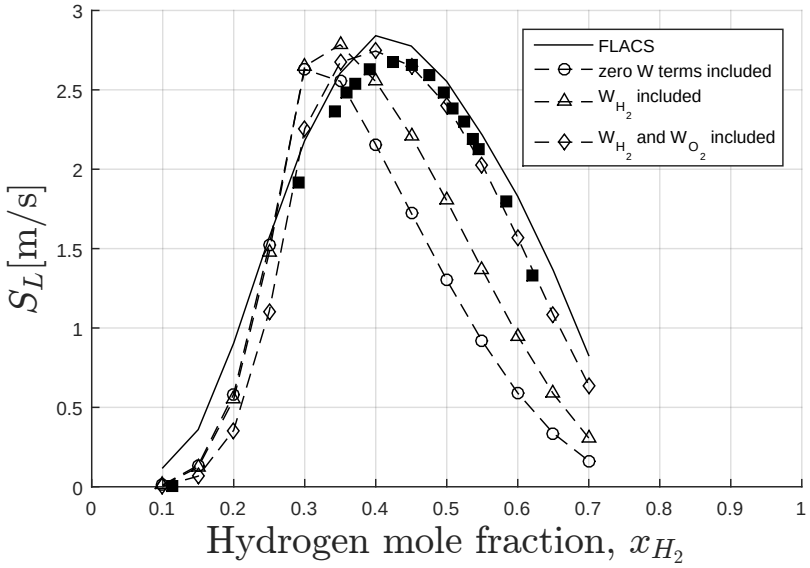

Figure 3.10: The effect of including 0-2 species mass fraction terms on the laminar burning velocity models curve shape

3.3.2 Initial approximation of the pre-exponential factor A_{prex}

In order to obtain a reasonable first guess for A_{prex}, mass fractions at the stoichiometric concentration in normal air were calculated for the $H_2 - \text{air}$ and $CH_4 - \text{air}$ mixtures. The S_L models (Equation (3.11)) expression for reaction rate gets greatly simplified at the stoichiometric concentration:

$$\omega_{stoich} = -A_{prex}\, e^{(-\frac{T_a}{T_P})} \cdot W_{F,stoich} \cdot W_{O,stoich} \ ,$$

or alternatively:

$$\omega_{stoich} = -A_{prex}\, e^{(-\frac{T_a}{T_P})} (\frac{Y_{F,stoich}}{Y_{F,stoich}})^a (\frac{Y_{O,stoich}}{Y_{O,stoich}})^b \ ,$$

which results in:

$$\omega_{stoich} = -A_{prex}\, e^{(-\frac{T_a}{T_P})} \cdot (1)^a \cdot (1)^b \ .$$

Utilization of the assumption that $S_L^2 \propto -\alpha \cdot \omega$, made it possible to calculate an estimate of what range the initial A_{prex} should lie within by inserting experimental values for S_L, α and product temperatures calculated from the chemical equilibrium calculator into Equation (3.13):

$$A_{prex} \propto \frac{S_L^2}{\alpha \cdot e^{(-\frac{T_a}{T_P})}} \tag{3.13}$$

The initial A_{prex} was calculated to be $6 \cdot 10^8\ \text{s}^{-1}$ for the $H_2 - \text{air}$ mixtures and $4 \cdot 10^8\ \text{s}^{-1}$ for the $CH_4 - \text{air}$ mixtures.

3.3.3 Choosing T_a and calculating reaction rate parameters

To simplify the S_L model, T_a was chosen to be 20 000 for all mixtures except 12 000 for the $CO - \text{air}$ mixtures, in order to obtain a reasonable fit. In comparison, Arntzen [8] calculated suited activation temperatures for paraffins and hydrogen to be 16 000 and 12 000, respectively. Better fits could be obtained if T_a varied for all the mixtures in the research. It proved very difficult and little scientific to find A_{prex} values and reaction orders by trial and error in Microsoft Excel. Therefore, a MATLAB algorithm was coded to calibrate the S_L model towards experiments, with the aim of finding A_{prex} values and reactions orders which best fit them.

3.3.4 MATLAB code

Some mixture concentrations in the proximity of the LFL and UFL that were not measured in experiments were evaluated by the S_L model (Equation 3.11). The S_L model was not calibrated towards these points. Assuming that the laminar burning velocity decays continuously towards the LFL and UFL, including these concentrations presented a nice opportunity to investigate the S_L models flammability limit validity later on in the research. For a given mixture, the S_L model was only calibrated towards the points lying within a 50% range of the maximum experimental laminar burning velocity. The reason for this was that the majority of measurements lied within this range, and some outliers at the high and low fuel concentrations had a tendency to skew and shift the modelled S_L curves into a more non-physical shape.

Thermodynamic data was transferred from Microsoft Excel to MATLAB, where a least square fit algorithm was used to calibrate pre-exponential factors and reaction orders. This deviation minimizing method was used to calculate the reaction rate parameters resulting in the least residual sum of squares (RSS) [30]:

$$RSS = \sum_{i=1}^{n} (S_L - S'_L)^2 \tag{3.14}$$

Where S_L is the experimental laminar burning velocity and S'_L is the least squared fitted laminar burning velocity.

The initial A_{prex} values calculated for different mixture types were first used for all the mixtures of that type, e.g $6 \cdot 10^8\ \mathrm{s}^{-1}$ for all $H_2 -$ air mixtures with varying air composition. Next, the code was used to calculate the reaction orders which resulted in the least RSS for that A_{prex} value. As mentioned, at least the two species mass fractions terms for fuel and oxidizer, e.g $(\frac{Y_{H_2}}{Y_{H_2,\mathrm{stoich}}})^a$ and $(\frac{Y_{O_2}}{Y_{O_2,\mathrm{stoich}}})^b$, and thereby two reactions orders, e.g a and b, were included in the S_L model. After the reaction orders were calculated, the code was used to calculate better fitted A_{prex} values for each distinct mixture. Eventually, the reaction orders were calibrated one last time using a smaller step size, to better fit the new pre-exponential factor (A_{prex}) values.

Reaction orders were calibrated over a range of -3 to 3, with step sizes of 0.1 and 0.01. A_{prex} was calibrated over a range of $\pm$ 10000% of the initial A_{prex}, with a step size of 10% of the initial A_{prex}. The algorithm outputted up to three RSS results, in order to compare S_L models with different numbers of species mass fraction terms (three in the case of H_2O or CO_2 diluted mixtures, including either W_{H_2O} or W_{CO_2} as well). A flowchart of the MATLAB code can be seen in Figure 3.11, and the least square fitting part of the code can be found in Appendix B.

The aim was to construct reaction rate parameter expressions as functions of the fraction of oxygen in air and inert gases; $\frac{O_2}{O_2+N_2+CO_2}$. After calibrated reaction rate parameters for each mixture were calculated, they were manually altered to increase their linear dependencies on $\frac{O_2}{O_2+N_2+CO_2}$. Next, the code was used to re-calibrate the manually altered reaction rate parameters, to further increase their fit and linear dependencies on $\frac{O_2}{O_2+N_2+CO_2}$. Linear expressions for the reaction rate parameters as a function of $\frac{O_2}{O_2+CO_2+N_2}$ were constructed using the polyfit and polyval function in MATLAB. Because the $\text{fuel} - \text{air}$ mixtures in the research did not include CO_2, and the $\text{fuel} - O_2 - CO_2$ mixtures included a very small amount of N_2, the reaction rate parameters were basically linearised as a function of $\frac{O_2}{O_2+N_2}$ and $\frac{O_2}{O_2+CO_2}$. Overall, this linearisation process increased the deviation from experimental results.

The aim for a convenient S_L model

Some of the linear expressions for A_{prex} and reaction orders were used to model mixtures of different types, e.g the linear expressions for H_2 and O_2 reaction orders and A_{prex} values calibrated towards the $H_2 - \text{air}$ mixtures, were also used to model the $H_2 - O_2 - CO_2$ mixtures. Experiments presented by Lewis Von Elbe show that an increased CO_2 concentration decreases the burning velocity more than when the N_2 concentration rises for $H_2 - \text{air}$ mixtures [19]. The choice to weight these different inert gases equally in the reaction rate parameter input ($\frac{O_2}{O_2+N_2+CO_2}$) could make the S_L model, Equation (3.11), deviate more from experiments if the air composition changes simultaneously as the CO_2 concentration. This was not the case for any of the mixtures in the research. This input scheme was chosen to make the S_L model convenient to use.

A better input scheme may be to linearise the reaction orders of species as functions their mole fraction, and the pre-exponential factor (A_{prex}) as function of the fuel mole fraction. The steam mixtures were first linearised as a function of $\frac{O_2}{O_2+N_2+H_2O}$, however, the steam concentrations in the research of $0 - 12\%$ impacted this fraction too little, and better shape results were obtained when the steam reaction order was linearised as a function of the mole fraction of steam (x_{H_2O}), instead of $\frac{O_2}{O_2+N_2+H_2O}$.

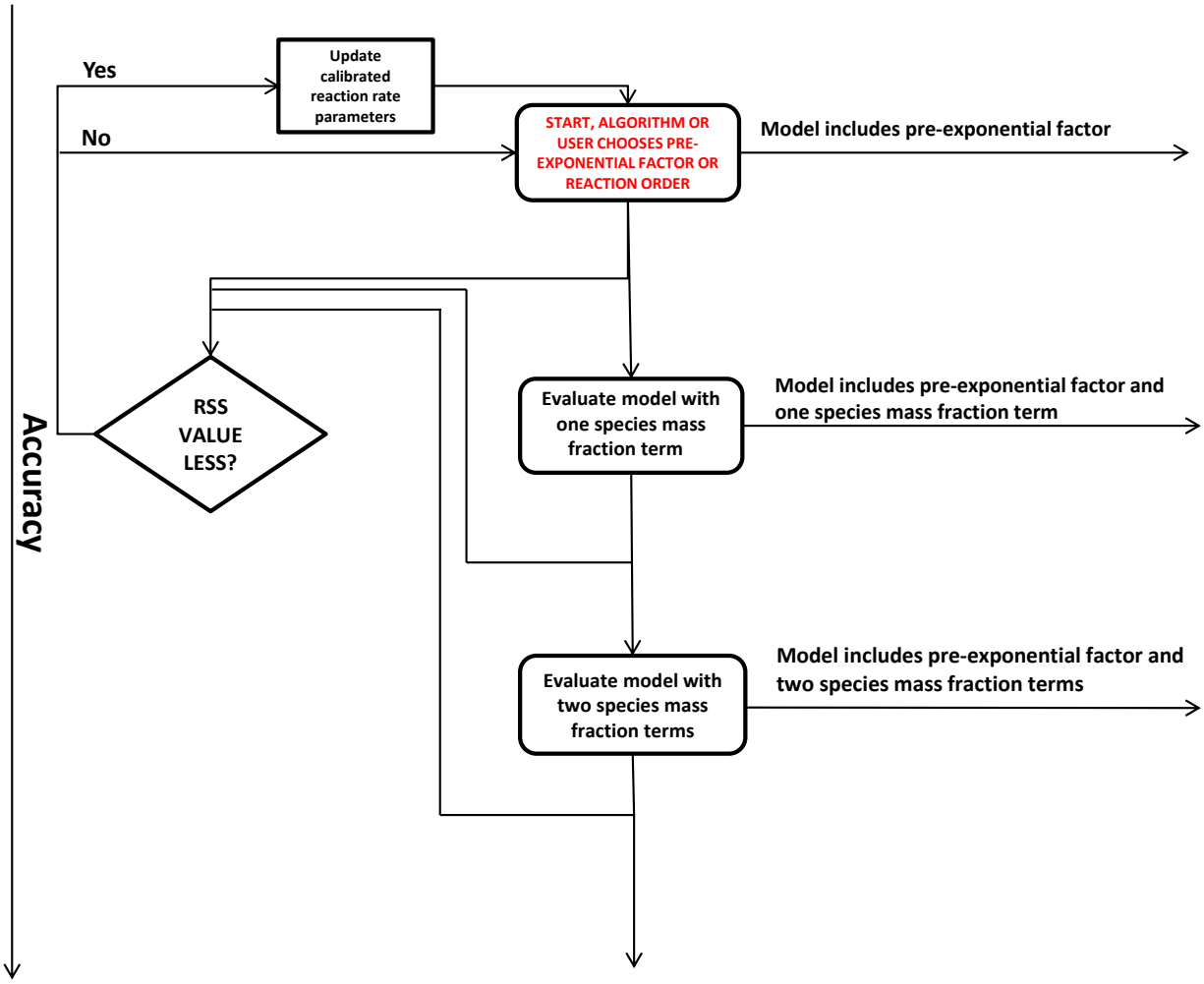

Figure 3.11: Flowchart of the algorithm used in MATLAB

4. Results and discussion

The complete model for S_L is presented in this chapter. Results are discussed with regard to different aspects of model validation. An assessment of whether FLACS or the S_L model produces the better results is presented.

4.1 Equations for reaction rate parameters A_{prex} and species mass fractions term reaction orders in the S_L model

S_L model:

$$S_L^2 = 2\alpha(v+1)A_{prex}\, e^{(-\frac{T_a}{T_P})} \cdot (\frac{Y_F}{Y_{F,stoich}})^a (\frac{Y_O}{Y_{O,stoich}})^b \cdots (\frac{Y_Z}{Y_{Z,stoich}})^z \,. \tag{4.1}$$

Table 4.1 displays the equations for reaction rate parameters as a function of $\frac{\mathrm{O_2}}{\mathrm{O_2+N_2+CO_2}}$, and steam reaction order as a function of $x_{\mathrm{H_2O}}$. T_a was chosen to be equal to 20 000 for all mixtures except 12 000 for the CO − air mixtures. The remaining equations for parameters in the S_L model can be found in Section 3.1.4.

Table 4.1: Linear expressions for reaction rate parameters A_{prex} and species mass fraction term reaction orders, for mixtures in the research

H_2 mixtures, $X = \frac{O_2}{O_2+N_2+CO_2}$	
a, in $(\frac{Y_{H_2}}{Y_{H_2,stoich}})^a$	$a = -2.76 \cdot X + 2.53$
b, in $(\frac{Y_{O_2}}{Y_{O_2,stoich}})^b$	$b = 2.80 \cdot X - 1.59$
c, in $(\frac{Y_{CO_2}}{Y_{CO_2,stoich}})^c$	$c = \begin{cases} 2 \cdot X - 0.80 \text{ if } X < 0.50 \\ -0.04, \text{ otherwise} \end{cases}$
d, in $(\frac{Y_{H_2O}}{Y_{H_2O,stoich}})^d$	$d = -1.4669 \cdot x_{H_2O} + 0.0052$
T_a	$T_a = 20\,000$
A_{prex}	$\begin{cases} A = 2.75 \cdot (3 \cdot X + 1.2) \cdot 10^8\ s^{-1} \text{ if steam present and } T = 50\,°C \\ A = 3.25 \cdot (3 \cdot X + 1.2) \cdot 10^8\ s^{-1} \text{ if steam present and } T = 150\,°C \\ A = 0.20 \cdot (3 \cdot X + 1.2) \cdot 10^8\ s^{-1} \text{ if steam present and } T = 200\,°C \\ A = (3 \cdot X + 1.2) \cdot 10^8\ s^{-1},\ 1.3 \cdot 10^9\ s^{-1} \text{ if } X \leq 0.35, \text{ otherwise} \end{cases}$
CH_4 mixtures, $X = \frac{O_2}{O_2+N_2+CO_2}$	
a, in $(\frac{Y_{CH_4}}{Y_{CH_4,stoich}})^a$	$a = 0.70 \cdot X + 1.16$
b, in $(\frac{Y_{O_2}}{Y_{O_2,stoich}})^b$	$b = -0.70 \cdot X - 0.26$
T_a	$T_a = 20\,000$
A_{prex}	$A = \begin{cases} (50 \cdot X - 8) \cdot 10^7\ s^{-1} \cdot 1.75 \text{ if } CO_2 \text{ in mixture} \\ (50 \cdot X - 8) \cdot 10^7\ s^{-1}, \text{ otherwise} \end{cases}$
CO mixtures, $X = \frac{O_2}{O_2+N_2+CO_2}$	
a, in $(\frac{Y_{CO}}{Y_{CO,stoich}})^a$	$a = \begin{cases} -1.53 \cdot X + 2.92 \text{ if } X > 0.30 \\ 2.60, \text{ otherwise} \end{cases}$
b, in $(\frac{Y_{O_2}}{Y_{O_2,stoich}})^b$	$b = \begin{cases} 1.96 \cdot X \text{ if } X > 0.17 \\ -1.40, \text{ otherwise} \end{cases}$
T_a	$T_a = 12\,000$
A_{prex}	$A = (50 \cdot X - 8) \cdot 10^7\ s^{-1}$

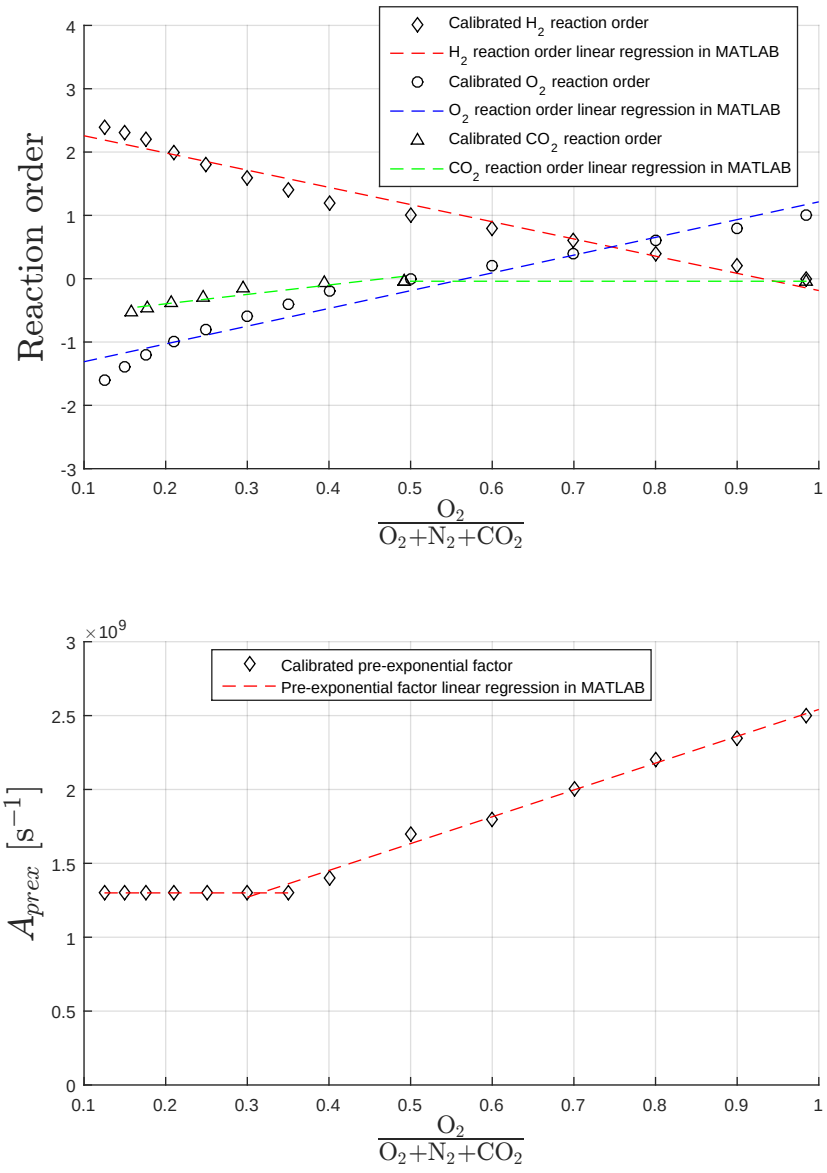

Figure 4.1: Linear regression of reaction rate parameters in MATLAB, for H_2 mixtures with different air compositions and inert gas contents.

Figures 4.1 and 4.2 display the calibrated and manually altered reaction rate parameters as well as the linear expressions made for them using the polyval and polyfit MATLAB functions, for two mixture types in the research. It can be seen that H_2 and O_2 reaction orders calibrated towards the H_2 – air mixtures deviate the most from a linear shape.

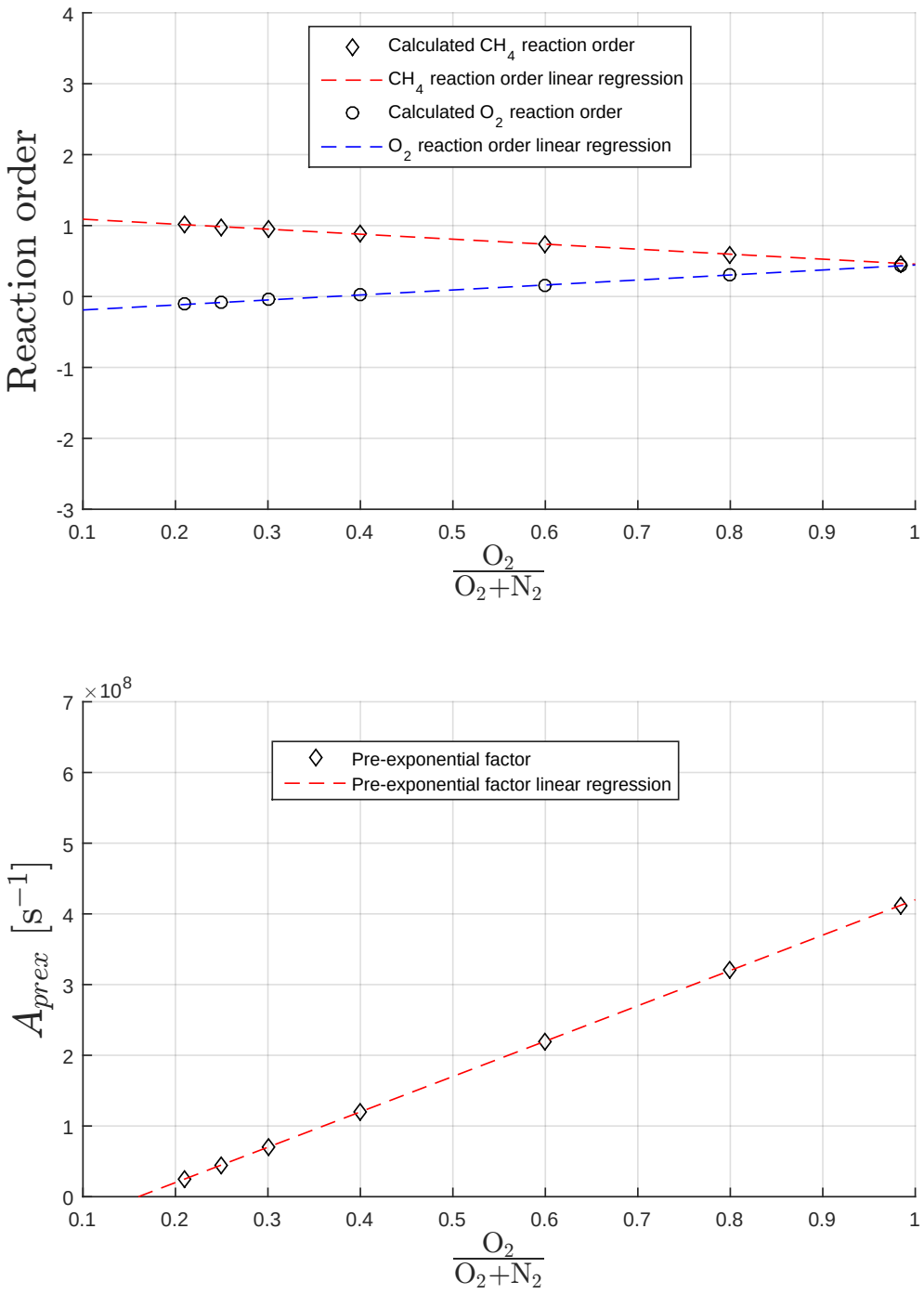

Figure 4.2: Linear regression of reaction rate parameters in MATLAB, for CH_4 mixtures with different air compositions and inert gas contents.

4.2 Laminar burning velocity model results

In this chapter S_L versus x_{fuel} graphs are presented and discussed. Mole fraction was chosen to quantify the amount of fuel in the mixtures, because this was the representation in most experiments used for calibration and comparison. The mole fraction ranges included in the respective graphs are mostly determined by the flammability limits of FLACS, for comparison.

4.2.1 H_2 – air mixtures

Nitrogen is sometimes used to inert explosive mixtures in order to narrow the flammability limit and thereby mitigate accident consequences. In Figures 4.3 and 4.4, two parameters vary with S_L; the air composition and the amount of hydrogen in the mixture. The intention was to get an impression of how the S_L model performs as a function of these two parameters.

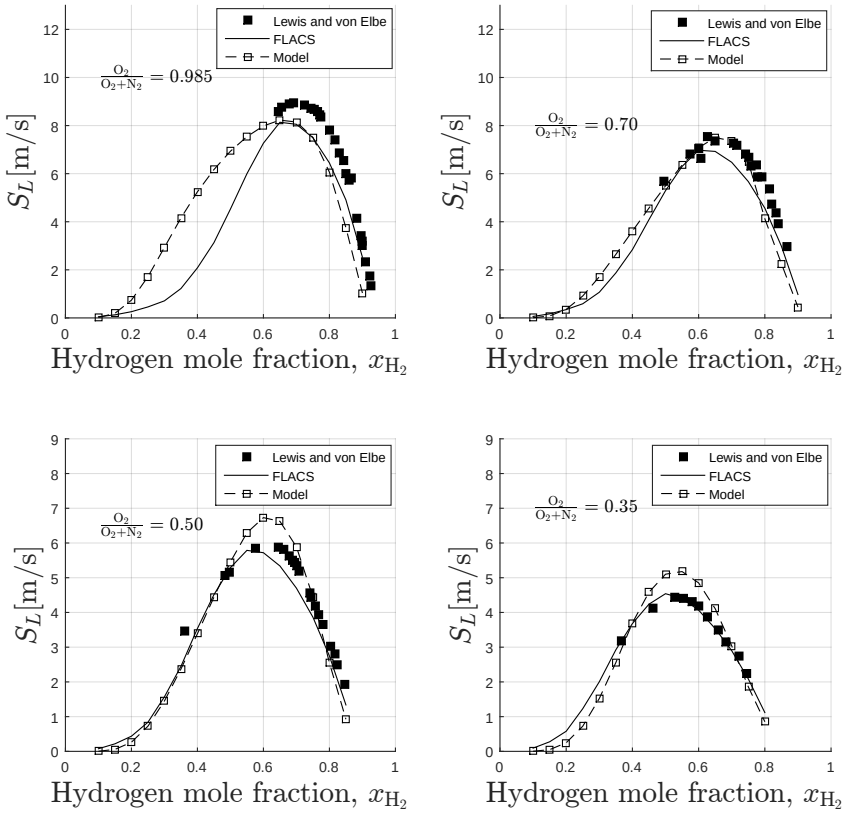

Figure 4.3: Laminar burning velocity results modelled by Equation (4.1), compared with calculated values from FLACS and experiments from Lewis and von Elbe [19]. H_2 – air mixture at atmospheric pressure and 20 °C with air compositions $\frac{O_2}{O_2+N_2} = 0.985, 0.7, 0.5$ and 0.35.

In Figure 4.3, for the oxygen rich air mixture with $\frac{O_2}{O_2+N_2} = 0.985$, the S_L model produces higher burning velocity values than FLACS in the low x_{H_2} range. In this range, no experimental data was found to use for validation. Nevertheless, the S_L model produces physically reasonable results where experimental data exists for this mixture ($x_{H_2} > 0.5$). The burning velocity maxima occurs at a hydrogen mole fraction approximately 5 % less than Lewis and Von Elbe. With nitrogen enriched air such as $\frac{O_2}{O_2+N_2} = 0.5, 0.35$ and 0.25, the S_L model and FLACS share shape characteristics with experiments, whilst the S_L model produces a higher maximum S_L value (approximately 15%) than FLACS and experiments.

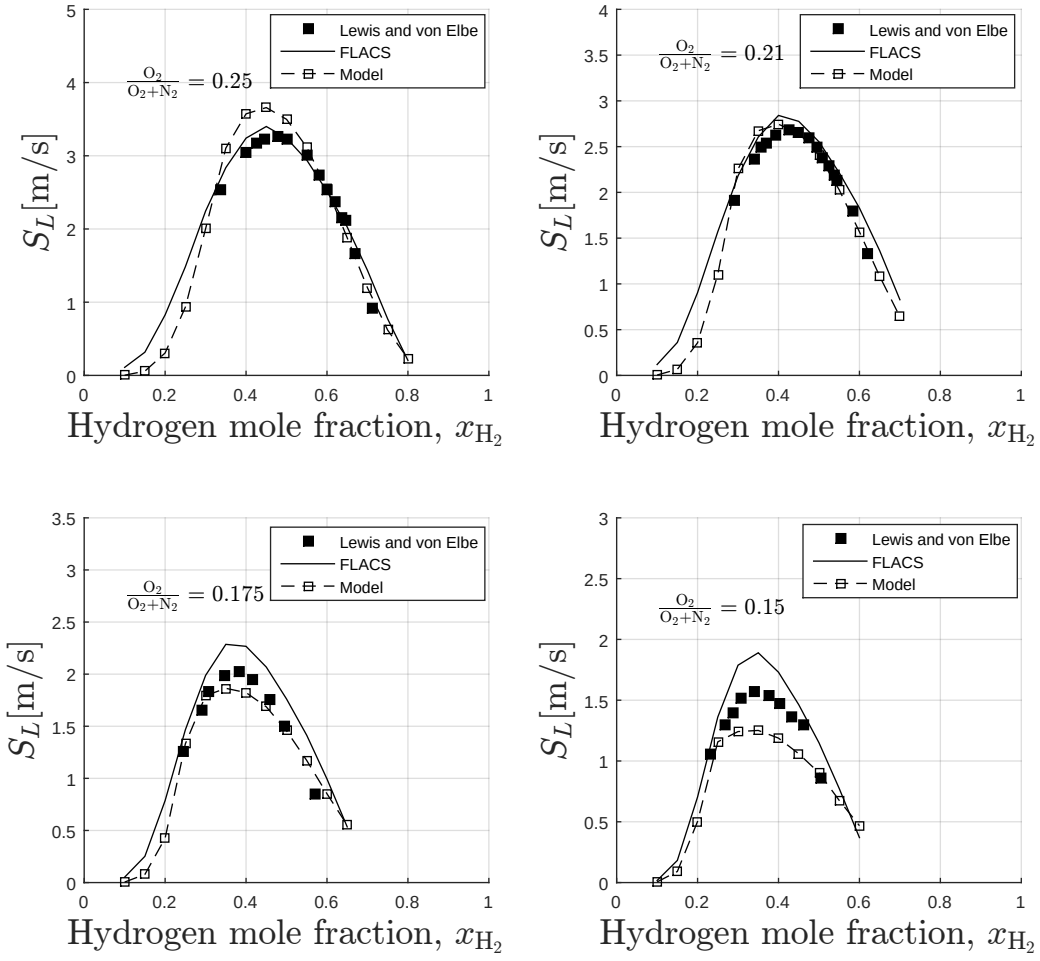

Figure 4.4: Laminar burning velocity results modelled by Equation (4.1), compared with calculated values from FLACS and experiments from Lewis and von Elbe [19]. $H_2 - \text{air}$ mixture at atmospheric pressure and 20 °C with air compositions $\frac{O_2}{O_2+N_2} = 0.25, 0.21, 0.175$ and 0.15.

This trend continues into Figure 4.4 as the nitrogen concentration in air increases, until the S_L models maximum value becomes less than FLACS with $\frac{O_2}{O_2+N_2} = 0.175$. The S_L model produces the most non-physical results when the nitrogen concentration in air is highest, with $\frac{O_2}{O_2+N_2} = 0.15$, where both the shape and magnitude of the curve deviate from experimental data. The deviation is likely caused by the manual altering of A_{prex} values for $\frac{O_2}{O_2+N_2} \leq 0.35$ to be constantly equal to $1.3 \cdot 10^9\ s^{-1}$. This choice was made to make the S_L model convenient and because the MATLAB calibrated A_{prex} values did not significantly vary in this range. For all air compositions $\frac{O_2}{O_2+N_2} < 0.35$, the S_L model produces slightly less burning velocities than FLACS for low fuel concentrations ($x_{H_2} = 0.1$ to 0.3). In many gas explosion scenarios, hydrogen burns in a normal atmosphere where $\frac{O_2}{O_2+N_2} = 0.21$. For the normal air composition mixture, the S_L model fits Lewis and von Elbes [19] experimental data better than FLACS, for concentrations it was calibrated towards. With normal air composition, calculated reaction orders with respect to H_2 and O_2, from the linear reaction order expressions in Table 4.1, were 1.95 and -1.00, respectively, and thereby:

$$S_L^2 \propto e^{(-\frac{20\,000}{T_P})} \cdot Y_{H_2}^{1.95} \cdot Y_{O_2}^{-1.00}\ , \tag{4.2}$$

for this mixture.

Overall, it is hard to ascertain whether FLACS or the S_L model produces the better results for the $H_2 -$ air mixtures.

Comparison with $H_2 - air$ mixtures' laminar burning velocities from different experiments

It is evident from the experiments presented by Liu and Macfarlane [25] and Dahoe et al. [1] that there exist an approximately 30% scatter in measured laminar burning velocities for hydrogen. Figure 4.5 shows how the S_L model compares to these experiments, as well as experiments conducted by Wulme Dery, a fellow student at UoB, who measured hydrogen laminar burning velocities using the pressure-time history and Schlieren measuring methods.

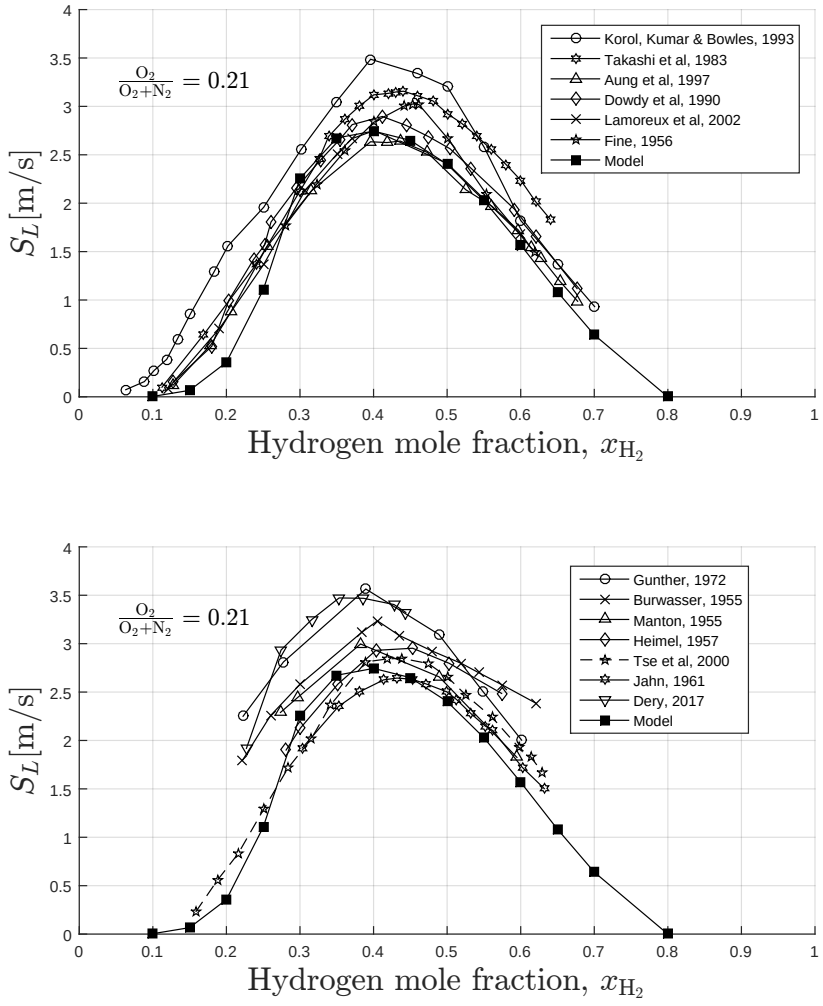

Figure 4.5: Comparison between S_L model (Equation 4.1) and experiments from Liu and Macfarlane [25], Dahoe et al. [1] and Dery, for $H_2 - air$ mixtures at atmospheric pressure and room temperature with normal air composition.

From Figure 4.5, it is evident that the S_L model produces lower S_L values than literature at low H_2 concentrations. At these low x_{H_2} values the burning velocity curve exhibits a

concave shape, unlike the convex shapes in literature. The largest cause of deviation in this range is likely the lack of experimental datapoints measured by Lewis and von Elbe [19] for $x_{H_2} < 0.3$, and thereby absence of calibration towards these concentrations. To achieve better fit at these concentrations, another possibility besides calibration is to upscale the S_L model by a suited factor. This is visualized in Figure 4.6 where the S_L model values have been upscaled by a factor of 1.35:

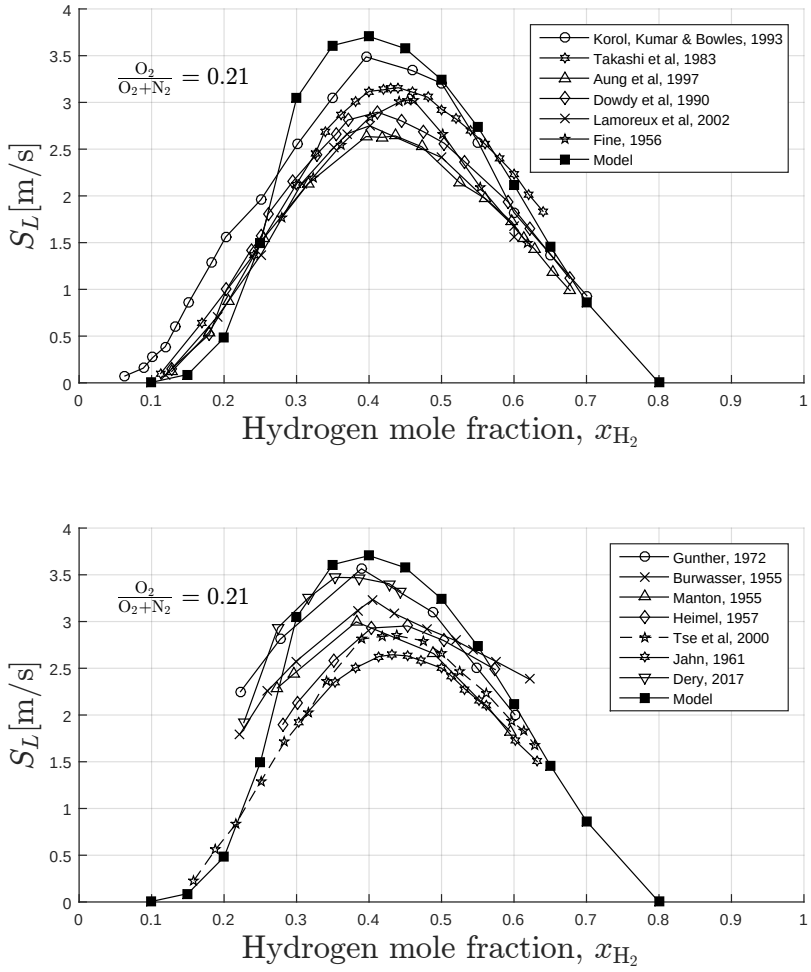

Figure 4.6: Comparison between upscaled S_L model (Equation 4.1) and experiments from Liu and Macfarlane [25], Dahoe et al. [1] and Dery, for $H_2 - $ air mixtures at atmospheric pressure and room temperature with normal air composition.

Evaluating the flammability limits produced by the S_L model for $H_2 - \text{air}$ mixtures

The prediction of flammability limits of gas mixtures is important for correct assessment of risk, and consequence mitigation. Assuming that S_L decays continuously towards the LFL and UFL, the S_L model can be used for approximation of flammability limits where $S_L \approx 0$. Table 4.2 displays some literature data for the flammability limits of $H_2 - \text{air}$ mixtures with normal air, collected from an article by Ren and Zhang [31]:

Table 4.2: Experimental UFL and LFL values for $H_2 - \text{air}$ mixtures at 25 °C and atmospheric pressure, with normal air composition.

UFL	LFL
75% (Coward and Jones, 1952)	4% (Kuznetsov et al., 2012)
74.7% (Wierzba and Wang, 2006)	4.2% (Ishizuka, 1991)
75.1% (Schröder and Molnarne, 2005)	$5\% \pm 0.5\%$ (Cashdollar et al., 2000)

Figure 4.6 shows that the S_L model approximates both an UFL and LFL approximately 5% greater than the tabulated values. From a safety aspect, overestimation is 'better' than underestimation because it leads to more conservative measures. Therefore, the UFL result is better than the LFL result. The S_L model will not propagate a flame in the mole fraction range $x_{H_2} \approx (0.04 - 0.10)$, where experiments in Table 4.2 have resulted in flame propagation.

Evaluating the effect of changing reaction temperature model

A simple comparison between different reaction temperature (T) models was conducted. The compared reaction temperature models were:

- The reaction temperature model implemented in S_L model, reaction temperature model 1: $T = T_P$
- Reaction temperature model 2: $T = \frac{3T_P + T_R}{4}$
- Reaction temperature model 3: $T = \frac{1}{2}(T_P + T_R)$

From Figure 4.7 it is evident that the chosen model for reaction temperature, reaction temperature model 1, shows the best agreement with experiments. In order to further assess if the other reaction temperature models could be better choices for the S_L model (Equation 4.1), they would have to be implemented into the S_L model, which would need to be re-calibrated towards experiments.

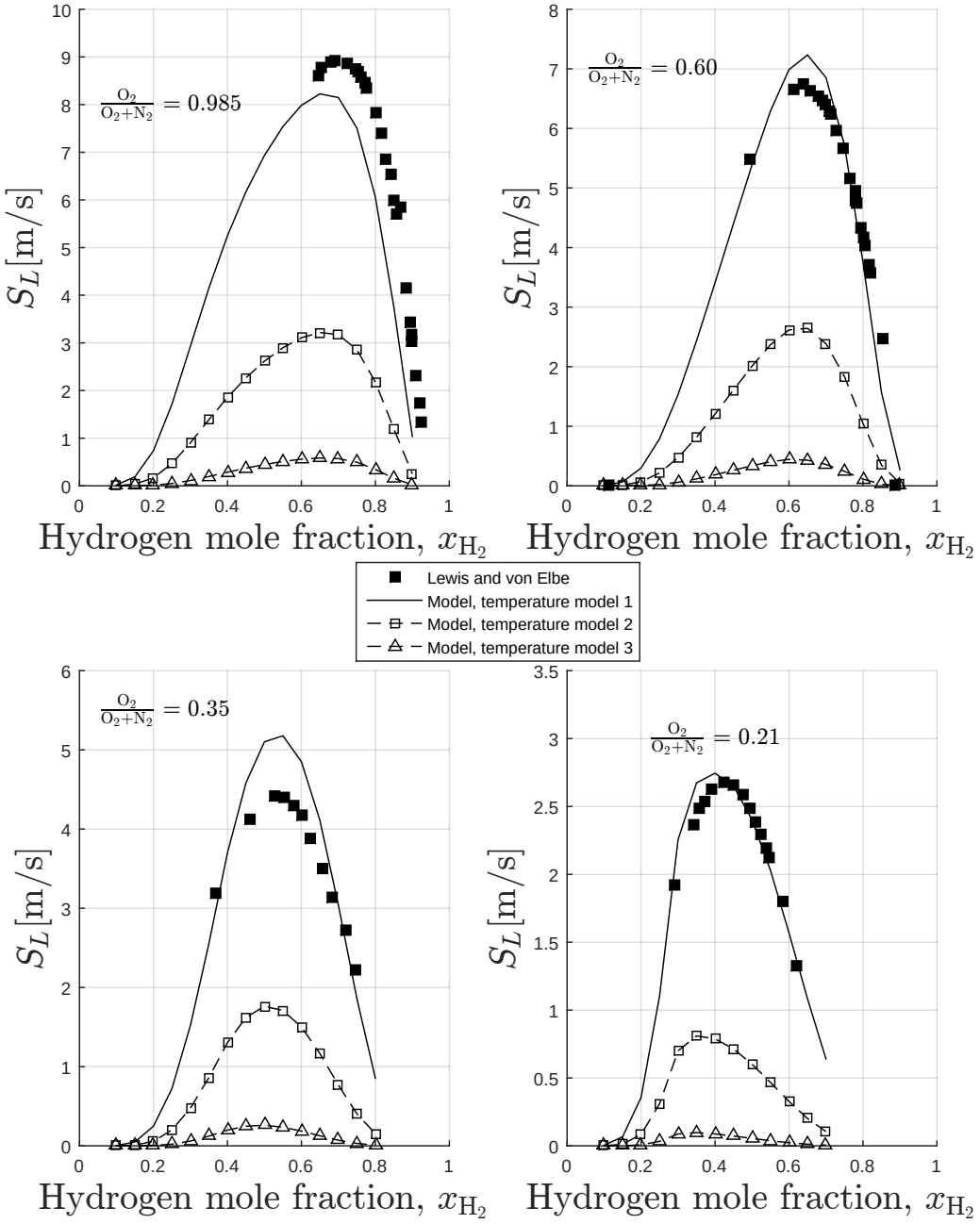

Figure 4.7: Effect of varying reaction temperature models in the laminar burning velocity model (Equation (4.1)), for a $H_2 - air$ mixture at atmospheric pressure and 20 °C, with air compositions $\frac{O_2}{O_2+N_2} = 0.985, 0.60, 0.35$ and 0.21.

4.2.2 $H_2 - O_2 - CO_2$ mixtures

Carbon dioxide inerted hydrogen mixtures may form during an accident scenario. In Figures 4.8 and 4.9, two parameters vary with S_L; the amount of oxygen in air with varying carbon dioxide dilution, and the amount of hydrogen in the mixture. The intention was to get an impression of how the S_L model performs as a function of these two parameters.

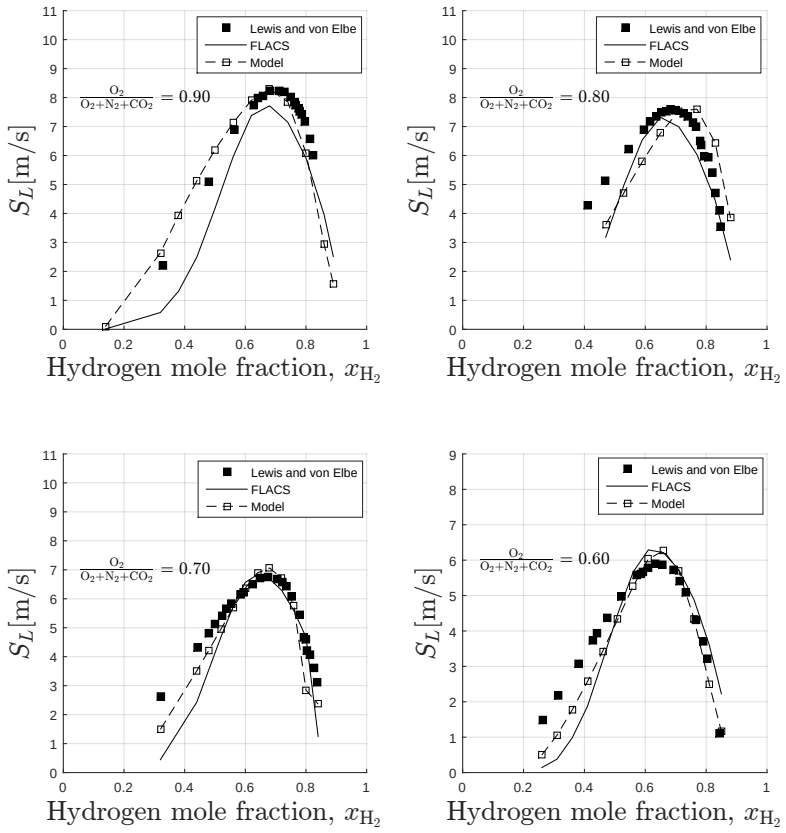

Figure 4.8: Laminar burning velocity results modelled by Equation (4.1), compared with calculated values from FLACS and experiments from Lewis and von Elbe [19]. $H_2 - O_2 - CO_2$ mixture at atmospheric pressure and 20 °C, with CO_2 dilutions $\frac{O_2}{O_2+N_2+CO_2} = 0.90, 0.80, 0.70$ and 0.60. O_2 contains 1.5% N_2.

To make the S_L model convenient to use, the A_{prex} expression as well as H_2 and O_2 reaction orders calibrated towards the H_2 – air mixtures were retained, and only a $H_2 - O_2 - CO_2$ mixture calibrated $(\frac{Y_{CO_2}}{Y_{CO_2,stoich}})^c$ term was added to the S_L model. The S_L model shows better agreement with experiments than FLACS for the weakly CO_2 diluted mixtures in Figure 4.8, except for the outlier mixture with $\frac{O_2}{O_2+N_2+CO_2} = 0.8$, which is skewed a little to the right compared to experiments and FLACS. Unlike for the H_2 – air mixtures (Figures 4.3 and 4.4), the S_L model does not underpredict S_L at low x_{H_2}, showing better agreement with experiments than FLACS there as well.

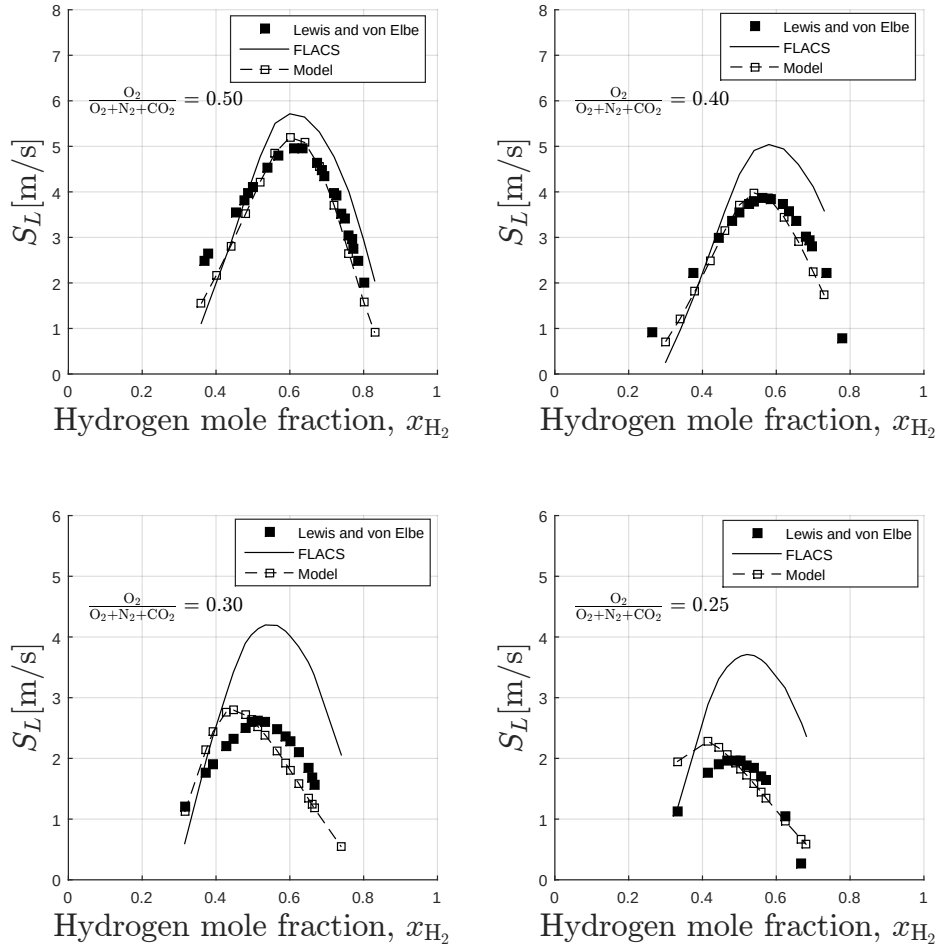

Figure 4.9: Laminar burning velocity results modelled by Equation (4.1), compared with calculated values from FLACS and experiments from Lewis and von Elbe [19]. $H_2 - O_2 - CO_2$ mixture at atmospheric pressure and 20 °C, with CO_2 dilutions $\frac{O_2}{O_2+N_2+CO_2} = 0.50, 0.40, 0.30$ and 0.25. O_2 contains 1.5% N_2.

It can be seen from Figure 4.9 that further increasing the CO_2 dilution makes both the FLACS and S_L model curve deviate more from the experimental results. With $\frac{O_2}{O_2+N_2+CO_2} \leq 0.30$, the shape of the S_L model curve and the shape and magnitude of the FLACS curve starts to deviate more noticeably. Even though the S_L model fails to replicate the experimental results with $\frac{O_2}{O_2+N_2+CO_2} = 0.25$, it produces shapes and magnitudes more alike experiments than FLACS overall for the $H_2 - O_2 - CO_2$ mixtures. The significant deviations with $\frac{O_2}{O_2+N_2+CO_2} = 0.30$ and 0.25 are likely caused by the linearisation process and the use of reaction rate parameters calibrated for the H_2 – air mixtures.

4.2.3 H_2 − air − steam mixtures

In nuclear power plants, water is boiled into steam which is used to produce electricity. When facing the high temperatures of a meltdown event (around 1500 K), water molecules may react with zirconium (used to store nuclear fuel) and break apart the hydrogen from the water molecule [32]. Explosive mixtures of hydrogen, air and steam may then form, like it did in Fukushima in 2011. A realistic model of the laminar burning velocity for mixtures of hydrogen, air and steam at elevated temperatures is required for FLACS to accurately assess such gas explosions.

The A_{prex} expression as well as H_2 and O_2 reaction orders calibrated for the H_2 − air mixtures were retained and only W_{steam} was added to the S_L model. The magnitudes of the experimental curves were approximately two times bigger than curves calculated by FLACS and the S_L model. A reason for this may be the use of the A_{prex} expression calibrated towards the H_2 − air mixtures. Because of this marked deviation, only the shape of FLACS and S_L model curves was compared, and RSS values in Table 4.3 were excluded for steam mixtures. Both FLACS and the S_L model were scaled in order to compare their shapes with experiments. The scaling factors used on the S_L model can be found in Table 4.1.

In Figures 4.10, 4.11 and 4.12, two parameters vary with S_L; the steam and hydrogen concentration in the mixture. The intention was to get an impression of how the S_L model performs as a function of these two parameters.

Mixture at 50 °C:

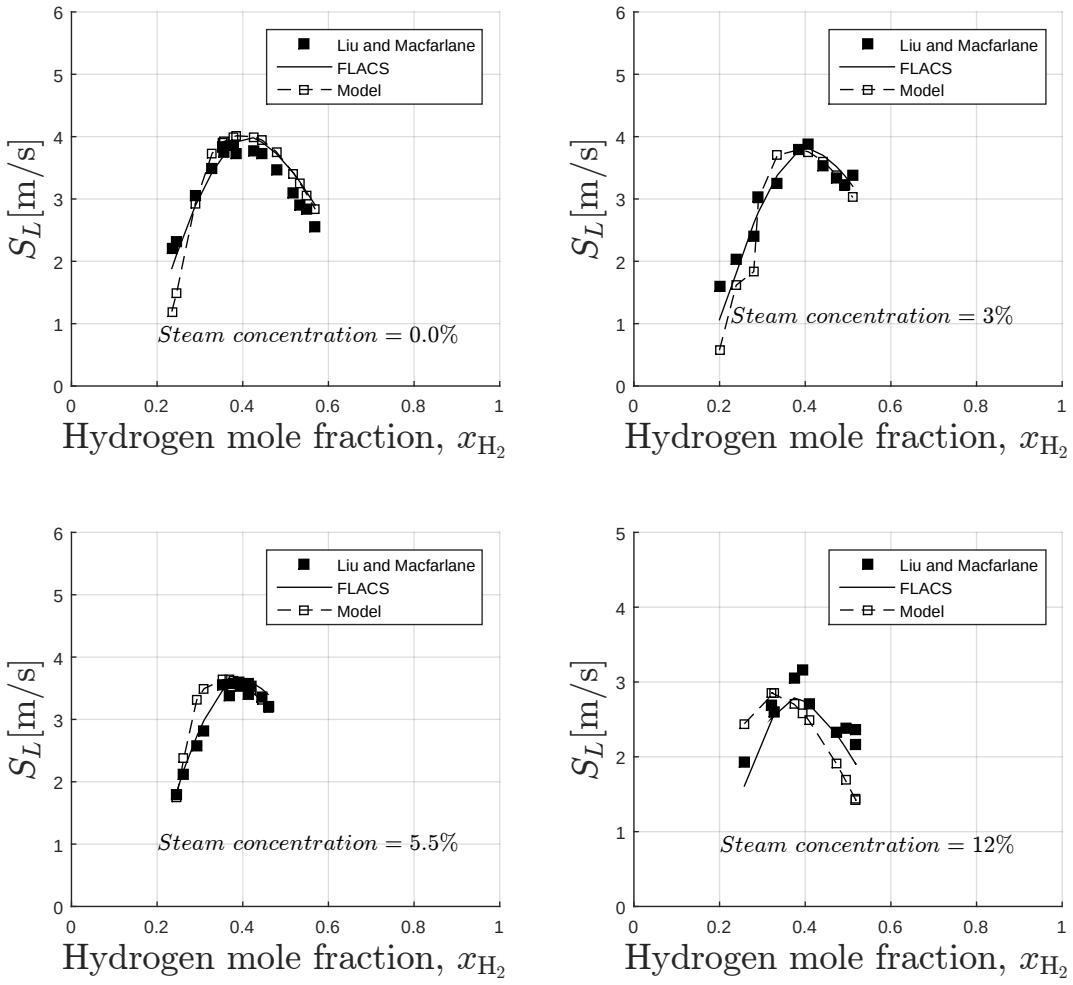

Figure 4.10: Laminar burning velocity results modelled by Equation (4.1), compared with calculated values from FLACS and experiments from Liu and MacFarlane [25]. $H_2 - \text{air} - \text{steam}$, normal air mixture at atmospheric pressure and 50 °C, with steam concentrations $= (0, 3, 5.5, 12)\%$.

In Figure 4.10, both FLACS and the S_L model show shape-wise agreement with experiments for all steam concentrations except the 12% steam mixture. Deviations at this steam concentration is likely caused by the linearisation process and use of reaction rate parameters calibrated towards the $H_2 - \text{air}$ mixtures. FLACS generally shows a slightly better agreement for low x_{H_2}, while the S_L model produces shapes more alike experiments around the maximum S_L.

Mixture at 150 °C

In Figure 4.11, the S_L model shows shape-wise agreement for all mixtures, except the one with 12% steam. Generally, FLACS shows better shape agreement than the S_L model for this mixture, but produces an overestimated outlier for both the 3% and 12% steam mixture curves around $x_{\mathrm{H_2}} = 0.22$.

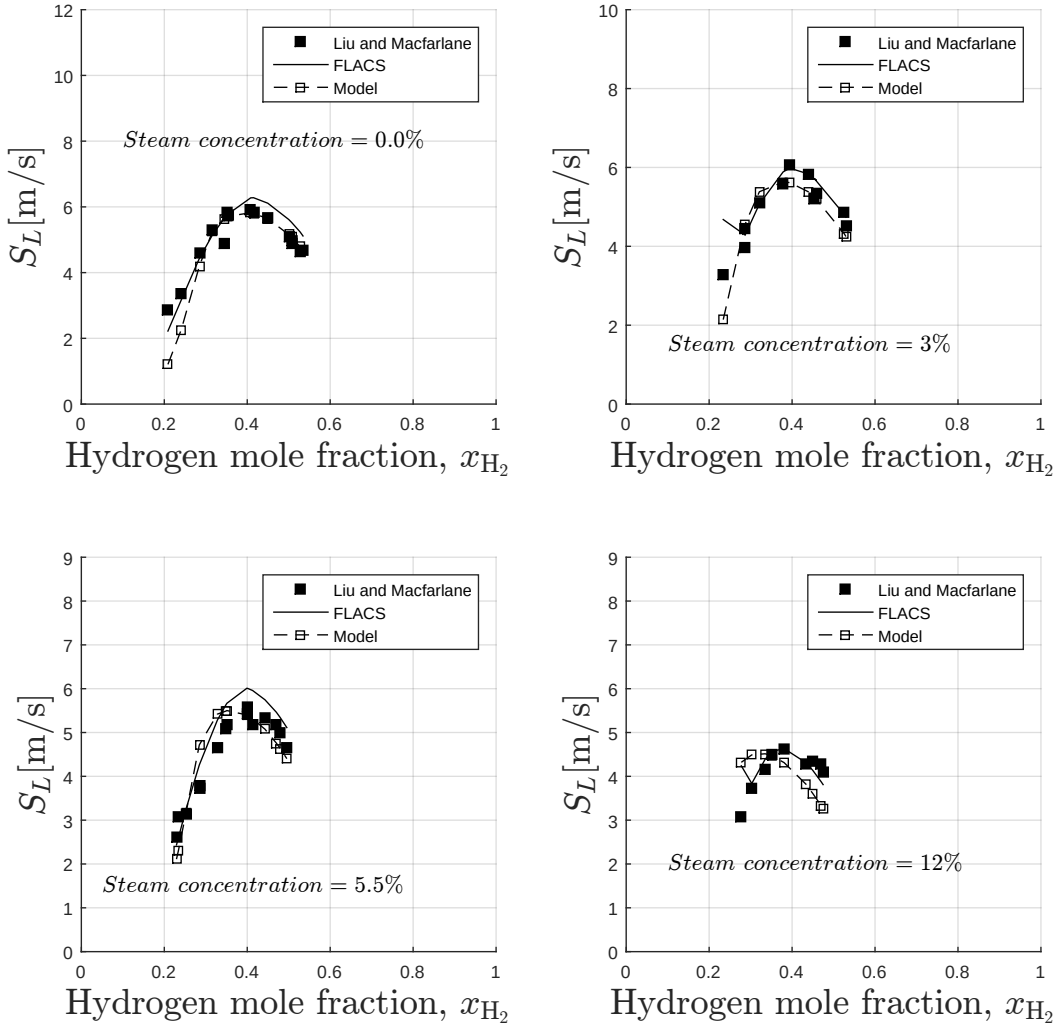

Figure 4.11: Laminar burning velocity results modelled by Equation (4.1), compared with calculated values from FLACS and experiments from Liu and MacFarlane [25]. $H_2 - \mathrm{air} - \mathrm{steam}$, normal air mixture at atmospheric pressure and 150 °C, with steam concentrations $= (0, 3, 5.5, 12)\%$.

Mixture at 200 °C

In Figure 4.12, it can be seen that both the S_L model and FLACS share shape characteristics with the experimental curve for all the different steam concentrations, except for the 12% steam curve, where the S_L model deviates noticeably from experimental data. As previously mentioned, this deviation is likely caused by the linearisation process and use of reaction rate parameters calibrated towards the $H_2 - air$ mixtures.

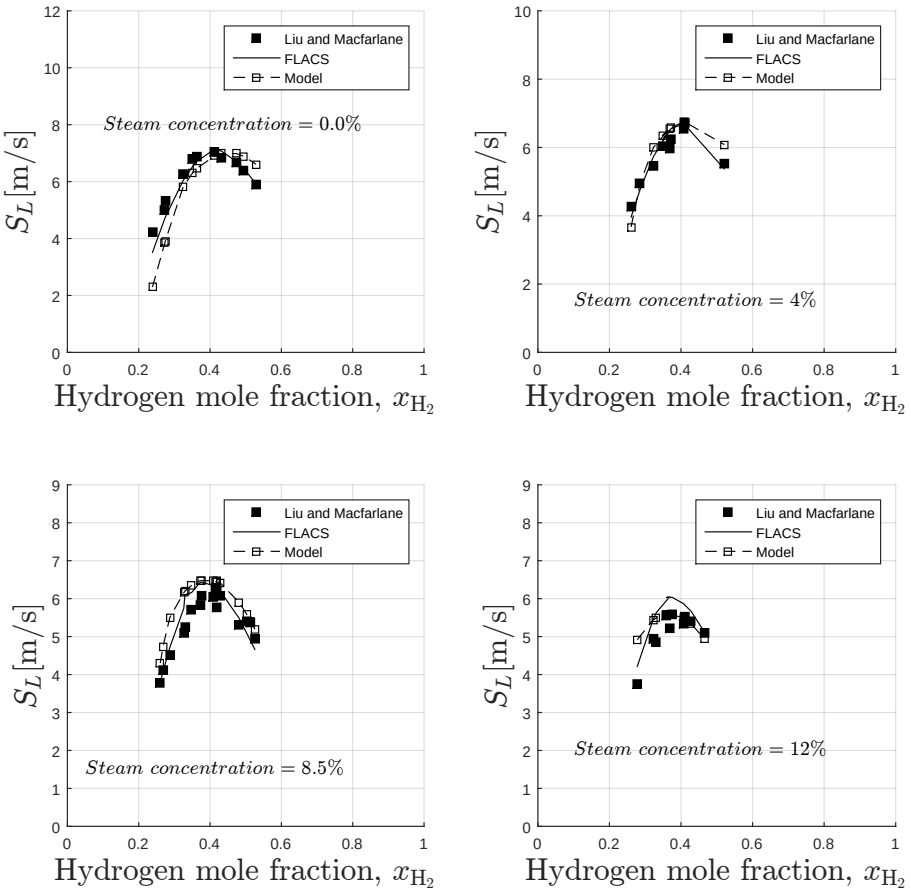

Figure 4.12: Laminar burning velocity results modelled by Equation (4.1), compared with calculated values from FLACS and experiments from Liu and MacFarlane [25]. $H_2 - air - steam$, normal air mixture at atmospheric pressure and 200 °C with steam concentrations = $(0, 4, 8.5, 12)\%$.

Summarizing, the S_L model shows fine shape agreement with experiments for all temperature elevated $H_2 - air - steam$ mixtures except the 12% steam mixtures. Deviations at this steam concentration are likely caused by the linearisation process and use of reaction rate parameters calibrated towards the $H_2 - air$ mixtures. Modelled laminar burning velocities could be significantly improved by the inclusion of $H_2 - air - steam$ calibrated reaction rate parameters such as A_{prex}, in the S_L model.

4.2.4 CH_4 – air mixtures

Methane may form explosive mixtures with air, responsible for many fatal mining accidents. An accurate model for the laminar burning velocity of methane is required for correct assessment of such gas explosions in FLACS. In Figure 4.13, two parameters vary with S_L; the air composition and the amount of methane in the mixture. The intention was to get an impression of how the S_L model performs as a function of these two parameters.

In Figure 4.13 it can be seen that the S_L model and FLACS show similarities to experimental curves. Both overestimate S_L compared to experiments, and FLACS overestimates the most. In the mixtures with $\frac{O_2}{O_2+N_2} = 0.60$ and 0.21, the S_L model curves show better agreement in the low x_{CH_4} range, but do however produce an outlier at $x_{CH_4} = 0.2$ for the mixture with $\frac{O_2}{O_2+N_2} = 0.30$. The outlier may be caused by the absence of calibration towards this concentration, or inaccuracies in the chemical equilibrium calculator, as the equilibrium temperature drop stagnates when x_{CH_4} increases from 0.18 to 0.20, only dropping from 2140 K to 2092 K [28]. The S_L models maxima for the mixture with normal air composition, $\frac{O_2}{O_2+N_2} = 0.21$, lies within the range of recent reported experimental values by Mitu et al. [33]. For this mixture, calculated reaction orders with respect to CH_4 and O_2, from the linear reaction order expressions in Table 4.1, were 1.30 and -0.40, respectively, and thereby:

$$S_L^2 \propto e^{(-\frac{20\,000}{T_P})} \cdot {Y_{CH_4}}^{1.30} \cdot {Y_{O_2}}^{-0.40} , \tag{4.3}$$

for this mixture.

Overall, the S_L model shows better agreement than FLACS with experiments, except for the outlier-mixture with $\frac{O_2}{O_2+N_2} = 0.30$. Deviations may be caused by the linearisation process of reaction rate parameters.

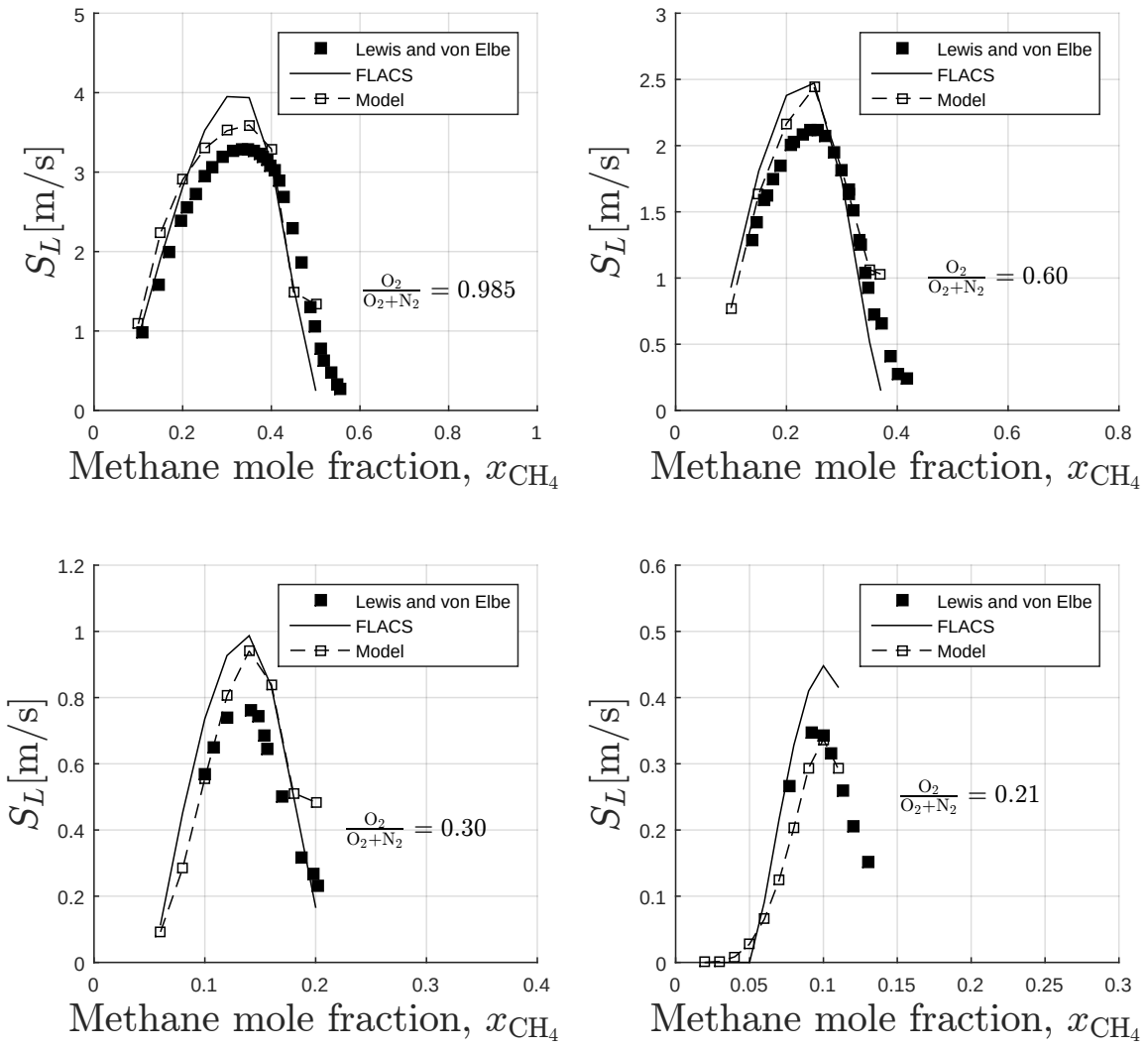

Figure 4.13: Laminar burning velocity results modelled by Equation (4.1), compared with calculated values from FLACS and experiments from Lewis and von Elbe [19]. $CH_4 - \text{air}$ mixture at atmospheric pressure and 20 °C with air compositions $\frac{O_2}{O_2+N_2} = 0.985, 0.60, 0.30, 0.21$.

4.2.5 $CH_4 - O_2 - CO_2$ mixtures

Carbon dioxide diluted methane mixtures may form during a mining accident scenario. An accurate model for the laminar burning velocity of carbon dioxide diluted methane mixtures is required for correct assessment of such gas explosions in FLACS. In Figures 4.14 and 4.15, two parameters vary with S_L; the amount of oxygen in air with varying carbon dioxide dilution and the amount of methane in the mixture. The intention was to get an impression of how the S_L model performs as a function of these two parameters.

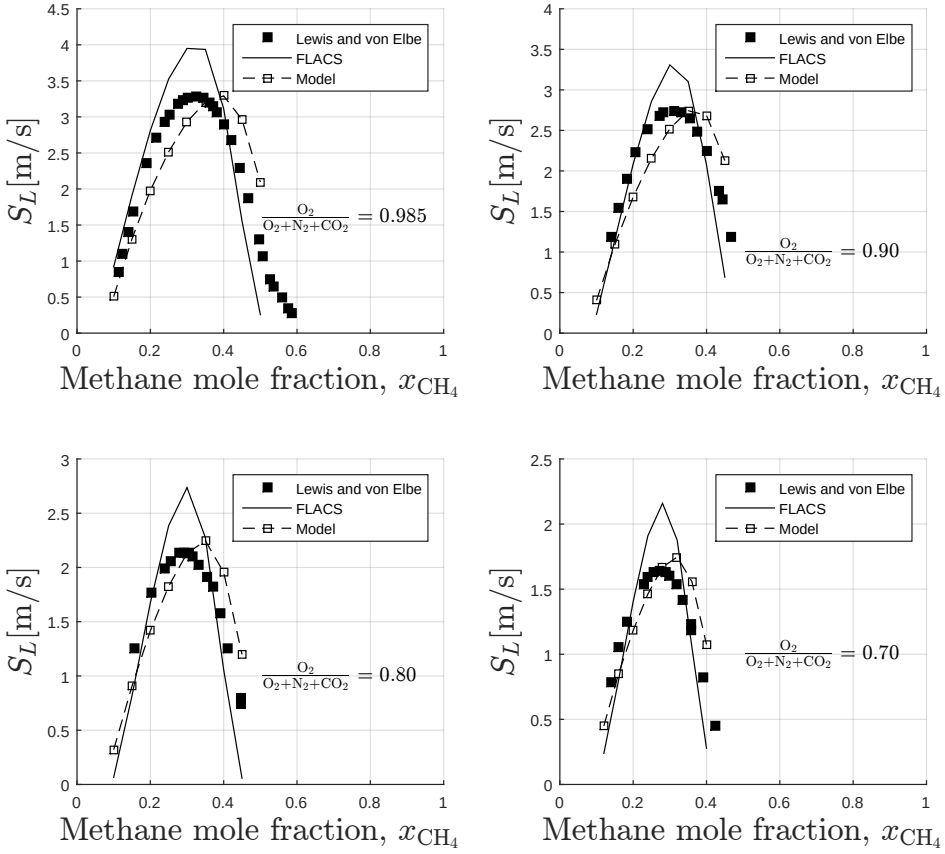

Figure 4.14: Laminar burning velocity results modelled by Equation (4.1), compared with calculated values from FLACS and experiments from Lewis and von Elbe [19]. $CH_4 - O_2 - CO_2$ mixture at atmospheric pressure and 20 °C with CO_2 dilutions $\frac{O_2}{O_2+N_2+CO_2} = 0.985, 0.90, 0.80, 0.70$. O_2 contains 1.5% N_2.

The pre-exponential factor (A_{prex}), upscaled by a factor of 1.75, and reaction orders calibrated towards the CH_4 – air mixtures were retained. Inclusion of W_{CO_2} calibrated towards the $CH_4 - O_2 - CO_2$ mixtures in the S_L model did not improve results, and was therefore excluded. Hence, the only differences in the S_L model for the CH_4 – air and

$CH_4 - O_2 - CO_2$ mixtures are the scaled A_{prex} expression and physical parameters, such as product temperature and thermal diffusivity. In the weakly CO_2 diluted mixtures from Figure 4.14, the S_L model produces curves with the same magnitude as experiments, while FLACS overestimates S_L. Shape-wise, the S_L model is shifted a bit to the right compared to experiments. Downscaling the relatively high-magnitude FLACS curves shows that their shapes are significantly thinner than experimental ones. With increased CO_2 dilution, presented in Figure 4.15, FLACS still overestimates the laminar burning velocity, while the S_L model shows better shape agreement with experiments as the CO_2 dilution increases. The S_L models shape deviations are likely caused by the linearisation process and use of $CH_4 - \text{air}$ calibrated reaction rate parameters. Overall the S_L model shows best agreement with experiments for the $CH_4 - O_2 - CO_2$ mixtures.

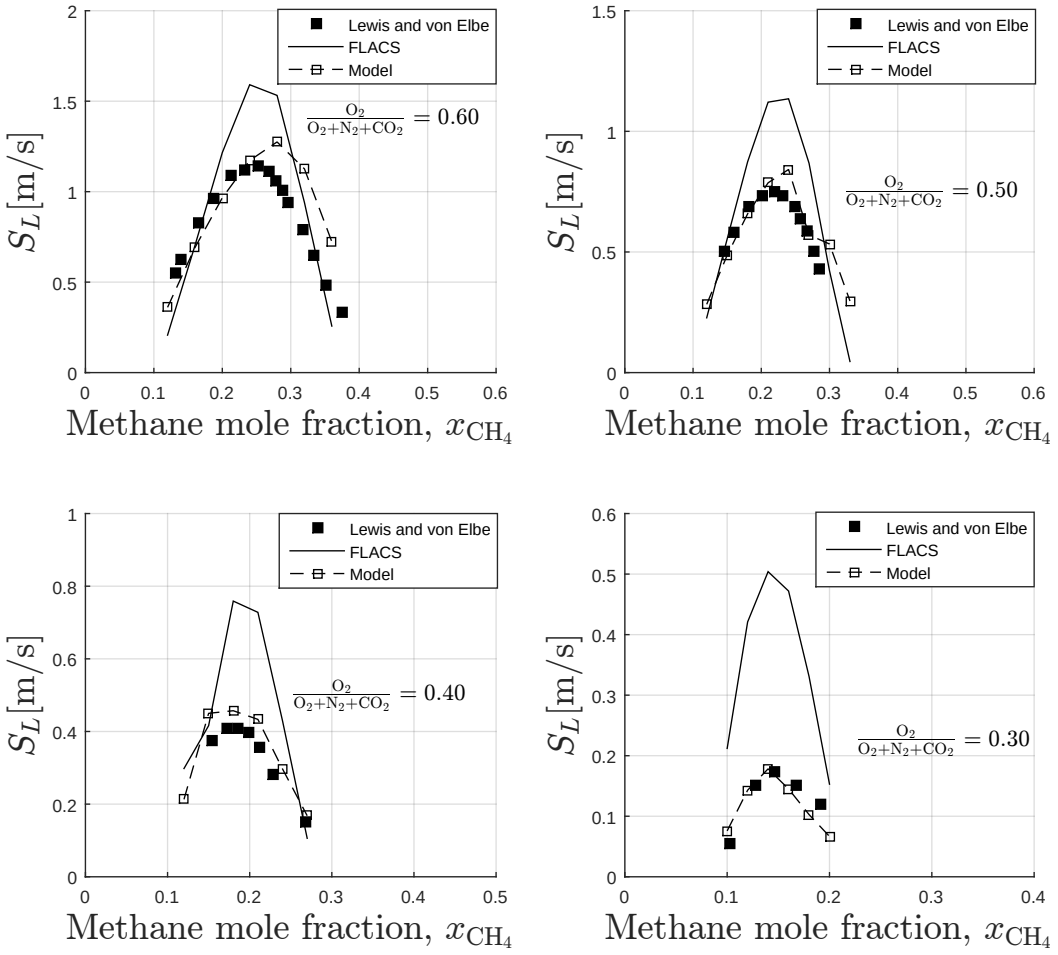

Figure 4.15: Laminar burning velocity results modelled by Equation (4.1), compared with calculated values from FLACS and experiments from Lewis and von Elbe [19]. $CH_4 - O_2 - CO_2$ mixture at atmospheric pressure and 20 °C with CO_2 dilutions $\frac{O_2}{O_2+N_2+CO_2} = 0.60, 0.50, 0.40, 0.30$. O_2 contains 1.5% N_2.

4.2.6 CO − air mixtures

Syngas is mainly composed of carbon monoxide, hydrogen and methane, with a fluctuating amount of diluents like nitrogen or carbon dioxide. Recently there has been an increased interest towards syngas due to its less destructive effect on the environment [34]. This is accompanied by an increased possibility of syngas production and applications were explosions may occur. Realistic predictions of carbon monoxide laminar burning velocities can be used to estimate the consequences of syngas explosions. In Figures 4.16 and 4.17, two parameters vary with S_L; the air composition and the amount of carbon monoxide in the mixture. The intention was to get an impression of how the S_L model performs as a function of these two parameters.

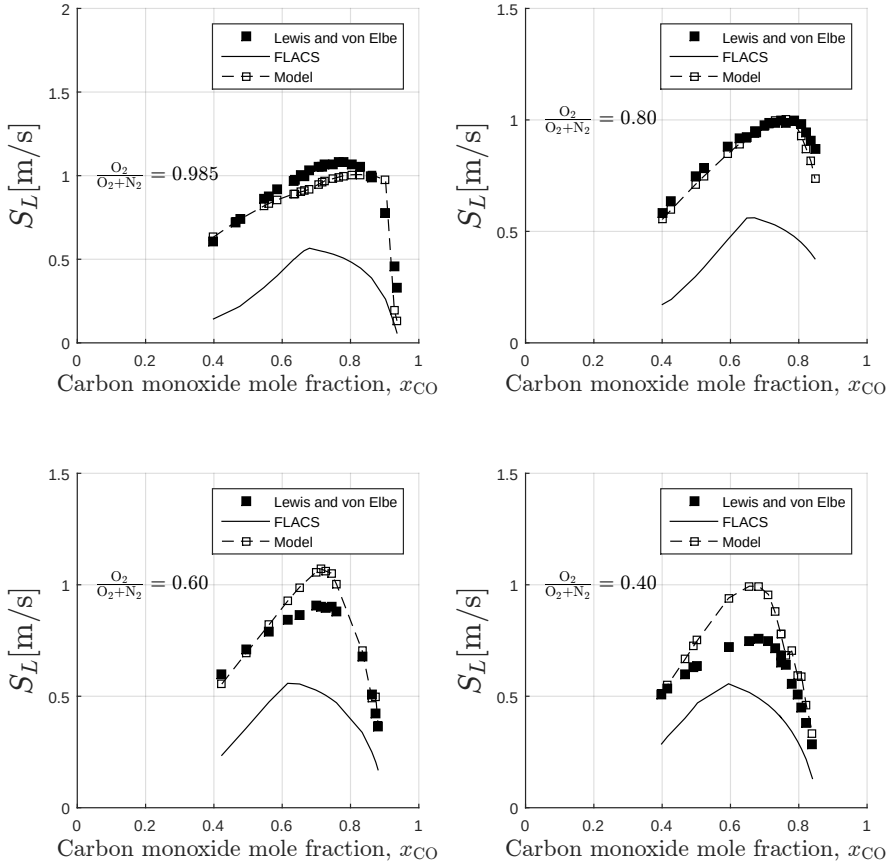

Figure 4.16: Laminar burning velocity results modelled by Equation (4.1), compared with calculated values from FLACS and experiments from Lewis and von Elbe [19]. CO − air mixture at atmospheric pressure and 20 °C with air compositons $\frac{O_2}{O_2+N_2} = 0.985, 0.80, 0.60, 0.40$.

From Figure 4.16 it is evident that the S_L model produces shapes and magnitudes showing better agreement with experiments than FLACS. With air compositions of $\frac{O_2}{O_2+N_2} = 0.985, 0.8$ and 0.6, the S_L model produces shapes and magnitudes showing significantly better agreement with experiments than FLACS.

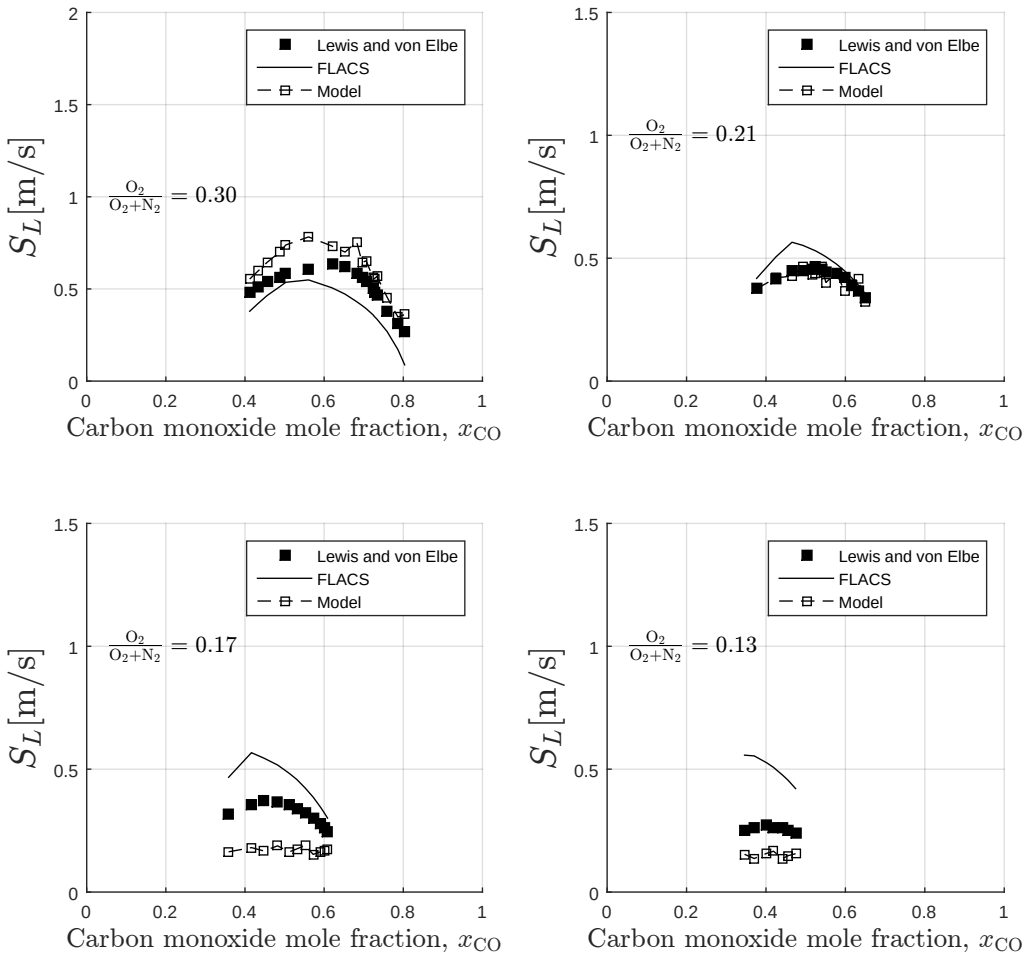

Figure 4.17: Laminar burning velocity results modelled by Equation (4.1), compared with calculated values from FLACS and experiments from Lewis and von Elbe [19]. CO − air mixture at atmospheric pressure and 20 °C with air compositions $\frac{O_2}{O_2+N_2} = 0.30, 0.21, 0.17, 0.13$.

As the nitrogen dilution increases to $\frac{O_2}{O_2+N_2} = 0.40$ and 0.30, the S_L model curve magnitude deviates slightly more from experimental ones, with FLACS producing a better fitted curve at $\frac{O_2}{O_2+N_2} = 0.30$. At this air composition, seen in Figure 4.17, the S_L model produces an outlier at $x_{CO} = 0.66$. This outlier may be caused by a stagnation in equilibrium temperature drop, calculated by the chemical calculator [28]. From $x_{CO} = 0.63$ to 0.66, the equilibrium temperature only drops from 1975 K to 1960 K, respectively. The S_L model shows good agreement with experimental data for the mixture with normal air composition. At all air compositions except $\frac{O_2}{O_2+N_2} = 0.30$ and 0.17, the S_L model produces better shapes and magnitudes than FLACS.

4.3 Validation

Oberkampf and Trucano [35] divide model validation into three aspects; comparison with experimental data, extrapolation of the model and associated uncertainty to its intended domain, and assessing whether the model meets certain precision requirements in its intended domain. These aspects are discussed in the following sections.

4.3.1 Comparison with experimental data

In order to quantitatively compare the FLACS calculated laminar burning velocity values to the modelled ones, residual sum of squares data was calculated for all mixtures except the $H_2 - air - steam$ mixtures. It is presented in Figures 4.18 and 4.19:

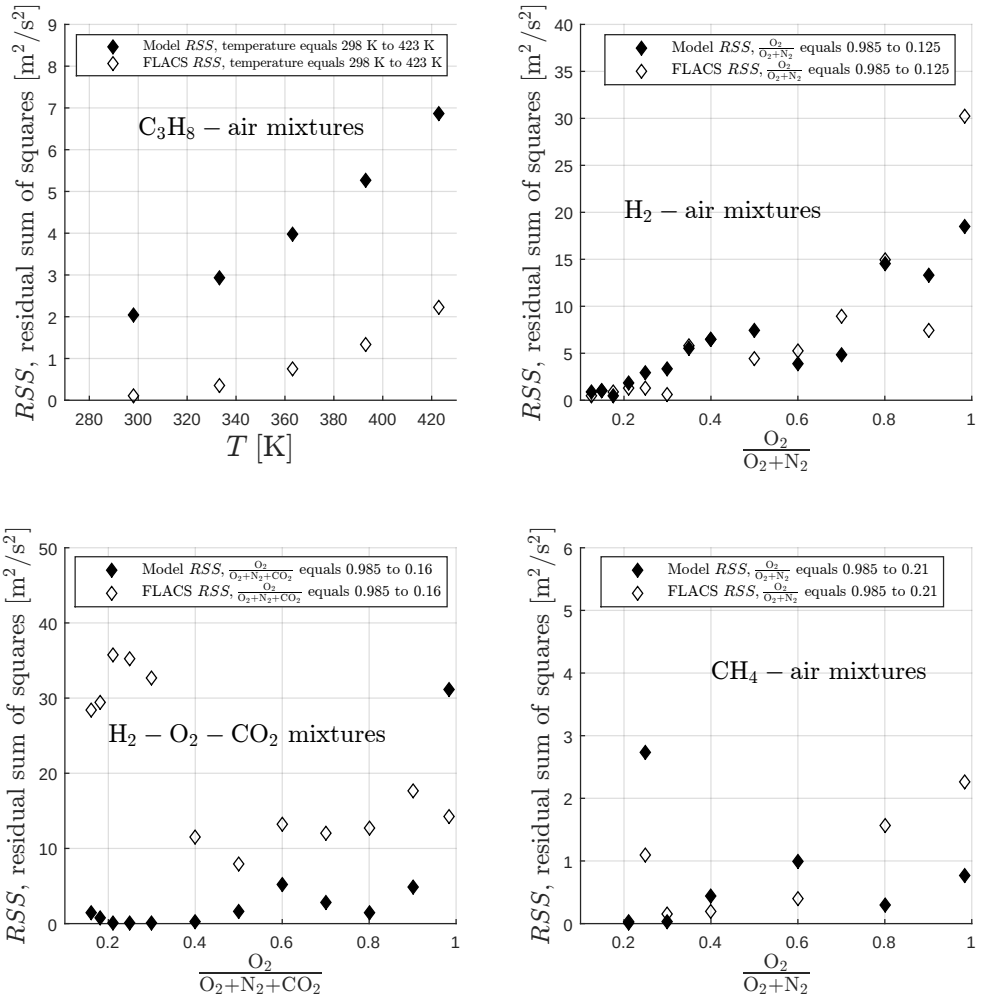

Figure 4.18: Residual sum of squares (RSS) values for $C_3H_8 - air$, $H_2 - air$, $CH_4 - air$ and $H_2 - CO_2 - O_2$ mixtures in the research.

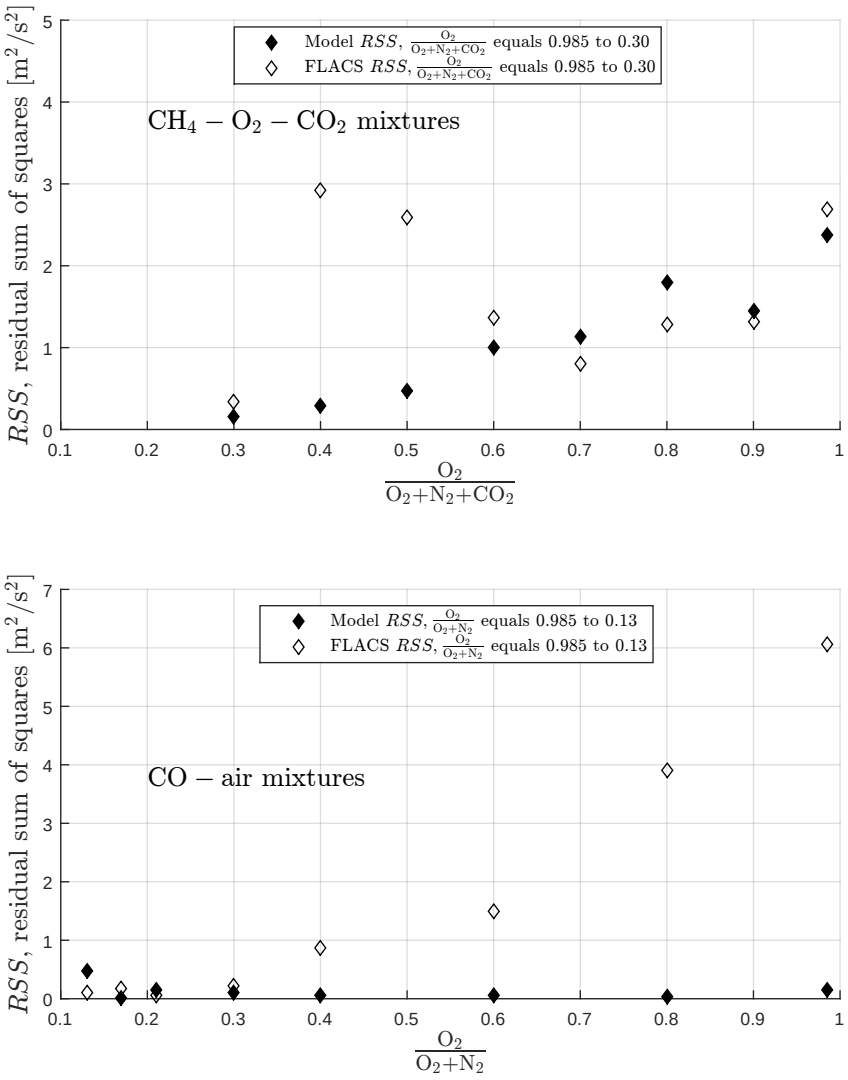

Figure 4.19: Residual sum of squares (RSS) values for $CH4 - O2 - CO_2$ and $CO - air$ mixtures in the research.

Tables 4.3 and 4.4 present an overview of the RSS values for mixtures in the research, as well as an assessment on whether the FLACS or S_L model shape and magnitude fit the experimental data, and the overall best fit for the given mixture. Shape, magnitude and overall fit will be characterised by variables "FLACS", "model", "both" or "none", depending on which one, if any, produces shapes and magnitudes adequately agreeing with experiments. In order to be characterized as an overall fit, both the shape and magnitude need to fit and the RSS needs to be reasonably low.

Table 4.3: Overview of RSS values and assessment of shape and magnitude fit for the mixtures in research, part 1.

Mixture	T [°C]	$\frac{O_2}{O_2+N_2+CO_2}$ or % steam	Model RSS	FLACS RSS	Shape fit	Magnitude fit	Overall fit
$H_2 - air - steam$	50	0% steam	-	-	model	-	none
$H_2 - air - steam$	50	3% steam	-	-	FLACS	-	none
$H_2 - air - steam$	50	5.5% steam	-	-	FLACS	-	none
$H_2 - air - steam$	50	8.5% steam	-	-	FLACS	-	none
$H_2 - air - steam$	50	8.5% steam	-	-	FLACS	-	none
$H_2 - air - steam$	150	0% steam	-	-	model	-	none
$H_2 - air - steam$	150	3% steam	-	-	model	-	none
$H_2 - air - steam$	150	5.5% steam	-	-	FLACS	-	none
$H_2 - air - steam$	150	8.5% steam	-	-	none	-	none
$H_2 - air - steam$	200	0% steam	-	-	FLACS	-	none
$H_2 - air - steam$	200	4% steam	-	-	model	-	none
$H_2 - air - steam$	200	8.5% steam	-	-	both	-	none
$H_2 - air - steam$	200	12% steam	-	-	FLACS	-	none
$H_2 - air$	20	0.99	18.54	30.18	FLACS	both	both
$H_2 - air$	20	0.90	13.33	7.41	model	model	model
$H_2 - air$	20	0.80	14.52	14.93	FLACS	FLACS	both
$H_2 - air$	20	0.70	4.80	9.00	both	both	both
$H_2 - air$	20	0.60	3.85	5.28	both	both	both
$H_2 - air$	20	0.50	7.45	4.46	model	FLACS	both
$H_2 - air$	20	0.40	6.41	6.41	both	both	both
$H_2 - air$	20	0.35	5.57	5.77	both	both	both
$H_2 - air$	20	0.30	3.40	0.55	FLACS	FLACS	both
$H_2 - air$	20	0.25	2.87	1.29	FLACS	FLACS	both
$H_2 - air$	20	0.21	1.78	1.23	model	model	both
$H_2 - air$	20	0.18	0.51	0.86	model	model	both
$H_2 - air$	20	0.15	1.09	0.96	FLACS	FLACS	FLACS
$H_2 - air$	20	0.13	0.86	0.43	FLACS	FLACS	FLACS
$H_2 - O_2 - CO_2$	20	0.99	31.11	14.29	both	both	FLACS
$H_2 - O_2 - CO_2$	20	0.90	4.80	17.60	both	both	model
$H_2 - O_2 - CO_2$	20	0.80	1.50	12.70	FLACS	both	FLACS
$H_2 - O_2 - CO_2$	20	0.70	2.78	12.10	model	both	model
$H_2 - O_2 - CO_2$	20	0.60	5.17	13.20	both	both	model
$H_2 - O_2 - CO_2$	20	0.50	1.70	7.90	model	model	model
$H_2 - O_2 - CO_2$	20	0.40	0.25	11.56	model	model	model
$H_2 - O_2 - CO_2$	20	0.30	0.10	32.75	none	model	none
$H_2 - O_2 - CO_2$	20	0.25	0.03	35.23	none	model	none
$H_2 - O_2 - CO_2$	20	0.20	0.02	35.70	none	none	none
$H_2 - O_2 - CO_2$	20	0.18	0.80	29.48	none	none	none
$H_2 - O_2 - CO_2$	20	0.16	1.48	28.47	none	none	none

Table 4.4: Overview of RSS values and assessment of shape and magnitude fit for the mixtures in research, part 2.

Mixture type	T [°C]	$\frac{O_2}{O_2+N_2+CO_2}$	Model RSS	FLACS RSS	Shape fit	Magnitude fit	Overall fit
$CH_4 - air$	20	0.99	0.77	2.64	both	both	model
$CH_4 - air$	20	0.80	0.30	1.57	both	both	model
$CH_4 - air$	20	0.60	1.00	0.40	both	both	none
$CH_4 - air$	20	0.40	0.44	0.20	both	both	FLACS
$CH_4 - air$	20	0.30	0.04	0.16	both	both	none
$CH_4 - air$	20	0.25	2.73	1.10	both	both	model
$CH_4 - air$	20	0.21	0.02	0.04	both	both	model
$CH_4 - O_2 - CO_2$	20	0.99	2.38	2.69	both	model	none
$CH_4 - O_2 - CO_2$	20	0.90	1.44	1.31	both	model	none
$CH_4 - O_2 - CO_2$	20	0.80	1.79	1.29	both	model	none
$CH_4 - O_2 - CO_2$	20	0.70	1.14	0.80	both	model	model
$CH_4 - O_2 - CO_2$	20	0.60	1.00	1.37	none	model	none
$CH_4 - O_2 - CO_2$	20	0.50	0.48	2.60	model	model	model
$CH_4 - O_2 - CO_2$	20	0.40	0.30	2.90	model	model	model
$CH_4 - O_2 - CO_2$	20	0.30	0.16	0.33	model	model	model
$CO - air$	20	0.99	0.15	6.07	model	model	model
$CO - air$	20	0.80	0.03	3.90	model	model	model
$CO - air$	20	0.60	0.07	1.49	model	none	model
$CO - air$	20	0.40	0.06	0.87	model	none	none
$CO - air$	20	0.30	0.10	0.21	none	none	none
$CO - air$	20	0.21	0.14	0.06	model	model	model
$CO - air$	20	0.17	0.01	0.18	none	none	none
$CO - air$	20	0.13	0.47	0.10	model	none	none
$C_3H_8 - air$	25	0.21	2.04	0.10	both	none	none
$C_3H_8 - air$	60	0.21	2.94	0.35	both	none	none
$C_3H_8 - air$	90	0.21	6.87	2.21	both	none	none
$C_3H_8 - air$	126	0.21	3.96	0.74	both	none	none
$C_3H_8 - air$	150	0.21	5.27	1.35	both	none	none

The S_L model shows best agreement with experiments in 18 of the 67 mixtures and FLACS shows best agreement with experiments in 5 of the 67 mixtures. It is hard to ascertain whether FLACS or the S_L model shows best agreement with experiments in 11 of the 67 mixtures, while in the remaining 37 mixtures neither FLACS nor the S_L model shows adequate agreement with experiments. The no-fit group includes the steam mixtures where neither FLACS nor the S_L model achieved magnitude-fit with experiments without being scaled. The S_L model struggles to fit experiments especially for the strongly nitrogen diluted $H_2 - air$ mixtures. Both FLACS and the S_L model struggle to fit experiments for the strongly CO_2 diluted $H_2 - O_2 - CO_2$ mixtures and strongly nitrogen diluted $CO - air$ mixtures. Overall, the S_L model shows better agreement with experiments for the

$CO - air$, $CH_4 - air$ and $CH_4 - O_2 - CO_2$ mixtures than FLACS. The S_L model and FLACS show equal agreement with experiments for the $H_2 - air$ and $H_2 - air - steam$ mixtures. FLACS shows a slightly better shape agreement with experiments for the $C_3H_8 - air$ mixtures, which the S_L model was not calibrated towards. Results for the $C_3H_8 - air$ mixtures are presented in Section 4.3.2. Neither FLACS nor the S_L model are adequately precise in the current work's domain, however the S_L model shows good promise should it be further enhanced.

4.3.2 The S_L models extrapolation ability

A model with good extrapolation ability produces sensible results when being exposed to changing input. Some model parameters may be over-sensitive to their respective input, which weakens the integrity of the model. As previously mentioned, the reaction rate parameters in the S_L model are calibrated toward specific mixtures and are sensitive to changes in mixture type. Propane and methane are both alkanes, which made propane a well suited candidate to evaluate if the S_L model produced physically reasonable results, should parameters like heat capacity, thermal conductivity and density change.

Expressions for A_{prex}, W_{O_2} and W_{CH_4} were used on $C_3H_8 - air$ mixtures at elevated temperatures. Experimental data was gathered from an article by Domnina Razus et al. [26]. FLACS S_L values were significantly low compared to experiments, while the S_L model generally overestimated the curve magnitude by approximately 60%. In the same manner as for the $H_2 - air - steam$ mixtures, the propane mixture curves were therefore mainly shape compared. Results in Figure 4.20 show that the S_L model extrapolates the laminar burning velocity of $C_3H_8 - air$ mixtures well at different temperatures. The S_L model deviates slightly more in shape than FLACS, which in turn is calibrated towards the experimental data.

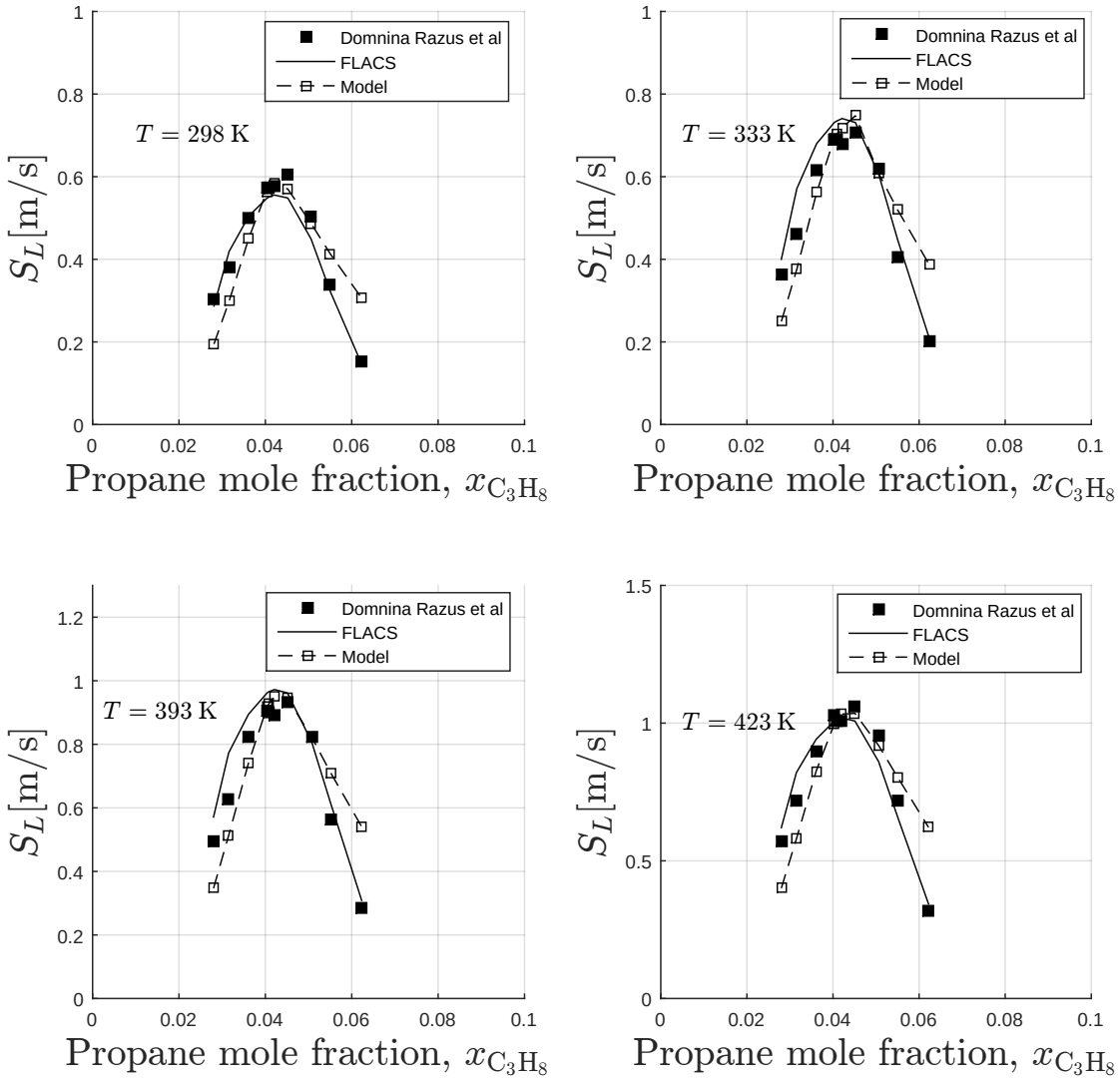

Figure 4.20: Laminar burning velocity results modelled by Equation (4.1), compared with calculated values from FLACS and experiments from Domnina Razus et al. [26]. $C_3H_8 - \text{air}$ mixture at atmospheric pressure and elevated temperatures.

4.3.3 Uncertainty to the S_L models intended domain

In this section uncertainties and possible reasons behind deviations are discussed.

- Experimental data:

  Differences in experimental measurement techniques and flame configurations lead to deviating laminar burning velocity results, as can be seen for the $H_2 - \text{air}$ mixture in in Figure 4.5. Distinct experimental setups are associated with their own equipment inaccuracies, which may be difficult to quantify. The next paragraph will shed a light on experimental deviation sources.

  Error in apparatuses which measure various parameters such as temperature and pressure, contributes to experimental uncertainty. In the $H_2 - \text{air} - \text{steam}$ experiments, the temperature measurement apparatus contributes to such an experimental uncertainty, as voltage fluctuations causes an $\pm 5\,^{\circ}\text{C}$ error in the measured temperature [25]. Another important deviation source are the models used to transform raw data, e.g laminar burning velocity stretch models (measurements of flame area are influenced by the flame stretch phenomena caused by non-uniformities in the flow field [36]). Such models suffer from missing or truncated physics which leads to a structural uncertainty. The chosen stretch models level of detail will influence the unstretched laminar burning velocity. The measurements in the experiments presented by Liu and Macfarlane [25] and Lewis and von Elbe [19], which the S_L model were calibrated towards, are not handled by such correction models and represent an average laminar burning velocity. Experiments of different setups lead to fluctuating heat loss, temperatures and pressures caused by the physical characteristics of the materials which constitute the setup. Some setups may have a greater number of monitors which cancel out "noise" in the raw data, other setups may not. These factors bring uncertainty to the raw data output of the experiments. When executing an experiment, the number of repetitions and preciseness of each repetition will influence the uncertainty of results as well. All the mentioned experimental uncertainty aspects above will propagate into the models calibrated towards the experiment in question.

- Model calibration

  The greatest cause of deviation in the S_L model is the calibration and linearisation process of reaction rate parameters, and the use of mixture-specific calibrated reaction rate parameters on other mixture types. For instance; when reaction rate parameters are calibrated for the $H_2 - \text{air}$ mixtures, they will make the S_L model mixtures fit the $H_2 - \text{air}$ experimental data. However, the best fitted reaction rate parameters strongly oscillate, requiring 6th degree polynomials to be made functions of $\frac{O_2}{O_2+N_2}$, making the model both less convenient to use and more sensitive with regard to input. Reaction rate parameters were therefore manually altered to attain more linear shapes. This alteration induces an error for the originally calibrated

reaction rate parameters. Next, the linearisation of the reaction rate parameters further increases this error.

- Truncated physics in the S_L model

  There are many deviation sources caused by truncated physics in the S_L model. The uncertainty associated with assuming that the included gases are ideal, propagates into calculations of other parameters in the S_L model such as density. The reaction rate of the S_L model is approximated by a one-step reaction equation, which greatly simplifies the reaction rate chemistry by excluding the vast number of intermediate reactions actually taking place. As discussed in Section 3.1.2, Equation (3.2) underestimates thermal diffusivities for many of the species that are part of the research, caused by an inaccurate thermal conductivity model. The 2nd degree specific heat capacity polynomials used in the current work had an uncertainty of approximately 2% which contributes to uncertainty [8]. Furthermore, many of the same physics-truncating assumptions presented by Turns [9] are also assumed for the S_L model in the current work, e.g constant pressure, a unity Lewis number and the neglection of kinetic and potential energies as well as thermal radiation.

- Extrapolating a faulty model

  The importance of including accurate models for thermodynamic parameters in the model is especially visible when extrapolating mixture-specific calibrated reaction rate parameters to other mixtures. Reaction rate parameters calibrated towards a mixture where, for instance, the thermal diffusivity of some species is misrepresented, will induce an extra uncertainty should they be used on a mixture-type or composition outside of the calibrated domain.

- Input data

  A lot of input data used in the S_L model was handled in the research. The burning velocities and concentrations gathered by use of the Microsoft Paint and GRABIT digitalisation methods (Section 3.2.1) induce uncertainty to this input data in the S_L model, caused by human error. Faulty calculation and handling of other data may have occurred, such as when calculating FLACS laminar burning velocities or balancing the mixtures' reaction equations in order to calculate $Y_{F,stoich}$. Obvious outliers and the data in general has been checked to minimize the probability for such errors.

5. Conclusion

In this thesis, a product temperature dependent laminar burning velocity model was constructed and evaluated for four different fuel − air gas mixtures, including 67 distinct mixtures. The gas mixtures evaluated were: hydrogen, methane, propane and carbon monoxide mixtures at different temperatures, with varying air compositions and inert gas dilutions. The purpose was to compare the behaviour of this so-called S_L model to literature data and tabulated values from the CFD program FLACS, in order to assess if it could replace the present laminar burning velocity model in FLACS.

Neither FLACS nor the S_L model are adequately precise in the current works domain. Overall, the S_L model showed a better agreement to literature for more mixtures than FLACS. For some cases however, none of them showed adequate agreement. The no-fit group included the $H_2 - air - steam$ mixture experiments by Liu and Macfarlane [25], where neither FLACS nor the S_L model achieved magnitude fit without being scaled. The S_L model struggled especially with the strongly nitrogen diluted $H_2 - air$ mixtures. Both FLACS and the S_L model struggled with the strongly CO_2 diluted $H_2 - O_2 - CO_2$ mixtures and strongly nitrogen diluted $CO - air$ mixtures. Overall, the S_L model showed better agreement to Lewis and von Elbe [19] than FLACS for the $CO - air$, $CH_4 - air$ and $CH_4 - O_2 - CO_2$ mixtures. The S_L model and FLACS showed equal agreement to Lewis and von Elbe for the $H_2 - air$ and $H_2 - air - steam$ mixtures. FLACS showed a slightly better shape agreement with Domnina Razus et al. [26] for the $C_3H_8 - air$ mixtures, which the S_L model was not calibrated towards.

A better fit than FLACS could have been achieved for all mixtures by the S_L model with construction of more advanced reaction rate parameter expressions, calibrated for each distinct mixture. However, aiming for a convenient model, some calibrated reaction rate parameters were used on mixtures which they were not calibrated towards. This is the main source of the S_L models deviation from literature. Another marked deviation source is the linearisation process of reaction rate parameters.

Because the study was limited to evaluating four different gas mixture types, calibration and validation of the S_L model towards other gas mixtures at various conditions is needed in order to determine if it can replace the model currently implemented in FLACS. It is conceivable that with further enhancement it may be possible to do so.

6. Suggestions for further work

- Improving fit for all mixtures by recalibration:

  With the deviating magnitudes for the $H_2 - air - steam$ mixtures as an example; Other reaction rate parameters besides the steam reaction order could be calibrated towards steam mixtures. This might result in better fitted curves.

- Inclusion of other gas mixture types:

  The model could be enhanced by the inclusion of reaction rate parameters calibrated for other gas mixture types.

- Inclusion of a blending law:

  A blending law for different fuels could be included in the model. Arntzen [8] suggests two blending laws in his PhD thesis.

- Inclusion of pressure dependence:

  The submodel for reaction rate (ω) in the S_L model could be improved by inclusion of a pressure dependent parameter.

- Flammability limit correction:

  A scheme to correct different mixtures' flammability limits could be included in the model.

- Replacing the thermal conductivity or thermal diffusivity model:

  The current thermal diffusivity model underestimates α for many species in the research, and should be replaced to lay a foundation for more valid results.

- Further simplifying the model:

  Currently, the model includes many variables that are specific to each gas mixture. If the model is further improved to the point where it is clearly better than the FLACS model, a sensitivity analysis could be performed to evaluate if some of these variables are not needed.

- Improving the model for turbulent burning velocity:

  The turbulent burning velocity model in FLACS may be improved by implementation of the S_L models reaction rate submodel (ω).

Bibliography

[1] A. Dahoe, "Laminar burning velocities of hydrogen-air mixtures from closed vessel gas explosions," vol. 18, 2005.

[2] J. Warnatz, U. Maas, and R. W. Dibble, *Combustion: physical and chemical fundamentals, modeling and simulation, experiments, pollutant formation.* Berlin ; New York: Springer, 4th ed., 2006.

[3] G. S. Settles, *Schlieren and shadowgraph techniques: visualizing phenomena in transparent media.* Experimental fluid mechanics, Berlin ; New York: Springer, 2001.

[4] K. J. Bosschaart and L. P. H. de Goey, "The laminar burning velocity of flames propagating in mixtures of hydrocarbons and air measured with the heat flux method," *Combustion and Flame*, vol. 136, pp. 261–269, Feb. 2004.

[5] M. I. Hassan, K. T. Aung, and G. M. Faeth, "Measured and predicted properties of laminar premixed methane/air flames at various pressures," *Combustion and Flame*, vol. 115, pp. 539–550, Dec. 1998.

[6] E. Ranzi, A. Frassoldati, R. Grana, A. Cuoci, T. Faravelli, A. Kelley, and C. Law, "Hierarchical and comparative kinetic modeling of laminar flame speeds of hydrocarbon and oxygenated fuels," *Progress in Energy and Combustion Science*, 2012.

[7] C. Law, "The 2011 Dryden Lecture: fuel options for next generation chemical propulsion.," *AIAA Journal 2011*, vol. 50, pp. 1–18.

[8] B. J. Arntzen, *Modelling of Turbulence and Combustion for Simulation of Gas Explosions in Complex Geometries.* PhD thesis, The Norwegian University of Science and Technology, May 1998.

[9] S. R. Turns, *An Introduction to Combustion.* Propulsion Engineering Research Center and Department of Mechanical and Nuclear Engineering, The Pennsylvania State University: McGraw -Hill, 2nd ed.

[10] T. H. Crowe, "Correlation of laminar flame velocities for hydrocarbon-oxygen-inert gas mixtures," 1955.

[11] G. D. Byrne and A. M. Dean, "The numerical solution of some kinetics models with VODE and CHEMKIN II," *Computers & Chemistry*, vol. 17, pp. 297–302, Sept. 1993.

[12] "Definition of combustion." [Online]. Available: http://www.merriam-webster.com/dictionary/combustion. (Accessed: 2016-09-06).

[13] R. K. Eckhoff, *Explosion hazards in the process industries*. Houston, TX: Gulf Pub, 2005.

[14] "Definition of heat." [Online]. Available: https://www.merriam-webster.com/dictionary/heat. (Accessed: 2016-09-07).

[15] I. Mills and International Union of Pure and Applied Chemistry, eds., *Quantities, units, and symbols in physical chemistry*. Cambridge, UK: RSC Pub, 3rd ed., 2007.

[16] M. Rausand and I. Bouwer Utne, *Risk analysis - theory and methods*. Fagbokforlaget, 2009.

[17] J. D. Anderson, *Computational fluid dynamics: the basics with applications*. McGraw-Hill series in mechanical engineering, New York: McGraw-Hill, 8th ed., 2001.

[18] H. Hisken Pedersen, "TECHNICAL NOTE - Modelling the flammability limits and laminar burning velocities of hydrogen and hydrocarbon mixtures in non-standard atmospheres.," tech. rep., Sept. 2012.

[19] B. Lewis and G. von Elbe, "Combustion, Flames and Explosions of Gases," pp. 394–405, Academic Press, INC., 3rd ed., 1987.

[20] E. Bourgin, M. Alveis, C. Yang, F. Fachini, and L. Bauwens, "Effects of Lewis numbers and kinetics on spontaneous ignition of hydrogen jets," *Proceedings of the Combustion Institute*, vol. 36, July 2016.

[21] D. R. Lide and Chemical Rubber Company, eds., *CRC handbook of chemistry and physics: a ready-reference book of chemical and physical data*. Boca Raton, FLa.: CRC Press, 90th ed., 2009.

[22] R. H. Perry and D. W. Green, eds., *Perry's chemical engineers' handbook*. Perry's chemical engineers' platinum edition, New York, NY: McGraw-Hill, 7th ed., 1999.

[23] "Thermal conductivity of common materials and gases." [Online]. Available: http://www.engineeringtoolbox.com/thermal-conductivity-d_429.html. (Accessed: 2016-10-24).

[24] J. R. Welty, C. E. Wicks, and R. E. Wilson, *Fundamentals of momentum, heat, and mass transfer*. New York: Wiley, 3rd ed., 1984.

[25] D. D. S. Liu and R. MacFarlane, "Laminar burning velocities of hydrogen-air and hydrogen-airsteam flames," *Combustion and Flame*, vol. 49, pp. 59–71, Jan. 1983.

[26] D. Razus, D. Oancea, V. Brinzea, M. Mitu, and C. Movileanu, "Experimental and computed burning velocities of propaneair mixtures," *Energy Conversion and Management*, vol. 51, pp. 2979–2984, Dec. 2010.

[27] "Grabit function - matlab central." [Online]. Available:https://se.mathworks.com/matlabcentral/fileexchange/7173-grabit. (Accessed: 2017-01-13).

[28] "Chemical equilibrium calculator - colorado state university." [Online]. Available:http://navier.engr.colostate.edu/~dandy/code/code-4/. (Accessed: 2016-09-20).

[29] G. A. , "FLACS v10.4 User's Manual." 2015.

[30] R. D. Cook and S. Weisberg, *Residuals and influence in regression*. Monographs on statistics and applied probability, New York: Chapman and Hall, 1982.

[31] S. Ren and Q. Zhang, "Influence of concentration distribution of hydrogen in air on measured flammability limits," *Journal of Loss Prevention in the Process Industries*, vol. 34, pp. 82–91, Mar. 2015.

[32] "Partial meltdowns led to hydrogen explosions at fukushima nuclear power plant - scientific american." [Online]. Available:https://www.scientificamerican.com/article/partial-meltdowns-hydrogen-explosions-at-fukushima-nuclear-power-plant/. (Accessed: 2017-03-20).

[33] M. Mitu, V. Giurcan, D. Razus, and D. Oancea, "Inert gas influence on the laminar burning velocity of methane-air mixtures," *Journal of Hazardous Materials*, vol. 321, pp. 440–448, Jan. 2017.

[34] J. Fu, C. Tang, W. Jin, L. D. Thi, Z. Huang, and Y. Zhang, "Study on laminar flame speed and flame structure of syngas with varied compositions using OH-PLIF and spectrograph," *International Journal of Hydrogen Energy*, vol. 38, pp. 1636–1643, Feb. 2013.

[35] T. Trucano and W. Oberkampf, "Verification and validation benchmarks," *Nucl Eng*, vol. 238, p. 43, Dec. 2008.

[36] D. Veynante and T. Poinsot, *Theoretical and numerical combustion*. Philadelphia: Edwards, 2005.

Appendix A

CO – air reaction order

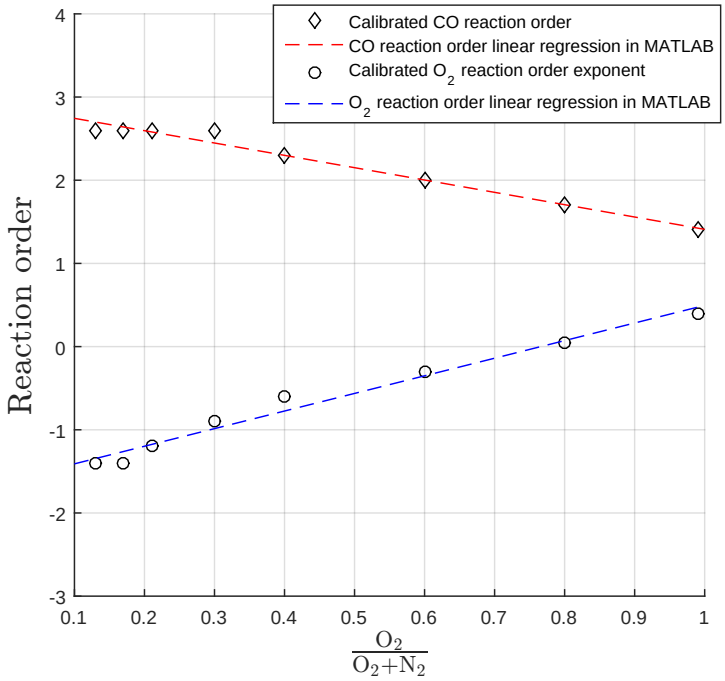

Figure 6.1: Linear regression of reaction orders for CO – air mixtures with different air compositions.

Appendix B

MATLAB code

```
1
2  % a = fuel reaction order
3  % b = oxygen reaction order
4  % c = inert reaction order
5  % d = nitrogen reaction order
6  %The following for-loops constitute the least square fit algorithm in the
7  %code. In the following instance, mixture 53(ch4 - o2 - co2) is checked
8  %for which number and values or reaction orders give the least RSS value
9  %for the chosen pre exponential fator 721875000.
10
11 for PREX_FACTOR = 721875000
12 for a=-3:0.01:3
13 for b=-3:0.01:3
14 for c=-3:0.01:3
15 for d=-3:0.01:3
16 for i =53:53
17     if((i>45)&&(i<61))
18 MW_fuel=MW_CH4;
19     end
20 if(i>60)
21     MW_fuel = MW_H2;
22 end
23 if((i>64)&&(i<73))
24     MW_fuel = MW_CO;
25 end
26 if(i>72)
27     MW_fuel = MW_C3H8;
28 end
29 b_masscalc=size(molefractionarray{i});
30 for ii = 1:b_masscalc(1);
31 if(exp_values{i}(ii)>0.5*max(exp_values{i}))
32     ii;
33 W_NOEXP_TEST=-((PREX_FACTOR*EXPONENT{i}(ii)*MW_fuel));
34 SL_NOEXP_TEST = (-2*THERMAL_DIFFUSIVITY{i}(ii)*((FUEL_OXIDIZER_RATIO{i}(ii))+1)*W_NOEXP_TEST
       /REACTANT_DENSITY{i}(ii))^(0.5);
35 error_NONE=abs((SL_NOEXP_TEST-exp_values{i}(ii)));
36 Errorculminated_NONE = Errorculminated_NONE+error_NONE^2;
37 W_A_TEST=-((PREX_FACTOR*(BURNED_DENSITY{i}(ii))^(a))*EXPONENT{i}(ii)*((FUEL_massfraction{i}(
       ii)/EQ1MF(i))^(a)))*MW_fuel;
38 SL_A_TEST=(-2*THERMAL_DIFFUSIVITY{i}(ii)*(FUEL_OXIDIZER_RATIO{i}(ii)+1)*W_A_TEST/
       REACTANT_DENSITY{i}(ii))^(0.5);
39 error_A=abs((SL_A_TEST-exp_values{i}(ii)));
40 Errorculminated_a = Errorculminated_a+error_A^2;
41 W_A_B_TEST=-((PREX_FACTOR*BURNED_DENSITY{i}(ii)^(a+b))*EXPONENT{i}(ii)*((FUEL_massfraction{i
       }(ii)/EQ1MF(i))^(a))*((O_massfraction{i}(ii)/EQ1MF_o2(i))^(b)))*MW_fuel;
42 SL_A_B_TEST=(-2*THERMAL_DIFFUSIVITY{i}(ii)*(FUEL_OXIDIZER_RATIO{i}(ii)+1)*W_A_B_TEST/
       REACTANT_DENSITY{i}(ii))^(0.5);
43 error_A_B=abs((SL_A_B_TEST-exp_values{i}(ii)));
44 Errorculminated_a_b = Errorculminated_a_b+(error_A_B)^(2);
45 error_FLACS = abs((FLACS_SL{i}(ii)-exp_values{i}(ii)));
46 errorculminated_a_b_FLACS = errorculminated_a_b_FLACS + (error_FLACS)^(2);
47 W_A_B_C_TEST = -((PREX_FACTOR*BURNED_DENSITY{i}(ii)^(a+b+c))*EXPONENT{i}(ii)*((
       FUEL_massfraction{i}(ii)/EQ1MF(i))^(a))*((O_massfraction{i}(ii)/EQ1MF_o2(i))^(b)...
```

```
)*((INERT_massfraction{i}(ii)/EQ1MF_inert(i))^(c)))*MW_fuel;
SL_A_B_C_TEST=(-2*THERMAL_DIFFUSIVITY{i}(ii)*(FUEL_OXIDIZER_RATIO{i}(ii)+1)*W_A_B_C_TEST/
    REACTANT_DENSITY{i}(ii))^(0.5);
if(i<20)
W_A_B_C_TEST = -((PREX_FACTOR*BURNED_DENSITY{i}(ii)^(a+b+c))*EXPONENT{i}(ii)*((
    FUEL_massfraction{i}(ii)/EQ1MF(i))^(a))*((O_massfraction{i}(ii)/EQ1MF_o2(i))^(b)...
)*((INERT_massfraction{i}(ii)/EQ1MF_inert(i))^(c)))*MW_fuel
SL_A_B_C_TEST=(-2*THERMAL_DIFFUSIVITY{i}(ii)*(FUEL_OXIDIZER_RATIO{i}(ii)+1)*W_A_B_C_TEST/
    REACTANT_DENSITY{i}(ii))^(0.5)
end
error_A_B_C=abs((SL_A_B_C_TEST-exp_values{i}(ii)));
Errorculminated_a_b_c = Errorculminated_a_b_c+(error_A_B_C)^(2);
error_FLACS_c = abs(FLACS_SL{i}(ii)-exp_values{i}(ii));
Errorculminated_a_b_c_FLACS = Errorculminated_a_b_c_FLACS + error_FLACS_c^(2);
if(i>64)
W_A_B_C_D_TEST = -((PREX_FACTOR*(BURNED_DENSITY{i}(ii)^(a+b+c+d))*EXPONENT{i}(ii)*((
    FUEL_massfraction{i}(ii)/EQ1MF(i))^(a))*((O_massfraction{i}(ii)/EQ1MF_o2(i))^(b))*((
    INERT_massfraction{i}(ii)/EQ1MF_inert(i))^(c))*((0.01/EQ1MF_H2EXTRA(i))^(d))*MW_fuel));
SL_A_B_C_D_TEST=(-2*THERMAL_DIFFUSIVITY{i}(ii)*(FUEL_OXIDIZER_RATIO{i}(ii)+1)*W_A_B_C_D_TEST
    /REACTANT_DENSITY{i}(ii))^(0.5);
error_A_B_C_D=abs((SL_A_B_C_D_TEST-exp_values{i}(ii)));
Errorculminated_a_b_c_d = Errorculminated_a_b_c_d+(error_A_B_C_D)^(2);
error_FLACS_d = abs(FLACS_SL{i}(ii)-exp_values{i}(ii));
Errorculminated_a_b_c_d_FLACS = Errorculminated_a_b_c_d_FLACS + error_FLACS_d^(2);
end
end
end
end
if(Errorculminated_a < Errorculminated_compare_a)
BEST_PREX_FACTOR_a = PREX_FACTOR;
BEST_A_EXPONENT_a = a;
Errorculminated_compare_a = Errorculminated_a;
end
if(Errorculminated_a_b < Errorculminated_compare_a_b)
BEST_PREX_FACTOR_a_b = PREX_FACTOR;
BEST_A_EXPONENT_a_b = a;
BEST_B_EXPONENT_a_b = b;
Errorculminated_compare_a_b = Errorculminated_a_b;
end
if(Errorculminated_a_b_c < Errorculminated_compare_a_b_c)

BEST_PREX_FACTOR_a_b_c = PREX_FACTOR;
BEST_A_EXPONENT_a_b_c = a;
BEST_B_EXPONENT_a_b_c = b;
BEST_C_EXPONENT_a_b_c = c;
Errorculminated_compare_a_b_c = Errorculminated_a_b_c;
end
if(Errorculminated_a_b_c_d < Errorculminated_compare_a_b_c_d)
BEST_PREX_FACTOR_a_b_c_d = PREX_FACTOR;
BEST_A_EXPONENT_a_b_c_d = a;
BEST_B_EXPONENT_a_b_c_d = b;
BEST_C_EXPONENT_a_b_c_d = c;
BEST_D_EXPONENT_a_b_c_d = d;
Errorculminated_compare_a_b_c_d=Errorculminated_a_b_c_d;
end
if(Errorculminated_a_b_c_FLACS < Errorculminated_compare_a_b_c_FLACS)
Errorculminated_compare_a_b_c_FLACS = Errorculminated_a_b_c_FLACS;
end
if(errorculminated_a_b_FLACS < Errorculminated_compare_a_b_FLACS)
errorculminated_compare_a_b_FLACS = errorculminated_a_b_FLACS;
end
if(Errorculminated_a_b_c_d_FLACS < Errorculminated_compare_a_b_c_d_FLACS)
Errorculminated_compare_a_b_c_d_FLACS = Errorculminated_a_b_c_d_FLACS;
end
Errorculminated_NONE = 0;
```

```
107 Errorculminated_a = 0;
108 Errorculminated_a_b = 0;
109 Errorculminated_a_b_c =0;
110 Errorculminated_a_b_c_d = 0;
111 errorculminated_a_b_FLACS = 0;
112 Errorculminated_a_b_c_FLACS = 0;
113 end
114 end
115 end
116 end
117 end
118 Errorculminated_compare_a_b_c_FLACS
119 errorculminated_compare_a_b_FLACS
120 Errorculminated_compare_a_b
121 Errorculminated_compare_a_b_c
```

Appendix C

Screenshot from MATLAB

A screenshot from MATLAB:

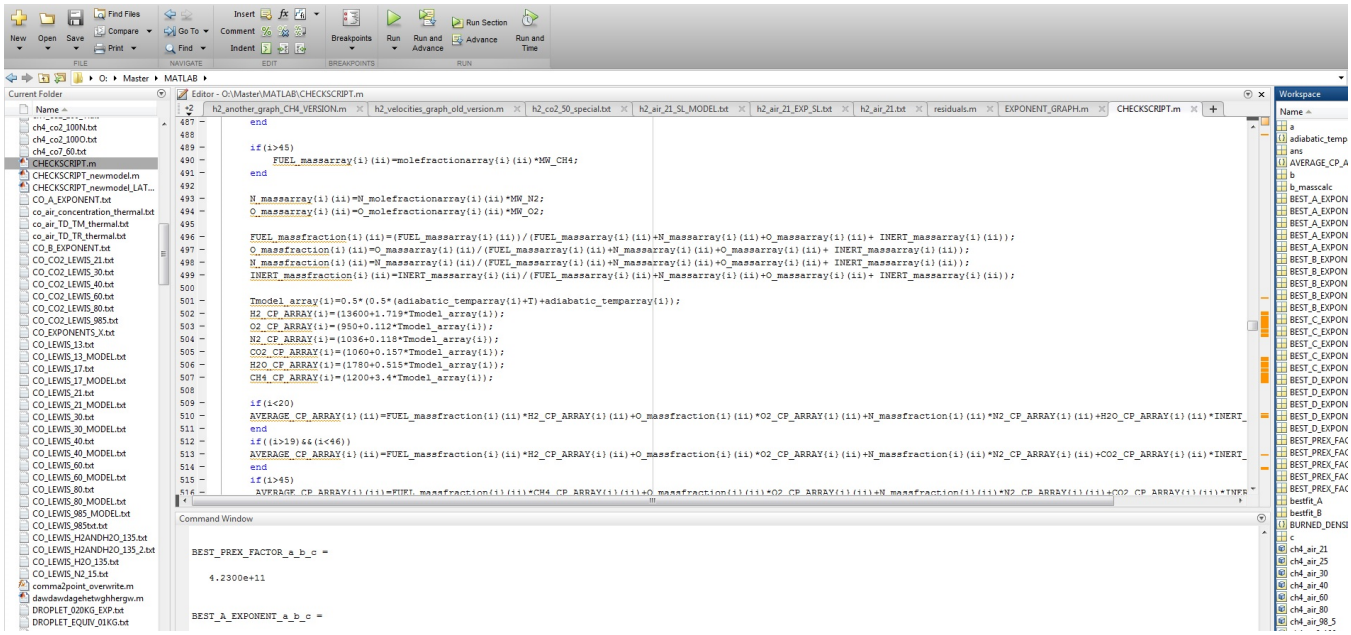

Figure 6.2: Screenshot of MATLAB code used to calibrate reaction rate parameters towards experimental results